NASA/TM—2003-212090

Specimen Designs for Testing Advanced Aeropropulsion Materials Under In-Plane Biaxial Loading

John R. Ellis
Glenn Research Center, Cleveland, Ohio

Ali Abul-Aziz
Cleveland State University, Cleveland, Ohio

January 2003

The NASA STI Program Office . . . in Profile

Since its founding, NASA has been dedicated to the advancement of aeronautics and space science. The NASA Scientific and Technical Information (STI) Program Office plays a key part in helping NASA maintain this important role.

The NASA STI Program Office is operated by Langley Research Center, the Lead Center for NASA's scientific and technical information. The NASA STI Program Office provides access to the NASA STI Database, the largest collection of aeronautical and space science STI in the world. The Program Office is also NASA's institutional mechanism for disseminating the results of its research and development activities. These results are published by NASA in the NASA STI Report Series, which includes the following report types:

- TECHNICAL PUBLICATION. Reports of completed research or a major significant phase of research that present the results of NASA programs and include extensive data or theoretical analysis. Includes compilations of significant scientific and technical data and information deemed to be of continuing reference value. NASA's counterpart of peer-reviewed formal professional papers but has less stringent limitations on manuscript length and extent of graphic presentations.

- TECHNICAL MEMORANDUM. Scientific and technical findings that are preliminary or of specialized interest, e.g., quick release reports, working papers, and bibliographies that contain minimal annotation. Does not contain extensive analysis.

- CONTRACTOR REPORT. Scientific and technical findings by NASA-sponsored contractors and grantees.

- CONFERENCE PUBLICATION. Collected papers from scientific and technical conferences, symposia, seminars, or other meetings sponsored or cosponsored by NASA.

- SPECIAL PUBLICATION. Scientific, technical, or historical information from NASA programs, projects, and missions, often concerned with subjects having substantial public interest.

- TECHNICAL TRANSLATION. English-language translations of foreign scientific and technical material pertinent to NASA's mission.

Specialized services that complement the STI Program Office's diverse offerings include creating custom thesauri, building customized databases, organizing and publishing research results . . . even providing videos.

For more information about the NASA STI Program Office, see the following:

- Access the NASA STI Program Home Page at ***http://www.sti.nasa.gov***

- E-mail your question via the Internet to help@sti.nasa.gov

- Fax your question to the NASA Access Help Desk at 301–621–0134

- Telephone the NASA Access Help Desk at 301–621–0390

- Write to:
  NASA Access Help Desk
  NASA Center for AeroSpace Information
  7121 Standard Drive
  Hanover, MD 21076

NASA/TM—2003-212090

Specimen Designs for Testing Advanced Aeropropulsion Materials Under In-Plane Biaxial Loading

John R. Ellis
Glenn Research Center, Cleveland, Ohio

Ali Abul-Aziz
Cleveland State University, Cleveland, Ohio

National Aeronautics and
Space Administration

Glenn Research Center

January 2003

This report contains preliminary findings, subject to revision as analysis proceeds.

Trade names or manufacturers' names are used in this report for identification only. This usage does not constitute an official endorsement, either expressed or implied, by the National Aeronautics and Space Administration.

Available from

NASA Center for Aerospace Information
7121 Standard Drive
Hanover, MD 21076

National Technical Information Service
5285 Port Royal Road
Springfield, VA 22100

Available electronically at http://gltrs.grc.nasa.gov

Specimen Designs for Testing Advanced Aeropropulsion Materials Under In-Plane Biaxial Loading

John R. Ellis
National Aeronautics and Space Administration
Glenn Research Center
Cleveland, Ohio 44135

Ali Abul-Aziz
Cleveland State University
Cleveland, Ohio 44115

1. Summary

A design study was undertaken to develop specimen designs for testing advanced aeropropulsion materials under in-plane biaxial loading. Materials of interest in this work include titanium-based alloys in both monolithic and composite forms and also nickel- and cobalt- based superalloys in plate form. The focus of initial work was on developing a specimen design suitable for deformation and strength tests to be conducted under monotonic loading. The type of loading initially assumed in this study was the special case of equibiaxial, tensile loading. A specimen design was successfully developed after a lengthy design and optimization process with overall dimensions of 12 by12 by 0.625 in., and a gage area of 3.875 by 3.875 by 0.080 in. Perhaps the most important feature of the design was the four sets of flexures which were incorporated to partially decouple the applied biaxial loading. This essential design feature resulted in a complex specimen configuration, presenting a challenge to manufacture and leading to high manufacturing costs. Subsequently, the scope of the work was extended to include the development of a second design tailored for tests involving cyclic loading. One obvious consideration here is buckling stability as these experiments involve both tensile and compressive loading. A specimen design suitably tailored to meet these requirements was successfully developed with overall dimensions of 12 by 12 by 0.500 in. and a gage area of 2.375 by 2.375 by 0.050 in. Compared to the earlier design, details of the design were simpler in the gripped region and also in the flexure region, but, overall, the geometry of the specimen remained complex. Finally, an investigation was made to determine whether the specimen designs developed in this study could be used without modification to investigate general forms of biaxial loading. It was concluded that the two specimen designs can be used to investigate deformation behavior under general forms of biaxial loading, provided measurement and observation is limited to the 1.0-in.-diameter circular region at the specimen center. However, the situation is more complicated in the case of experiments investigating strength and fracture behavior. For best results, it was concluded that specimen designs need to be optimized and tailored to meet the loading requirements of individual research programs.

2. Introduction

One technique for investigating material behavior under complex stress states is to use in-plane biaxial loading. Using this approach, cruciform specimens fabricated from plate material are gripped at four locations and loaded along two orthogonal axes as illustrated in figure 1. Servohydraulic loading systems are used in this application which are similar to those used for uniaxial testing. Thus, the technique has the advantage that the loading arrangement is relatively straightforward and uses

equipment which has seen extensive development over the past thirty years. Also, the test method allows a wide range of biaxial stress states to be investigated with minimum complication from the load application viewpoint. For these reasons, the test method has been used to generate a sizable body of biaxial test data for both monolithic and composite materials (refs. 1 to 29).

One difficulty facing these investigations has been the selection and/or development of the most suitable specimen design for the particular program. It should be noted that consensus standards do not exist for this method of testing and so the experimentalist is faced with a wide range of possibilities. A major complication here is that use of the cruciform specimen configuration and associated gripping fixtures results in "coupling" between the two loading directions. In the present research, specimens are positioned in the load frame using four hydraulic grips which rigidly constrain the specimen over the gripped regions. It follows that loading applied in one direction is partially reacted by the specimen and partially by the grips associated with loading in the second direction. One method of minimizing this effect is to use specimen designs which incorporate fairly complicated arrangements of flexures as illustrated in figure 2. It has been demonstrated that flexures with low bending stiffness in the plane of loading can be used to minimize the constraint imposed by specimen gripping. Also, it has been shown that the geometry of these flexures can be optimized to give near-uniform stress/strain conditions in the gage area for specific biaxial loading conditions.

One obvious disadvantage of using flexures is that regions of high stress concentration can be introduced into specimens in close proximity to the gage area. Of particular concern are stress concentrations at the ends and intersection points of the flexures. This raises the possibility that failure can be initiated outside of the gage area in regions where stress/strain conditions are ill-defined. Traditionally, this problem has been addressed by incorporating a gage area within which specimen thickness is reduced significantly from the value in the gripped regions. In the case of conventional structural alloys, experience has shown that thickness reduction factors as high as ten are needed to achieve acceptable performance. That is failure initiating within the gage area where stress/strain conditions are both relatively uniform and relatively well defined.

The primary goal of the present work was to develop specimen designs for testing advanced aeropropulsion materials under in-plane biaxial loading. Materials of interest in this research included nickel- and cobalt-based superalloys and also titanium-based alloys in both monolithic and composite forms. The plan was to first conduct a series of tests under monotonic loading to investigate deformation and strength behavior in titanium alloys in unreinforced plate form. Subsequently, the intent was to extend the scope of the study to include cyclic loading with the aim of investigating fatigue and fracture in the same materials and product forms. The most immediate goal of this work was to develop specimen designs which would be fully compatible with the in-plane biaxial testing systems recently installed at the NASA Glenn Research Center (GRC) (ref. 27).

3. Specimen Designs for Testing Under Monotonic Loading

The focus of initial work was on developing a specimen design suitable for deformation and strength testing under monotonic loading. One requirement here was for a specimen with a relatively large gage area to meet instrumentation needs. A further requirement was to keep the overall specimen thickness to a minimum to keep manufacturing costs within acceptable limits. The approach adopted in developing an initial specimen design was to use the design proposed by Brown & Miller (ref. 18) as a starting point.

Note that it was not possible to use the exact same design in this work because of a number of differences in testing and material requirements. These requirements are outlined in the following along with the results of design and analysis work.

3.1 Initial Design

The first step in the design process was to select overall specimen dimensions. Consideration was given here to a number of test system features and characteristics including:

1. Load capacity of specimen grips, hydraulic actuators, load cells, and load frame.
2. Size envelope available within the load frame for specimen installation and gripping.
3. Gripping arrangement and size restrictions imposed by the hydraulic specimen grips.
4. The size and type of the heating system available for planned elevated temperature testing.
5. Specimen gage area needed to meet strain measurement and other instrumentation needs.

Preliminary design and analysis showed that the overall specimen dimensions best meeting testing requirements were 12 by 12 by 0.500 in. (fig. 3). Note that a relatively large gage area, 5 by 5 in., was selected for the monotonic specimen design as it would allow specimens to be highly instrumented with minimum installation difficulty.

As noted earlier, in-plane biaxial testing requires that the plate specimens be gripped at four locations. The gripping area provided for each specimen grip was 6 by 1.500 in. which meets the size requirements and load transfer requirements of the hydraulic grips available for this work. Inspection of figure 3 will show that the depth of sections available for gripping is 1.800 in. Additional material was provided to avoid gripping the specimen in close proximity to the flexures to avoid adverse interactions between stress concentrations resulting from gripping with those at the ends of the flexures resulting from biaxial loading.

The initial flexure configuration shown in figure 3 resulted from close inspection of the Brown and Miller design. Also, the design was based in part on an early series of stress analyses aimed at checking the load capacity of the design. Specifically, the width and length selected for the flexures was 0.188 and 1.387 in., and the spacing was 0.375 in. in 12 locations and 0.438 in. in the remaining 24 locations. Regarding the thickness of the gage area, consideration was given to the intended application for the advanced metallics of interest in this study. It was anticipated that in aeropropulsion service, the thickness of the plate material would most likely fall in the range 0.050 to 0.100 in. With this in mind, a gage area thickness of 0.100 in. was selected as being at the upper end of the intended use range. For simplicity, it was decided to use a straight taper in transitioning from the 0.500 in. overall thickness to the 0.100 in. gage area thickness (fig. 4). Later in the optimization process, the straight taper was replaced by a radius to minimize stress concentrations in the blend region. The remaining dimensions were selected using “engineering judgment.”

3.2 Stress Analysis Details

The three dimensional model shown in figures 5 and 6 was generated using the MSC/PATRAN computer code (ref. 30). The model consists of 6300 eight-node isoparametric solid brick elements and 9000 nodes. As indicated in figure 5, a relatively fine mesh was introduced through the thickness to capture stress distributions with a reasonable degree of accuracy. Note that only 1/8 of the total specimen

was modeled to keep the size of the finite element model within reasonable limits. This was possible because of the symmetry of the specimen and because of the straightforward nature of the loading conditions applied. Linear elastic stress analyses were conducted using the MARC finite element code, version K5.2 (ref. 31). Analytical runs were conducted on the Cray YMP main frame computer at GRC. Individual runs required about 500 computer processing units (CPU) to complete. Note that the material properties used in this work were handbook values for Inconel 718, and that the results of stress analysis are expressed in the form of von Mises equivalent stress unless otherwise stated.

As noted earlier, the external loadings assumed in the analyses were applied over eight 6 by 1.5 in. areas, including both the top and bottom specimen surfaces. The approach followed was to simulate infinitely stiff grips by constraining all surface nodes within the gripped regions to move 0.005 in. in the loading direction so as to produce a state of equibiaxial tension in the gage area. This value was selected to give von Mises equivalent stress levels of about 50,000 psi at the center of the gage area. Also, the surface nodes within the gripped area were constrained to move 0.0002 in. in the thickness direction to simulate clamping by the hydraulic grips.

3.3 Stress Analysis Results

Results of finite element analyses performed using the above approach are given in figures 7 to 9. Considering overall conditions in the gage area, it can be seen that:

1. The stress distribution is relatively uniform, falling for the most part within the range 43,600 to 48,800 psi.
2. "Through thickness" variations in stress distribution are relatively minor (see figs. 7 and 8).
3. Stress levels are significantly below average in the corner region and are significantly above average at the ends of the center-most flexures.

A more detailed analysis of the results showed that the maximum stress in the gage area occurred at location N (fig. 7) and was about 53,000 psi. These analyses also showed that the minimum stress in the gage area occurred at location P and was about 39,400 psi. Thus, the deviation of stress over the entire gage area was within ±15 percent of the mean at the start of the optimization process.

Considering the balance of the specimen (fig. 9), the maximum stress was found to occur at location D and was 69,700 psi. As expected, a large stress concentration also was found to exist at the corners joining the two sets of flexures, location F in figure 9. Here, the maximum stress was determined to be 64,000 psi. Note that the "hidden regions" in this figure were examined in a similar manner using isometric projections to allow stress concentrations to be quantified throughout the part. These examinations showed that the maximum stress in these regions was 55,000 psi and occurred at location G (fig. 7). Overall, the results summarized above were viewed as being very encouraging and appeared to confirm the effectiveness of the Brown and Miller approach to specimen design. However, it was apparent that additional work was needed to improve the uniformity of stress in the gage area and also to reduce stress concentrations at the ends of the flexures.

3.4 Optimization Method

The optimization method used in achieving these goals focused on two straightforward design requirements.

1. The maximum stress in the specimen should occur within the gage area.
2. The distribution of stress within the gage area should be relatively uniform, for instance, within ±5 percent of the mean.

The optimization process simply involved making systematic changes to the specimen design and repeating stress analysis as necessary until the two design requirements had been met. This process was performed manually since the finite element code available for this work did not include a formal optimization package.

More specifically, the approach followed in developing a fully optimized design involved conducting the work in three stages. Consideration was given first to the thickness transition details. Of primary interest here was whether acceptable specimen performance in terms of stress uniformity in the gage area could be obtained using a single step reduction in specimen thickness. Clearly, this is the preferred approach as it results in a simpler design with low associated machining costs. The design variables of interest during this stage of the process were the gage area thickness and the thickness transition radius. Second, consideration was given to the detailed design of the flexures. Inspection of figure 3 will show that there are a large number of possibilities available with the subject design which can be used to influence the stress distribution in the gage area. These include the number, the size, the spacing and the configuration of the flexures.

Up to this stage of the process, no attempt was made to incorporate blend radii at the ends of the flexures. The goal here was to keep the size of the finite element model within reasonable limits during the early stages of the work. The final stage of the optimization process was to include such radii so as to get a more realistic picture of the stress concentrations at the ends of the flexures. It was anticipated that inclusion of these radii would produce only local effects on the stress distribution and would not have a marked effect on the gage area stress distribution. Clearly, the possibility existed that the above procedure would have to be repeated if less than ideal choices of dimensions and configurations were made at any stage of the optimization process.

3.5 Final Design

As expected, development of a final design using the above process proved to be lengthy and involved over 80 design interactions. Early in the process, it became apparent that the two design goals could not be achieved using the 12 by 12 by 0.500 in. configuration selected at the outset of this work. To correct this situation, it was decided to increase the overall thickness of the specimen to 0.625 in., primarily with the aim of reducing stress levels at the ends of the flexures. Also, it proved necessary to adopt a two-step reduction in gage area thickness. Again, this approach was adopted because it proved impossible to meet the design requirements using the single-step approach. Apart from these differences, the plan was to make minor changes to the flexure design to further improve stress uniformity in the gage area.

The finite element model used in achieving a fully optimized design is shown in figures 10 and 11. Here it can be seen that the configuration of the final design, designated no. 228.1, is similar in overall configuration to the initial design. In addition to the changes noted above, it can be seen that the width of

the center-most flexures was reduced and steps were added to the outermost flexures. The effect of these changes in terms of gage section stress distribution can be seen in figure 12. In this case, stress levels over the major part of the gage area fell within the range 54,000 to 59,200 psi. This increase over values reported earlier resulted from the increase in overall specimen thickness and the "fixed displacement" mode of specimen loading used to simulate biaxial testing. More detailed analysis of the results showed that the maximum stress, 58,300 psi, occurred at the corner and that the minimum stress, 53,000 psi, occurred at the center line. The corresponding deviation is about ±5 percent which means design no. 228.1 meets the design goal regarding stress uniformity in the gage area.

The stress distribution in the flexures is shown in figure 13. Detailed analysis showed that the maximum stress at locations D, E, and F fell in the range of 57,700 to 58,600 psi. The maximum stress in the specimen was found to be 59,500 psi and occurred at location C. This value exceeds the maximum gage section stress by about 2 percent which is a significant improvement over earlier designs. Given this encouraging result, the design study progressed to its final stage and blend radii were incorporated at the ends of the flexures. As noted earlier, the intent here was to refine the finite element model so as to obtain a more meaningful measure of local stresses at these locations.

The approach adopted in modeling these radii is shown in figure 14 for the case of the blend radius at the corner fillet region. About 80 additional elements were used to model the 0.063 in. radius shown. The effect of these radii on the local stress distribution is shown in figure 15. As expected, the local stress distribution in the corner fillet region is modified significantly by the addition of the blend radius. Detailed analysis showed that the maximum stress in this region was 55,800 psi which represents a 4 percent reduction from the earlier value. Also, it can be seen that the maximum stress location was shifted from the corner along the length of the flexure. Further analysis showed that use of larger radii produced a negative result in that stress levels in the flexures were increased over the above value. For this reason, the 0.063 in. radius was selected for use with the subject design.

The above stress values are summarized along with earlier data in table I. These data clearly show the performance gains at the various stages of design and optimization process. It can also be seen that specimen design no. 228.2 meets the design requirements regarding uniformity of gage area stress and location of maximum stress in the part. However, it should be noted that this level of performance is met with little if any margin of conservatism.

Details of specimen design no. 228.2 in final form are given in figures 16 to 18. It can be seen that the optimization process resulted in a number of changes to overall specimen dimensions. Specifically, the effective gage area dimension was reduced to 3.780 by 3.780 in. and the inner corner fillet radii was reduced to 0.575 in. Corresponding changes in the thickness transition details can be seen in figure 17. The final flexure configuration is shown in figure 18 and can be seen to be complex. Inspection of these figures will show that blend radii of 0.063 in. were used at the critical corner locations and also in locations where the width of flexures was "stepped." Also, it can be seen that a blend radius of 0.125 in. was used at the ends of the flexures in a total of 152 locations. The relative merits of this and subsequent specimen designs are discussed later in the paper.

4. Specimen Designs for Testing Under Cyclic Loading

The second design exercise was aimed at developing a specimen suitable for investigating material behavior under cyclic loading. As noted earlier, the types of experiment of interest in this research included low-cyclic fatigue tests and fatigue crack growth tests. One important consideration here is

buckling stability since these experiments involve both tensile and compressive loadings. As a result of preliminary analysis, the gage area was reduced to 2.375 by 2.375 in. to better meet cyclic testing requirements. One advantage of reducing the size of the gage area was that it was possible to incorporate a number of significant design changes at the outset based on experience gained thus far into the design study. These changes are described in the following along with the results of design and analysis work.

4.1 Initial Design

Details of the initial specimen configuration, designated no. 232.1, are given in figures 19 and 20. The overall dimensions chosen as best meeting cyclic testing requirements were 12 by 12 by 0.500 in. Based on experience gained with the earlier designs, a "two-step" reduction in thickness was used to obtain the 2.375 by 2.375 in. gage area as illustrated in figure 20. Here it can be seen that the thickness of the gage area and the intermediate step were 0.080 and 0.150 in., and a single thickness transition radius, 0.500 in., was used throughout. The remaining gage area dimensions for design no. 232.1 were again selected using "engineering judgment."

With regard to specimen gripping, inspection of figure 19 shows that the area available for gripping, 4.125 by 1.500 in., is also reduced from the earlier value. Checkout experiments conducted on the earlier design showed that a gripping area of about 6.0 in^2 met the loading requirements of the planned test programs. This result allowed the width of the material available for gripping to be reduced to 4.125 in. and the specimen configuration to be simplified in the gripped region. A further modification to the gripped regions is the incorporation of sixteen 0.063-in.-wide slots. The goal here was to provide "relief" which would allow localized stresses due to gripping to be distributed more uniformly. Also, the incorporation of slots was expected to be advantageous in minimizing thermal stresses in the gripped region during elevated temperature tests.

One important advantage associated with reducing the gage area is that it allowed the length of the flexures to be increased to 2.000 in. This represents a 40 percent increase over the value used in the earlier design. Inspection of figure 19 will show that the number of flexures used in each loading arm was ten and that the width of individual flexures was 0.188 in. It can also be seen in this figure that blend radii were not included at the ends and intersection points of the flexures. As before, the plan was to incorporate these radii once the optimum flexure configuration had seen established.

The details of the finite element analyses conducted on design no. 232.1 were identical to those described earlier. The three dimensional model shown in figure 21 was generated using PATRAN, and linear elastic stress analyses were conducted using the MARC finite element code. As before, all surface nodes in the gripped regions were constrained to move 0.005 in. in the X and Y directions to produce a state of equibiaxial tension in the gage area. Also, surface nodes in the gripped region were constrained to move 0.0002 in. in the thickness direction to simulate clamping in the hydraulic grips. As in the case of the earlier work, elastic constants used in these analyses were handbook values for Inconel 718.

The results of the finite element analyses are given in figures 22 to 25. As in the case of the earlier designs, the stress distribution over the major part of the gage area is relatively uniform, falling within the range 48,800 psi to 54,000 psi (fig. 23). More detailed analyses showed that the maximum stress, 55,000 psi, occurred at location P and that the minimum stress, 44,500 psi, occurred at location M. Thus, the deviation of stress in the gage area prior to optimization was within ±11 percent of the mean. Considering the balance of the specimen, figures 24 and 25, the maximum stress was found to occur at location D and was about 55,000 psi. The next highest stresses occurred at locations B and C and were

54,800 psi and 54,000 psi. Interestingly, the stress levels at the intersection point of the flexures, location F in figure 24, were relatively low in this particular design and were not viewed as being problematical. Based on these results, the primary focus of the optimization process was on improving the uniformity of stress within the gage area.

4.2 Final Design

The optimization process leading to the final design was relatively straightforward and involved 37 design iterations. In this case, the optimization process consisted of making systematic changes to the design of the flexures and determining the effect of these changes on the stress distribution in the gage area. As noted earlier, the goal was to get the distribution of stress in the gage area within ±5 percent of the mean. The procedure followed was simply to remove material from the flexures until the above target had been achieved. The flexures were treated in sequence starting at the centerline and working out toward the corner between loading arms. In the event, it proved necessary to modify eight of the flexures in each of the four loading arms.

One of the finite element models used in developing a final design is shown in figure 26. This particular design, designated no. 269.1, does not include blend radii at the ends of the flexures. The results of stress analyses performed on this particular design are shown in figures 27 to 30. The stress distribution over the entire gage area falls within the range, 43,600 psi to 48,800 psi. A more detailed analysis showed that the maximum stress, 46,600 psi, occurred at location P and that the minimum stress, 45,000 psi, occurred at location M. In this case, the deviation about the mean was ±2 percent which meets the original design requirement. The stress distribution in the balance of the specimen is shown in figures 29 and 30. The maximum stress in the flexures was found to occur at location D and was 46,975 psi. The next highest stresses were found to occur at locations A, B, and C and fall within the range, 45,375 to 46,500 psi. These results were viewed as being encouraging and the subject flexure configuration was adopted for the final design.

As before, the final stage of the design process was to incorporate blend radii. This procedure was followed and a series of finite element analyses were performed to establish optimum radius values. In summary, best results in terms of uniformity of stress in the gage area and local stress values were obtained using a radius of 0.125 in. at the four corner locations and a 0.063 in. radius in all other locations. One of the finite element models used in establishing this result is shown in figure 31. This particular model contains 9600 eight-node, isoparametric, solid brick elements and 13,300 nodes with three degrees of freedom. Initial results showed that the maximum stresses in the flexures were about the same as those in the gage area. To add a margin of conservatism, the decision was made to reduce the thickness of the gage area from 0.080 to 0.050 in. This necessitated some minor changes to the configuration of the gage area as will be described later in the paper.

Stress analysis results for the modified design, designated 269.2, are shown in figures 32 and 33. The stress distribution in the gage area is relatively uniform, falling within the range 54,000 psi to 59,200 psi. Detailed analysis showed that the maximum stress, 58,800 psi, occurred at location P and that the minimum stress, 54,000 psi, occurred at location M. In this case, the deviation of stress about the mean is about ±5 percent which meets the original design goal. The stress distribution in the flexure region is shown in figures 34 and 35. The maximum stress in this region occurred at locations A and B and was 55,000 psi. The next highest stresses occurred at locations C and D and were 54,500 psi and 53,200 psi. The above stresses are summarized in table II. Here, it can be seen that the ratio of the maximum stress in the flexures over the maximum stress in the gage area is 0.94 for specimen design no. 269.2. Thus, this

particular design met both design requirements regarding stress uniformity in the gage area and location of maximum stress in the specimen.

Details of specimen design no. 269.2 in final form are given in figures 36 and 37. Final dimensions for the gage area were 2.300 by 2.300 in. and the thickness was 0.050 in. The thickness transition details can be seen to be similar to those used earlier with the exception of some minor changes needed to accommodate the 0.050 in. thickness. The final flexure configuration was relatively straight forward and unlike earlier designs, did not involve the use of "steps." The eight outer-most flexures were 0.188 in. wide and the balance were 0.125 in. wide. The four central slots were 0.250 in. wide and the remaining slots were 0.313 in. wide. As noted earlier, the radius used in the corner locations was 0.125 in. and a radius of 0.063 in. was used in all remaining locations. Overall, the final specimen design was thought to be relatively simple and a significant improvement over earlier designs.

5.0 Performance Under General Forms of Biaxial Loading

One limiting feature of the design/optimization work described this far is that it focused entirely on a single form of biaxial loading. This was the special case of equibiaxial tensile loading. One advantage of using this type of loading was that it caused symmetrical stress states to be introduced into the specimens. This simplified the optimization process by effectively reducing the number of variables involved. Regardless of such efforts, the process of developing fully optimized designs remained complex and time consuming. Given this result, it was apparent that major savings in time and effort would be realized if it could be demonstrated that the equibiaxial specimen design could be used without modification to investigate more general forms of biaxial loading. Possible issues to be addressed here included the location of the maximum stress and also the uniformity of stress in the specimen gage area.

5.1 Stress Analysis Details

The specimen configuration selected for further study was specimen no. 269.2, details of which are given in figures 36 and 37. One goal in conducting this work was to maintain a reference state of stress at the center of the specimen gage area so as to allow meaningful comparison of performance under the various loading conditions investigated. The approach adopted in achieving this goal is shown schematically in figure 38. Here it can be seen that a single value of von Mises equivalent stress, 50,000 psi, was used throughout. Further, six stress ratios (θ) in the range ±45° were selected to investigate specimen performance over a single quadrant of biaxial stress space. In the case of isotropic materials, stress states in the remaining quadrants can be inferred from the symmetry of the von Mises ellipse. The components of stress, σ_x and σ_y, corresponding to the six reference conditions were calculated in a straightforward manner using the relationships shown in figure 38 and the results of these calculations are summarized in table III. It remained to establish the grip displacements needed to achieve the reference stress states in planned finite element analyses.

As noted earlier, loading in the subject in-plane biaxial tests is introduced into specimens by means of four hydraulic grips. These grips rigidly constrain the gripped region of the specimen over 1.5 by 4.125 in^2 areas (fig. 19). This was simulated in earlier finite element analyses by constraining all surface nodes in the gripped regions to displace predetermined amounts in the two loading directions. The plan was to use the same general approach in the present investigation. To determine the required grip displacements, it was assumed that stress components at the center of the gage area, σ_x and σ_y, are related to corresponding grip displacements, Δ_x and Δ_y, by the expressions:

$$\Delta_x = K_1\,\sigma_x + K_2\,\sigma_y \tag{1}$$

$$\Delta_y = K_1\,\sigma_y + K_2\,\sigma_x \tag{2}$$

Where K_1 and K_2 are constants.

Since K_1 and K_2 were unknown, it was necessary to conduct a preliminary finite element analysis to effectively calibrate these expressions. The approach was to apply known grip displacements to the model and to calculate the corresponding values of σ_x and σ_y. It was then possible to solve equations (1) and (2) for K_1 and K_2.

Regarding the boundary conditions and loading used in the preliminary analysis, clamping in the rigid grips was simulated as before by constraining surface nodes in the gripped regions to displace the same amount in a given loading direction. Loading was introduced into the finite element model by applying a simulated grip displacement of 0.005 in. in the Y direction. The condition in the transverse direction was "gripped" but free-to-displace in this direction. The value of Δ_x calculated as a result of this loading was –0.0000567 in. and the calculated values of σ_y and σ_x were 52,523 and 2078 psi. These values along with the known value of Δ_y were substituted in the equations (1) and (2) and solved for K_1 and K_2 with the following results:

$$K_1 = 9.5371\times10^{-8}\ \text{(in.)(psi)}^{-1}$$

$$K_2 = -4.85267\times10^{-9}\ \text{(in.)(psi)}^{-1}$$

At this stage, it was possible to solve equations (1) and (2) to determine the required grip displacements. These values are summarized in table III along with the target stress values.

5.2 Stress Analysis Results

The results obtained in subsequent finite element analyses are shown in figures 39 to 44. The first application of these data was to assess the accuracy of the stress analysis approach described above. This simply involved determining the stress components, σ_x and σ_y, at the center of the gage area and comparing them to the target values. The stresses calculated for the six loading cases are summarized in table III along with the earlier data. Overall, the two data sets were found to be in good agreement. This result provided some degree of confidence in the analysis approach adopted.

In the case of experiments investigating strength and fracture behavior, the focus is on the magnitude and the location of the maximum stress in the specimen. The results shown in figures 39 to 44 were analyzed further from this particular viewpoint. In this case, stress states were analyzed along individual axes to identify the magnitude and location of the maximum stress. The three axes considered in these analyses were the x, y, and 45° axes. The results of these analyses are summarized in tables IV to IX. Here, the six components of stress are given for particular locations in the gage area along with the corresponding value of von Mises equivalent stress. This level of detail was provided to facilitate comparison with experimental data to be determined in planned specimen evaluation experiments. Further analysis of these data was performed to establish the magnitude and the location of the maximum value of von Mises equivalent stress in the specimen. The results of these analyses are summarized in table X.

Finally, the same data is shown in graphical form in figures 45 to 50. One goal of presenting the data in this form was to allow more quantitative analysis of the data. These plots were used for example to establish regions in the gage area where stress values fell within ±5 percent of the mean. Determination of such regions of relatively uniform stress was of interest in establishing the optimum location for instrumentation to be used in planned deformation experiments. These results along with data summarized in tables IV to X are discussed in detail in the following section of the paper.

6.0 Discussion

As noted in the introduction, the aim of this research was to develop specimen designs suitable for testing advanced metallic materials under in-plane biaxial loading. A range of experiments was planned in this research including equibiaxial tension tests and equibiaxial fatigue tests. In the case of tests involving monotonic loading, the requirement was for a relatively large gage area which would allow extensive instrumentation with minimum installation difficulty. In addition, it was required that the stress distribution in the gage area should be reasonably uniform, for instance, within ±5 percent of the mean. This was to ensure that in-situ measurements were made in relatively uniform stress/strain fields. Also, it was required that the maximum stress in the specimen should occur within this gage area, preferably with some reasonable margin of conservatism. The aim here was to ensure that failure would be initiated within the gage area where stress/strain conditions are relatively well defined.

The results summarized in table I show that these requirements were met in part during the first optimization exercise. At the start of this process, the deviation of stress within the gage area of design no. 146.1 was ±15 percent. Also, the ratio of the maximum stress in the flexures over the maximum stress in the gage area, termed R ratio in table I, was 1.32. A lengthy optimization process involving over 80 design iterations resulted in the development of a number of improved designs. In the case of specimen design no. 228.2, the deviation in gage area stress was ±5 percent and the R ratio was 1.00. Perhaps the most significant design change made during this process was that a two-step reduction in thickness was used to achieve the 3.875 by 3.875 in. gage area. Also, the thickness of the gage area was reduced to 0.080 in. and the overall thickness of the specimen was increased to 0.625 in. These changes were made reluctantly since the two-step feature adds complexity to the design and leads to increased manufacturing costs.

The most time consuming aspect of the optimization process for design no. 228.2 was in developing an improved flexure configuration. One obvious difficulty here is that there are a large number of variables involved including the number, the size, the spacing, and the shape of the flexures. Another difficulty is that the stress distribution in the gage area is highly sensitive to small changes in the flexure configuration. Details of specimen design no. 228.2, including the final flexure configuration, are given in figures 16 to 18. One feature of this design is that the two outer-most flexures in each loading arm incorporate “steps,” resulting in a relatively complex design.

Turning to the development of the specimen design for cyclic loading, the process in this case was less protracted, primarily because the specimen design selected at the outset featured a number of improvements. These improvements were based on experience gained during the first design exercise and also on the results of evaluation experiments conducted on the earlier specimen design. Regarding the more important design changes, a “two-step” reduction in specimen thickness was used from the outset to obtain the 2.375 by 2.375 in. gage area. One advantage of this approach was that it allowed the length of the flexures to be increased by about 40 percent. Also, the reduced gage area offered improved buckling stability in experiments involving both tensile and compressive loadings. In addition to meeting design

goals regarding uniformity of gage area stress and location of the maximum stress, the aim was to develop a simpler design with improved margins of conservatism.

The results shown in table II indicate that these requirements were met in total during the second design exercise. In the case of specimen design no. 232.1, the deviation of stress within the gage area is ±11 percent and the R ratio is 1.00. Another encouraging result was that the stresses at the four corner locations were low relative to the average stress in the gage area. Given this starting point, the primary focus of the optimization effort was on refining the flexure design to improve the uniformity of stress in the gage area. The final specimen design, designated no. 269.2, was developed after 37 design iterations and met all of the performance requirements. In the case of the design with no blend radii, no. 269.1, the deviation of gage area stress was ±2 percent and the R ratio was 1.00. Clearly this represents a major improvement over earlier designs in regard to the uniformity of the gage area stress.

The final stage of the optimization process was to perform a series of analyses to establish optimum blend radius values. Best results were obtained using a 0.125 in. radius at the four corner locations and a 0.063 in. radius in all other locations. However, analysis showed that the R ratio for this particular configuration was still about 1.00. It was decided, therefore, to reduce the thickness of the gage area to 0.050 in. to achieve some margin of conservatism. Details of the fully optimized design, designated no. 269.2, are given in figures 36 and 37. Stress analysis results for this design are summarized in table II. Here it can be seen that the deviation of gage area stress was ±5 percent and that the R ratio was 0.94. Thus, design no. 269.2 meets the design goals regarding uniformity of gage area stress and location of maximum stress. Further, inspection of figure 36 will show that the flexure configuration did not include “steps,” resulting in a less complicated design. Based on these results, design no. 269.2 appeared to both meet and exceed all requirements for planned experiments involving cyclic loading.

The design work this far was focused on the development of specimens optimized for testing under equibiaxial loading. Given the length and complexity of the optimization process, one obvious question is whether these designs can be used for testing under more general forms of loading without compromising the validity of the results. Further analyses addressing this specific question were performed on specimen design no. 269.2. As described earlier, the goal was to load the specimen so as to produce given reference states of stress in the central elements. Loading was introduced into the specimen using the displacement controlled mode described earlier. Equations relating grip displacement, specimen stiffness, and local stress in the central reference elements were calibrated using the results of finite element analyses. Also as described earlier, these relationships were used to calculate the grip displacements needed to achieve the required stress states. These displacements are summarized in table III along with back-calculated values of stress obtained from finite element analyses conducted to check the accuracy of the procedure. Comparison of the two data sets showed that the finite element results were within ±2 percent of the target values in the case of σ_x and were within ±4 percent in the case of σ_y. Similarly, the values of von Mises equivalent stress were found to be within ±1 percent of the target value. These results were judged to be acceptable for the present comparative study and detailed analyses were conducted investigating the six stress ratios selected for the study.

The results of these analyses are shown in figures 39 to 44 in the form of color plots. The same data for the X, Y and 45° axes are shown in graphical form in figures 45 to 50 and in tabular form in tables IV to X. These data were used first to assess the uniformity of stress over the entire specimen gage area with the results shown in table X. As described earlier, the optimized form of specimen no. 269.2 was developed using equibiaxial tensile loading which corresponds to stress ratio (θ) = +45.0°. Not surprisingly, the stress distribution for this loading case shown in figure 39 is fairly uniform with stress levels falling within ±3 percent of the mean over the entire gage area. Analysis of the data shown in

figures 40 to 44 showed that the deviations of stress are significantly higher for the other stress ratios. More specifically, it can be seen in table X that the deviations for the other five stress ratios fall in the range ±11 to ±19 percent. Clearly, these results do not meet the original design requirement that stresses within the gage area should be uniform within ±5 percent of the mean.

As would be expected, a much improved situation holds for stress distributions within a more limited area at the center of the specimen's gage area. The data shown in figures 45 to 50 were analyzed further to determine the area within which the stress distributions met the original design requirement. This analysis showed that the ±5 percent target was met within a 1.0-in.-diameter circular region at the center of the specimen gage area. This result suggests that the equibiaxial design can be used to investigate deformation behavior under general forms of biaxial loading, provided measurement and observation is limited to this central 1.0-in.-diameter region.

In the case of experiments investigating strength and fracture behavior, the focus is on the magnitude and the location of the maximum stress in the specimen. The results shown in figures 39 to 44 were analyzed further with this particular viewpoint in mind. In this case, stress states were analyzed along individual axes to identify the magnitude and the location of the maximum stress. The results of these analyses for the X, Y and 45° axes are summarized in table X. As expected, the location of the maximum stress is highly dependent on the loading direction or stress ratio. In the case of equibiaxial loading, $\theta = 45.0°$, the maximum stress occurred on the 45.0° axis at the outer perimeter of the gage area. For stress ratios of 0°, 15.0° and 30.0°, the maximum stress location fell on the x-axis, again at the gage section outer perimeter. Interestingly, this pattern of behavior was not repeated for negative stress ratios. For $\theta = -22.5°$ and $-45.0°$, the maximum stress was located at the specimen center. Clearly, the behavior described above complicates interpretation of any strength or fracture tests involving general forms of biaxial loading.

In summary, this study showed that the equibiaxial specimen designs can be used without modification to investigate deformation behavior under general forms of biaxial loading. This is assuming that all measurements and observations are limited to the 1.0-in.-diameter circular region at the specimen center. It was also shown that the equibiaxial design can be used within limits for other forms of testing for stress ratios of +45.0°, 0°, –22.5°, and –45.0°. This recognized that data for $\theta = 0°$ can be generated under uniaxial loading using a simpler test setup. In the case of the negative stress ratios, the location of the maximum stress occurs at the specimen center within a region of uniform specimen thickness. This facilitates measurement of both strain and temperature at the critical location as stress/strain conditions in this region were shown to be relatively uniform. For the remaining stress ratios, $\theta = +15.0°$ and +30.0°, some modifications to the specimen design are necessary. For best results, it appears that specimen designs need to be optimized and tailored to meet the loading requirements of individual research programs.

7.0 Conclusions

The following conclusions were drawn from this design study aimed at developing specimen designs for testing advanced aeropropulsion materials under in-plane biaxial loading.

1. A specimen design was developed for deformation and strength tests with overall dimensions, 12 by 12 by 0.625 in. and gage section dimensions, 3.875 by 3.875 by 0.080 in. The configuration of the specimen was complex, presenting a challenge to manufacture and leading to high manufacturing costs. The design criteria regarding uniformity of stress in the gage area and the

location of the maximum stress in the specimen were both met with this design, but with little, if any, margin of conservatism.

2. A second specimen design was developed for tests involving cyclic loading with overall dimensions, 12 by 12 by 0.500 in., and with gage area dimensions, 2.375 by 2.375 by 0.050 in. Details of this design were simpler in the gripped region and also in the flexure region compared to the earlier design but, overall, the configuration of the specimen remained complex. This design met the various design criteria adopted for the study, but did so with relatively small margins of conservatism.

3. The two specimen designs were optimized for the special case of equibiaxial, tensile loading. Further study showed that the designs can be used without modification to investigate deformation behavior under general forms of biaxial loading, provided measurement and observation is limited to the 1.0-in.-diameter circular region at the specimen center. In the case of experiments investigating strength and fracture, for best results, specimen designs need to be optimized and tailored to meet the loading requirements of individual research programs.

4. The optimization process used in this study involved making systematic changes to the specimen design and repeating stress analysis as necessary until the various design requirements had been met. This process was performed manually since the finite element analysis code available for this work did not include a formal optimization package. This procedure proved to be both time consuming and inefficient as a large number of design iterations were needed to achieve a fully optimized design.

Future Work

The scope of this study will be extended to investigate the feasibility of using simple specimen designs and reusable fixturing for in-plane biaxial tests planned for advanced composite materials. Fiber reinforced composite systems of interest include: polymeric matrix composites; metal and intermetallic matrix composites; and ceramic matrix composites.

References

1. Johnson, A.E.: "Creep Under Complex Stress Systems at Elevated Temperatures," *Proc. Instn. Mech. Engrs.,* Vol. 164, No. 4, 1951, pp. 432–447.
2. Monch, E. and Galster, D.: "A Method for Producing a Defined Uniform Biaxial Tensile Stress Field," *British J. App. Phys.,* Vol. 14, 1963, pp. 810–812.
3. Pascoe, K.J. and DeVillers, J.W.R.: "Low-Cycle Fatigue of Steels Under Biaxial Straining," *Journal of Strain Analysis,* Vol. 2, No. 2, 1967, pp. 117–126.
4. Wilson, I.H. and White, D.J.: "Cruciform Specimens for Biaxial Fatigue Tests: An Investigation Using Finite Element Analysis and Photoelastic Coating Techniques," *J. Strain Analysis,* Vol. 6, 1971, pp. 27–37.
5. Pascoe, K.J.: "Low Cycle Biaxial Fatigue Testing at Elevated Temperatures," *Proc. 3rd Int. Conf Fracture,* Munich, Verein Deutscher Eisenhuttenleute, Dusseldorf, 1973, Vol. 6, paper V–524/A.
6. Hayhurst, D.R.: "A Biaxial-Tension Creep Rupture Testing Machine," *J. Str. Analysis,* Vol. 8, No. 2, 1973, pp. 119–123.

7. Parsons, M.W. and Pascoe, K.J.: "Low Cycle Fatigue Under Biaxial Stress," *Proc. Instn. Mech. Engrs.,* Vol. 188, 1974, 657–671.
8. Morrison, C.J.: "Development of a High Temperature Biaxial Testing Machine," Leicester University report, Vol. 71, No. 13, 1974.
9. Odqvist, F.K.G.: "Mathematical Theory of Creep Rupture," Oxford Mathematical Monographs, Second Edition, Clarendon Press, Oxford, 1974.
10. Weerasooriya, T.: "Fatigue Under Biaxial Loading at 565 °C and Deformation Characteristics of 2¼% Cr-1% Mo Steel," Ph.D. Thesis, University of Cambridge, Jan. 1978.
11. Duggan, M.F.: "An Experimental Evaluation of the Slotted-Tension Shear Test for Composite Materials," *Experimental Mechanics,* 1980, pp. 233–239.
12. Charvat, I.M.H. and Garrett, G.G.: "The Development of Closed Loop Servo-Hydraulic Test System for Direct Stress Monotonic and Cyclic Crack Propagation Studies under Biaxial Loading," *J. Test. Eval.,* Vol. 8, 1980, pp. 9–17.
13. Brown, M.W.: "Low Cycle Fatigue Testing Under Multiaxial Stresses at Elevated Temperature," *Measurement of High Temperature Properties of Materials,* M.S. Loveday, M.F. Day, and B.F. Dyson, Eds., HMSO, 1982, pp. 185–203.
14. Henderson, J. and Dyson, B.F.: "Multiaxial Creep Testing," *Measurement of High Temperature Properties of Materials,* M.S. Loveday, M.F. Day, and B.F. Dyson, Eds., HMSO, 1982, pp. 171–184.
15. Jones, D.L., Poulose, P.K., and Liebowitz, H.: "Effect of Biaxial Loads on the Static and Fatigue Properties of Composite Materials," *Multiaxial Fatigue,* ASTM STP 853, K.J. Miller and M.W. Brown, Eds., American Society for Testing and Materials, Philadelphia, 1985, pp. 413–427.
16. Radon, J.C. and Wachnicki, C.R.: "Biaxial Fatigue of Glass Fiber Reinforced Polyester Resin," *Multiaxial Fatigue,* ASTM STP 853, K.J. Miller and M.W. Brown, Eds., American Society for Testing and Materials, Philadelphia, 1985, pp. 396–412.
17. Found, M.S.: "A Review of the Multiaxial Fatigue Testing of Fiber Reinforced Plastics," *Multiaxial Fatigue,* ASTM STP 853, K.J. Miller and M.W. Brown, Eds., American Society for Testing and Materials, Philadelphia, 1985, pp. 381–395.
18. Brown, M.W., and Miller, K.J.: "Mode I Fatigue Crack Growth Under Biaxial Stress at Room and Elevated Temperature," *Multiaxial Fatigue,* ASTM STP 853, K.J. Miller and M.W. Brown, Eds., American Society for Testing and Materials, Philadelphia, 1985, pp. 135–152.
19. Sakane, M. and Ohnami, M.: "Creep-Fatigue in Biaxial Stress Using Cruciform Specimens," *Third International Conference on Biaxial Multiaxial Fatigue,* Vol. 2, University Stuttgart, Paper No. 46, 1989, pp. 1–18.
20. Susuki, L: "Fatigue Damage of Composite Laminate under Biaxial Loads," *Mechanical Behavior of Materials-VI, Vol.* 2 (ICM 6), Pergamon Press, Oxford, 1991, pp. 543–548.
21. Trautman, K.-H., Doker, H., and Nowack, H.: "Biaxial Testing," *Materials Research and Engineering,* H. Buhl, Ed., Springer Verlag, Berlin, 1992, pp. 308–319.
22. Makinde, A., Thibodeau, L., and Neale, K.W.: "Development of an Apparatus for Biaxial Testing Using Cruciform Specimens," *Experimental Mechanics,* Vol. 32, 1992, pp. 138–144.
23. Demmerle, J. and Boehler, J.P.: "Optimal Design of Biaxial Tensile Cruciform Specimens," *J. of the Mechanics and Physics of Solids*, Vol. 41, No. 1, 1993, pp. 143–181.
24. Boehler, J.P., Demmerle, S., and Koss, S.: "A New Direct Biaxial Testing Machine for Anisotropic Materials," *Experimental Mechanics*, Vol. 34, 1994, pp. 1–9.
25. Wang, J.Z. and Socie, D.F.: "A Biaxial Tension-Compression Test Method for Composite Laminates," *J. of Composites Technology & Research*, Vol. 16, No. 4, Oct. 1994, pp. 336–342.
26. Masumoto, H., and Tanaka, M.: "Ultra High Temperature In-Plane Biaxial Fatigue Testing System with In-Situ Observation," *Ultra High Temperature Mechanical Testing*, R.F. Lohr, and M. Steen, Eds., Woodhead Publishing Limited, Cambridge, 1995, pp. 193–207.

27. Bartolotta, P.A., Ellis, J.R., and Abdul-Aziz, A.: "A Structural Test Facility for In-Plane Biaxial Testing of Advanced Materials," *Multiaxial Fatigue and Deformation Testing Techniques*, ASTM STP1280, S. Kalluri and P.J. Bonacuse, Eds., American Society for Testing and Materials, 1997, pp. 25–42.
28. Trautmann, K.-H., Maldfeld, E., and Nowack, H.: "Crack Propagation in Cruciform IMI 834 Specimens Under Variable Biaxial Loading," *Multiaxial Fatigue and Deformation Testing Techniques*, ASTM STP 1280, S. Kalluri and P.J. Bonacuse, Eds., American Society for Testing and Materials, 1997, pp. 290–309.
29. Dalle Donne, C., and Doker, H.: "Plane Stress Crack Resistance Curves of an Inclined Crack Under Biaxial Loading," *Multiaxial Fatigue and Deformation Testing Techniques*, ASTM STP 1280, S. Kalluri and P.J. Bonacuse, Eds., American Society for Testing and Materials, 1997, pp. 243–263.
30. *MSC/PATRAN Graphics and Finite Element Package, Volumes I and II*, McNeal—Schwendler Corporation, Costa Mesa, California, 1997.
31. *Marc General Purpose Finite Element Analysis Program, Vol. A; User Information Manual, Vol. F; Theoretical Manual*, Marc Analysis Research Corporation, Palo Alto, California, 1996.

TABLE I.—STRESS DISTRIBUTION IN SPECIMEN DESIGNS FOR TESTING UNDER MONOTONIC LOADING

Specimen No. & Type	Gage Area Stress			Max. Stress in Flexures at Location Indicated, psi				Ratio of Maximum Stresses (R)+
	Max., psi	Min., psi	Deviation	C*	D	E	F	
146.1 (no blend radii)	53,000 (N*)	39,400 (P)	±15	--------	69,700	--------	64,000	1.32
228.1 (no blend radii)	58,300 (P)	53.000 (M)	±5	59,500	58,600	57,700	58,100	1.02
228.2 (with blend radii)	57,750 (P)	52,000 (M)	±5	52,500	49,500	57,750	55,800	1.00

Notes: *Reference locations are given in figure 7.
+R = ratio of maximum stress in flexures over maximum stress in gage area.

TABLE II.—STRESS DISTRIBUTION IN SPECIMEN DESIGNS FOR TESTING UNDER CYCLIC LOADING

Specimen No. & Type	Gage Area Stress			Max. Stress in Flexures at Location Indicated, psi				Ratio of Maximum Stresses (R)+
	Max., psi	Min., psi	Deviation	A*	B	C	D	
232.1 (no blend radii)	55,000 (P*)	44,500 (M)	±11	53,000	54,800	54,000	55,000	1.00
269.1 (no blend radii)	46,600 (P)	45,000 (M)	±2	46,500	45,375	45,375	46,975	1.00
269.2 (with blend radii)	58,800 (P)	54,000 (M)	±5	55,000	55,000	54,500	53,200	0.94

Notes: * Reference locations are given in figure 7.
+R = ratio of maximum stress in flexures over maximum stress in gage area.

TABLE III.—GLOBAL DISPLACEMENTS (Δ_X AND Δ_Y) GIVING REQUIRED STRESS RATIO (θ) AND VON MISES EQUIVALENT STRESS ($\bar{\sigma}$) IN CENTRAL REFERENCE ELEMENTS

Stress Ratio, θ	Calculated Values				Finite Element Results		
	σ_x, psi	σ_y, psi	Δ_x, in.	Δ_y, in.	σ_x, psi	σ_y, psi	$\bar{\sigma}$, psi
45.0	50,000	50,000	0.004526	0.004526	49,929	50,089	50,011
30.0	57,506	33,201	0.005324	0.002887	57,501	33,085	49,978
15.0	55,767	14,943	0.005246	0.001155	56,259	14,644	50,542
0.0	50,000	0	0.004768	-0.000243	49,790	-601	50,084
-22.5	39,705	-16,446	0.003867	-0.001761	39,474	-16,929	50,136
-45.0	28,868	-28,868	0.002893	-0.002893	28,392	-29,883	50,473

TABLE IV.—STRESS DISTRIBUTION IN SPECIMEN NO. 269.2: STRESS RATIO θ = 45.0°

Location	Element No.	Coordinates x	y	z	Stress Component, psi σ_{xx}	σ_{yy}	σ_{zz}	σ_{xy}	σ_{yz}	σ_{xz}	Von Mises Equiv. Stress, psi
Stress distribution along center line in Y-direction											
Uniform Gage Area	9321	0.058	0.139	0.016	49929	50089	-1	-83	1	-3	50011
	9320	0.058	0.300	0.016	49559	50453	19	-179	-1	-2	49994
	9319	0.058	0.462	0.016	48921	51081	22	-279	2	-4	50017
	9317	0.061	0.784	0.016	46808	53166	29	-504	26	-4	50270
	9316	0.063	0.946	0.016	45287	54641	-66	-651	-94	1	50698
	9315	0.066	1.107	0.016	43576	56477	325	-828	321	-7	50972
Thickness Transition	9136	0.068	1.211	0.017	41219	52197	1243	-868	3047	-48	46802
	9135	0.068	1.259	0.022	38142	41158	1699	-737	5289	-93	39155
	9134	0.068	1.306	0.030	35248	30520	1325	-620	5469	-84	33221
	9133	0.068	1.352	0.041	32940	22557	-334	-540	3814	-59	30259
Stress distribution along center line in X-direction											
Uniform Gage Area	9077	0.139	0.058	0.016	50091	49927	-1	-83	-3	1	50011
	9070	0.300	0.058	0.016	50456	49557	19	-179	-2	-1	49994
	9063	0.462	0.058	0.016	51083	48919	22	-279	-4	2	50017
	9056	0.623	0.059	0.016	51982	48002	20	-385	-4	-7	50096
	9049	0.784	0.061	0.016	53167	46807	29	-504	-4	26	50271
	9039	1.107	0.066	0.016	56479	43575	325	-827	-7	321	50974
Thickness Transition	8866	1.211	0.068	0.017	52199	41218	1243	-868	-48	3047	46803
	8862	1.259	0.068	0.022	41159	38140	1699	-737	-93	5289	39156
	8858	1.306	0.068	0.030	30521	35247	1325	-619	-84	5470	33221
	8854	1.352	0.068	0.041	22557	32939	-335	-540	-59	3814	30259
Stress distribution along 45° diagonal											
Uniform Gage Area	9373	0.174	0.247	0.022	49862	50164	-25	-445	3	-2	50045
	9380	0.290	0.355	0.022	49813	50228	-32	-1062	5	-6	50088
	9387	0.406	0.464	0.022	49775	50279	-40	-1946	7	-6	50184
	9394	0.522	0.576	0.022	49741	50325	-50	-3101	9	-10	50375
	9399	0.638	0.688	0.022	49701	50359	-42	-4511	11	-7	50686
	9404	0.754	0.802	0.022	49623	50375	-109	-6108	10	-15	51221
	9656	0.844	0.888	0.022	49739	50440	-90	-7362	-2	-2	51779
	9655	0.906	0.945	0.022	49826	50420	-26	-8255	25	6	52151
	9654	0.968	1.003	0.022	49814	50307	-70	-9126	-90	-86	52566
	9653	1.029	1.063	0.022	50067	50420	134	-9719	334	274	52872
Thickness Transition	9584	1.075	1.112	0.024	48244	48003	809	-11200	2483	2021	51462
	9583	1.107	1.148	0.031	43197	41802	1247	-13692	4197	3419	48522
	9582	1.138	1.183	0.042	38168	36046	2094	15306	4577	3649	45125
	9581	1.168	1.218	0.057	32091	29639	480	-16383	2780	2159	42154

TABLE V.—STRESS DISTRIBUTION IN SPECIMEN NO. 269.2: STRESS RATIO θ = 30.0°

Location	Element No.	Coordinates x	y	z	Stress Component, psi σ_{xx}	σ_{yy}	σ_{zz}	σ_{xy}	σ_{yz}	σ_{xz}	Von Mises Equiv. Stress, psi
Stress distribution along center line in Y-direction											
Uniform Gage Area	9321	0.058	0.139	0.016	57479	33084	9	-80	1	-3	49960
	9320	0.058	0.300	0.016	56951	33427	31	-163	-0.73	-3	49542
	9319	0.058	0.462	0.016	56050	34001	35	-254	1	-5	48878
	9317	0.061	0.784	0.016	53070	35914	38.22	-468	18	-5	46880
	9316	0.063	0.946	0.016	50932	37287	-42	-614	-66	-0.49	45723
	9315	0.066	1.107	0.016	48426	39013	250	-790	225	-7.18	44258
Thickness Transition	9136	0.068	1.211	0.017	45846	36356	892	-829	2120	-46	41250
	9135	0.068	1.259	0.022	43276	28795	1186	-695	3707	-89	37614
	9134	0.068	1.309	0.030	40894	21446	930	-571	3844	-87	35264
	9133	0.068	1.352	0.041	38964	15926	-244	-483	2688	-65	34467
Stress distribution along center line in X-direction											
Uniform Gage Area	9077	0.139	0.058	0.016	57649	32961	-11	-70	-2	1	50107
	9070	0.300	0.058	0.016	57966	32819	4	-161	-0.87	-0.87	50344
	9063	0.462	0.058	0.016	58529	32564	5	-251	-2	2	50792
	9056	0.623	0.059	0.016	59336	32194	3	-343	-2	-7	51449
	9049	0.784	0.061	0.016	60394	31717	14	-444	-3	28	52318
	9044	0.946	0.063	0.016	61693	31099	-77	-565	2	-104	53506
	9039	1.107	0.066	0.016	63292	30505	338	-709	-6	356	54557
Thickness Transition	8866	1.211	0.068	0.017	58195	28816	1360	-743	-40	3400	49633
	8862	1.259	0.068	0.022	45760	25811	1891	-640	-79	5874	39404
	8858	1.306	0.068	0.030	33836	22953	1471	-552	-64	6064	30414
	8854	1.352	0.068	0.041	24934	20702	-362	-496	-41	4221	24634
Stress distribution along 45° diagonal											
Uniform Gage Area	9373	0.174	0.247	0.022	57307	33230	-17	-410	3	-1	49861
	9380	0.29	0.355	0.022	57098	33426	-22	-969	5	-5	49737
	9387	0.406	0.464	0.022	56841	33673	-29	-1771	6	-5	49630
	9394	0.522	0.576	0.022	56535	33972	-38	-2821	8	-9	49572
	9399	0.638	0.688	0.022	56163	34322	-25	-4098	10	-5	49575
	9404	0.754	0.802	0.022	55634	34646	-130	-5499	9	-15	49707
	9656	0.844	0.888	0.022	55555	34978	-98	-6663	1	0.22	50089
	9655	0.906	0.945	0.022	55481	35156	-26	-7480	18	8	50338
	9654	0.968	1.003	0.022	55328	35214	-72	-8271	-58	-96	50644
	9653	1.029	1.063	0.022	55565	35372	116	-8837	215	323	50968
Thickness Transition	9584	1.075	1.112	0.024	53207	34053	706	-10242	1637	2361	49590
	9583	1.107	1.148	0.031	47070	30351	1095	-12570	2734	4047	46594
	9582	1.138	1.183	0.042	41196	26715	1849	-14051	2858	4508	43210
	9581	1.168	1.218	0.057	34087	22378	360	-14911	1632	2805	39805

TABLE VI.—STRESS DISTRIBUTION IN SPECIMEN NO. 269.2: STRESS RATIO θ = 15.0°

Location	Element No.	Coordinates x	y	z	Stress Component, psi σ_{xx}	σ_{yy}	σ_{zz}	σ_{xy}	σ_{yz}	σ_{xz}	Von Mises Equiv. Stress, psi
Stress distribution along center line in Y-direction											
Uniform Gage Area	9321	0.058	0.139	0.016	56259	14645	16	-66	0.9	-3	50542
	9320	0.058	0.300	0.016	55672	14923	36	-127	-0.51	-4	49888
	9319	0.058	0.462	0.016	54677	15374	41	-199	1	-5	48812
	9317	0.061	0.784	0.016	51386	16882	41	-375	10	-5	45341
	9316	0.063	0.946	0.016	49027	17986	-18	-501	-35	-1	42983
	9315	0.066	1.107	0.016	46201	19390	156	-653	117	-6	40077
Thickness Transition	9136	0.068	1.211	0.017	43780	18429	483	-685	1071	-39	37752
	9135	0.068	1.259	0.022	41971	14747	605	-567	1906	-74	36584
	9134	0.068	1.306	0.030	40328	11098	479	-454	1989	-79	35919
	9133	0.068	1.352	0.041	38968	8326	-137	-371	1400	-62	35727
Stress distribution along center line in X-direction											
Uniform Gage Area	9077	0.139	0.058	0.016	56412	14570	-18	-50	-0.84	1	50734
	9070	0.300	0.058	0.016	56646	14637	-9	-124	0.5	-0.74	50937
	9063	0.462	0.058	0.016	57077	14735	-10	-193	-0.13	2	51329
	9056	0.623	0.059	0.016	57695	14869	-12	-261	0.07	-7	51893
	9049	0.784	0.061	0.016	58499	15053	0.13	-333	-0.8	27	52616
	9044	0.946	0.063	0.016	59470	15270	-76	-414	2	-98	53553
	9039	1.107	0.066	0.016	60646	15687	304	-509	-4	338	54322
Thickness Transition	8866	1.211	0.068	0.017	55527	14778	1278	-533	-28	3246	49280
	8862	1.259	0.068	0.022	43562	12228	1802	-467	-56	5586	38887
	8858	1.306	0.068	0.030	32135	9771	1398	-415	-38	5759	29286
	8854	1.352	0.068	0.041	23623	7858	-337	-387	-21	4002	22250
Stress distribution along 45° diagonal											
Uniform Gage Area	9373	0.174	0.247	0.022	56023	14830	-9	-324	2	-0.3	50286
	9380	0.29	0.355	0.022	55711	15108	-10	-759	3	-4	49929
	9387	0.406	0.464	0.022	55310	15482	-17	-1383	5	-4	49495
	9394	0.522	0.576	0.022	54822	15948	-24	-2202	6	-4	49010
	9399	0.638	0.688	0.022	54230	16509	-8	-3195	8	-3	48473
	9404	0.754	0.802	0.022	53407	17041	-129	-4245	7	-13	47919
	9656	0.844	0.888	0.022	53184	17546	-91	-5179	4	2	47857
	9655	0.906	0.945	0.022	52991	17861	-23	-5824	10	9	47792
	9654	0.968	1.003	0.022	52750	18049	-65	-6444	-23	-92	47807
	9653	1.029	1.063	0.022	52951	18220	86	-6914	88	323	48051
Thickness Transition	9584	1.075	1.112	0.024	50455	17983	529	-8075	720	2342	46274
	9583	1.107	1.148	0.031	44202	16844	827	-9972	1160	4051	42373
	9582	1.138	1.183	0.042	38384	15447	1406	-11156	1054	4646	38571
	9581	1.168	1.218	0.057	31333	13400	213	-11729	463	2983	34310

TABLE VII.—STRESS DISTRIBUTION IN SPECIMEN NO. 269.2: STRESS RATIO θ = 0.0°

Location	Element No.	Coordinates x	y	z	Stress Component, psi σ_{xx}	σ_{yy}	σ_{zz}	σ_{xy}	σ_{yz}	σ_{xz}	Von Mises Equiv. Stress, psi
Stress distribution along center line in Y-direction											
Uniform Gage Area	9321	0.058	0.139	0.016	49790	-601	20	-51	0.63	-3	50084
	9320	0.058	0.300	0.016	49211	-395	37	-90	-0.3	-4	49392
	9319	0.058	0.462	0.016	48231	-74	42	-141	0.3	-5	48249
	9317	0.061	0.784	0.016	44999	1002	39	-273	3	-5	44490
	9316	0.063	0.946	0.016	42687	1805	3	-371	-8	-2	41819
	9315	0.066	1.107	0.016	39878	2840	70	-491	24	-5	38511
Thickness Transition	9136	0.068	1.211	0.017	37800	3244	130	-515	184	-30	36231
	9135	0.068	1.259	0.022	36733	2820	112	-419	376	-56	35362
	9134	0.068	1.306	0.030	35798	2289	96	-325	410	-65	34672
	9133	0.068	1.352	0.041	34992	1842	-44	-252	302	-53	34141
Stress distribution along center line in X-direction											
Uniform Gage Area	9077	0.139	0.058	0.016	50068	-211	-17	-77	1.2	-0.57	50197
	9070	0.300	0.058	0.016	50070	-418	-18	-86	1.4	-0.6	50290
	9063	0.462	0.058	0.016	50368	-68	-20	-134	1	1	50412
	9056	0.623	0.059	0.016	50794	427	-22	-179	1	-6	50594
	9049	0.784	0.061	0.016	51346	1084	-10	-224	0.62	23	50820
	9044	0.946	0.063	0.016	51997	1897	-68	-270	2.7	-84	51114
	9039	1.107	0.066	0.016	52770	3020	250	-324	-2	292	51199
Thickness Transition	8866	1.211	0.068	0.017	48153	2778	1094	-340	-17	2816	46527
	8862	1.259	0.068	0.022	37707	815	1561	-307	-35	4832	37483
	8858	1.306	0.068	0.030	27763	-1099	1209	-286	-17	4976	29095
	8854	1.352	0.068	0.041	20369	-2566	-286	-280	-5	3454	22721
Stress distribution along 45° diagonal											
Uniform Gage Area	9373	0.174	0.247	0.022	49528	-403	-1	-234	1	0.4	49733
	9380	0.29	0.355	0.022	49165	-88	-1	-539	2	-3	49220
	9387	0.406	0.464	0.022	48690	349	-6	-977	3	-3	48551
	9394	0.522	0.576	0.022	48106	902	-11	-1553	4	-6	47746
	9399	0.638	0.688	0.022	47395	1574	6	-2247	5	-1	46791
	9404	0.754	0.802	0.022	46415	2219	-118	-2940	5	-10	45699
	9656	0.844	0.888	0.022	46094	2813	-78	-3615	5	3	45233
	9655	0.906	0.945	0.022	45821	3206	-18	-4072	3	9	44874
	9654	0.968	1.003	0.022	45525	3479	-53	-4505	5	-79	44606
	9653	1.029	1.063	0.022	45664	3651	54	-4856	-15	289	44725
Thickness Transition	9584	1.075	1.112	0.024	43312	4250	343	-5715	-36	2087	42499
	9583	1.107	1.148	0.031	37607	5134	543	-7091	-129	3637	37625
	9582	1.138	1.183	0.042	32420	5544	933	-7924	-395	4270	33341
	9581	1.168	1.218	0.057	26128	5405	83	-8216	-453	2809	28266

TABLE VIII.— STRESS DISTRIBUTION IN SPECIMEN NO. 269.2: STRESS RATIO θ = -22.5°

Location	Element No.	Coordinates x	y	z	Stress Component, psi σ_{xx}	σ_{yy}	σ_{zz}	σ_{xy}	σ_{yz}	σ_{xz}	Von Mises Equiv. Stress, psi
Stress distribution along center line in Y-direction											
Uniform Gage Area	9321	0.050	0.139	0.016	39334	-17311	23	-29	0.3	-2	50272
	9320	0.058	0.300	0.016	38806	-17200	35	-42	-0.04	-3	49684
	9319	0.058	0.462	0.016	37918	-17048	40	-66	-0.26	-4	48725
	9317	0.061	0.784	0.016	34989	-16532	34	-139	-6	-4	45559
	9316	0.063	0.946	0.016	32898	-16120	25	-201	22	-2	43271
	9315	0.066	1.107	0.016	30312	-15567	-29	-276	-80	-3	40423
Thickness Transition	9136	0.068	1.211	0.017	28761	-13692	-266	-290	-805	-18	37620
	9135	0.068	1.259	0.022	28584	-10502	-439	-226	-1335	-32	35234
	9134	0.068	1.306	0.030	28495	-7565	-332	-159	-1356	-45	33131
	9133	0.068	1.352	0.041	28357	-5423	62	-104	-927	-40	31445
Stress distribution along center line in X-direction											
Uniform Gage Area	9077	0.139	0.058	0.016	39423	-17293	-23	-7	1	0.27	50354
	9070	0.300	0.058	0.016	39474	-16929	-27	-37	2	-0.35	50136
	9063	0.462	0.058	0.016	39599	-16323	-30	-57	3	1	49816
	9056	0.623	0.059	0.016	39780	-15463	-31	-73	3	-4	49371
	9049	0.784	0.061	0.016	40006	-14329	-21	-84	2	17	48783
	9044	0.946	0.063	0.016	40246	-12910	-54	-87	3	-63	48040
	9039	1.107	0.066	0.016	40505	-11081	173	-89	-0.09	221	46987
Thickness Transition	8866	1.211	0.068	0.017	36742	-10571	815	-94	-3	2151	42952
	8862	1.259	0.068	0.022	28677	-11753	1189	-100	-9	3670	36328
	8858	1.306	0.068	0.030	21043	-12942	917	-115	8	3771	30315
	8854	1.352	0.068	0.041	15384	-13823	-210	-135	14	2612	25732
Stress distribution along 45° diagonal											
Uniform Gage Area	9373	0.174	0.247	0.022	39061	-17113	7	-114	0.02	1	49871
	9380	0.29	0.355	0.022	38671	-16781	9	-252	0.75	-1	49255
	9387	0.406	0.464	0.022	38149	-16307	6	-451	1	-0.72	48416
	9394	0.522	0.576	0.022	37505	-15701	4	-714	2	-3	47369
	9399	0.638	0.688	0.022	36720	-14957	21	-1026	2	1	46092
	9404	0.754	0.802	0.022	35645	-14239	-96	-1273	2	-6	44590
	9656	0.844	0.888	0.022	35246	-13593	-58	-1615	6	4	43766
	9655	0.906	0.945	0.022	34911	-13146	-12	-1832	-5	8	43138
	9654	0.968	1.003	0.022	34582	-12800	-36	-2029	36	-61	42610
	9653	1.029	1.063	0.022	34654	-12645	16	-2226	-128	233	42590
Thickness Transition	9584	1.075	1.112	0.024	32618	-11170	116	-2700	-865	1672	39803
	9583	1.107	1.148	0.031	27887	-8117	195	-3417	-1539	2949	33683
	9582	1.138	1.183	0.042	23733	-5745	352	-3816	-1964	3583	28644
	9581	1.168	1.218	0.057	18685	-3773	-66	-3786	-1433	2438	22476

TABLE IX.—STRESS DISTRIBUTION IN SPECIMEN NO. 269.2: STRESS RATIO θ = -45.0°

Location	Element No.	Coordinates x	y	z	Stress Component, psi σ_{xx}	σ_{yy}	σ_{zz}	σ_{xy}	σ_{yz}	σ_{xz}	Von Mises Equiv. Stress, psi
Stress distribution along center line in Y-direction											
Uniform Gage Area	9321	0.050	0.139	0.016	28340	-29941	24	-10	-0.011	-1.51	50479
	9320	0.058	0.300	0.016	27887	-29915	31	0.5	0.17	-2.95	50069
	9319	0.058	0.462	0.016	27128	-29911	36	-0.2	-0.7	-3.5	49419
	9317	0.061	0.784	0.016	24629	-29886	28	-21	-12	-3	47287
	9316	0.063	0.946	0.016	22847	-29819	42	-49	45	-2.7	45750
	9315	0.066	1.107	0.016	20603	-29696	-109	-84	-159	-1.5	43791
Thickness Transition	9136	0.068	1.211	0.017	19579	-26731	-575	-88	-1567	-6.6	40321
	9135	0.068	1.259	0.022	20143	-20774	-863	-54	-2654	-10.7	35742
	9134	0.068	1.306	0.030	20753	-15176	-663	-13	-2720	-26	31663
	9133	0.068	1.352	0.041	21171	-11043	145	24	-1878	-27	28524
Stress distribution along center line in X-direction											
Uniform Gage Area	9077	0.139	0.058	0.016	28392	-29883	-24	13	1.59	-0.03	50473
	9063	0.462	0.058	0.016	28333	-28641	-36	8	3.58	0.65	49342
	9070	0.300	0.058	0.016	28356	-29419	-32	5	3	-0.14	50038
	9056	0.623	0.059	0.016	28301	-27535	-37	18	3.7	-2.86	48358
	9049	0.784	0.061	0.016	28246	-26079	-29	36	3.28	11.35	47062
	9044	0.946	0.063	0.016	28136	-24253	-40	68	2.72	-42.45	45416
	9039	1.107	0.066	0.016	27957	-21956	99	108	1.6	149.7	43329
Thickness Transition	8866	1.211	0.068	0.017	25125	-20861	537	114	8	1473	39950
	8862	1.259	0.068	0.022	19509	-21331	811	76	13	2491.5	35677
	8858	1.306	0.068	0.030	14238	-21852	622	32	29	2551.9	31879
	8854	1.352	0.068	0.041	10350	-22198	-134	-8	29	1760.9	28946
Stress distribution along 45° diagonal											
Uniform Gage Area	9373	0.174	0.247	0.022	28076	-29756	13	-10	-0.81	1.72	50092
	9380	0.29	0.355	0.022	27686	-29429	17	-2	-0.51	-0.16	49473
	9387	0.406	0.464	0.022	27159	-28954	16	7	-0.59	0.8	48607
	9394	0.522	0.576	0.022	26505	-28342	16	17	-0.5	-0.58	47512
	9399	0.638	0.688	0.022	25707	-27586	2	39	-0.18	2.6	46169
	9404	0.754	0.802	0.022	24621	-26852	-72	171	0.02	-3	44595
	9656	0.844	0.888	0.022	24183	-26203	-37	123	7	5	43649
	9655	0.906	0.945	0.022	23817	-25738	-6	116	-11	7	42928
	9654	0.968	1.003	0.022	23481	-25356	-20	125	59	-41	42306
	9653	1.029	1.063	0.022	23494	-25224	-16	66	-213	173	42206
Thickness Transition	9584	1.075	1.112	0.024	21843	-23121	-77	-61	-1492	1230	39104
	9583	1.107	1.148	0.031	18203	-18479	-101	-195	-2600	2203	32314
	9582	1.138	1.183	0.042	15150	-14645	-145	-214	-3129	2799	26818
	9581	1.168	1.218	0.057	11433	-11063	-184	78	-2147	1983	20210

TABLE X.—SUMMARY OF STRESS STATES IN GAGE AREA FOR GENERAL FORMS OF BIAXIAL LOADING

Stress ratio, θ	Overall Variation of Stress in Gage Area		Stress States Along Individual Axes						Maximum Overall Stress and Location
			X-Axis		Y-Axis		45°-Axis		
	Average, ksi	Deviation, percent	Maximum, ksi	Average, ksi	Maximum, ksi	Average, ksi	Maximum, ksi	Average, ksi	
45.0	51.2	±3	51.0	50.2	51.0	50.3	52.9	51.2	52.9 ksi at OP on 45° axis
30.0	49.8	±11	54.6	51.9	50.0	47.6	51.0	50.0	54.6 ksi at OP on X axis
15.0	49.1	±18	54.3	52.2	50.5	46.3	50.3	48.7	54.3 ksi at OP on X axis
0	47.6	±19	51.2	50.7	50.1	45.4	49.7	46.7	51.2 ksi at OP on X axis
-22.5	47.1	±14	50.4	49.1	50.3	46.3	49.9	45.8	50.4 ksi at center of gage area
-45.0	47.1	±12	50.5	47.7	50.5	47.8	50.1	45.7	50.5 ksi at center of gage area

Note: OP indicates outer perimeter of gage area

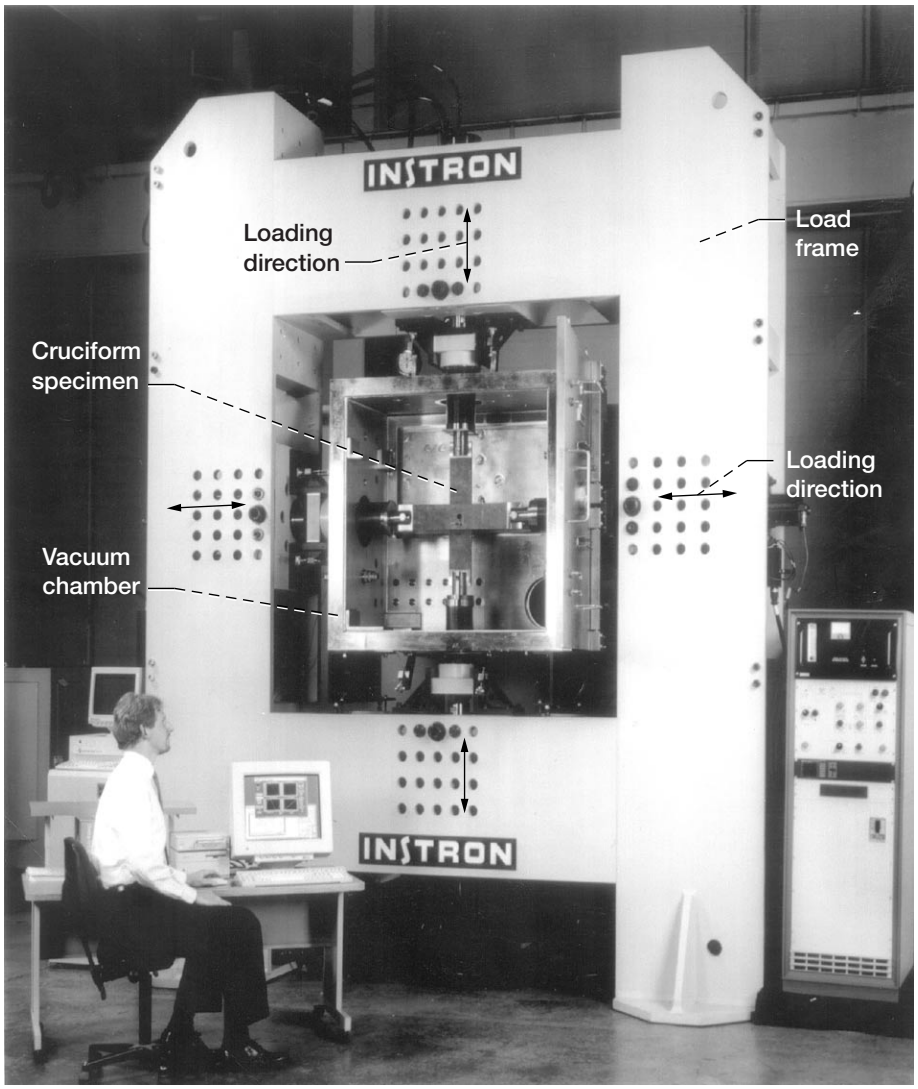

Figure 1.—In plane biaxial test system.

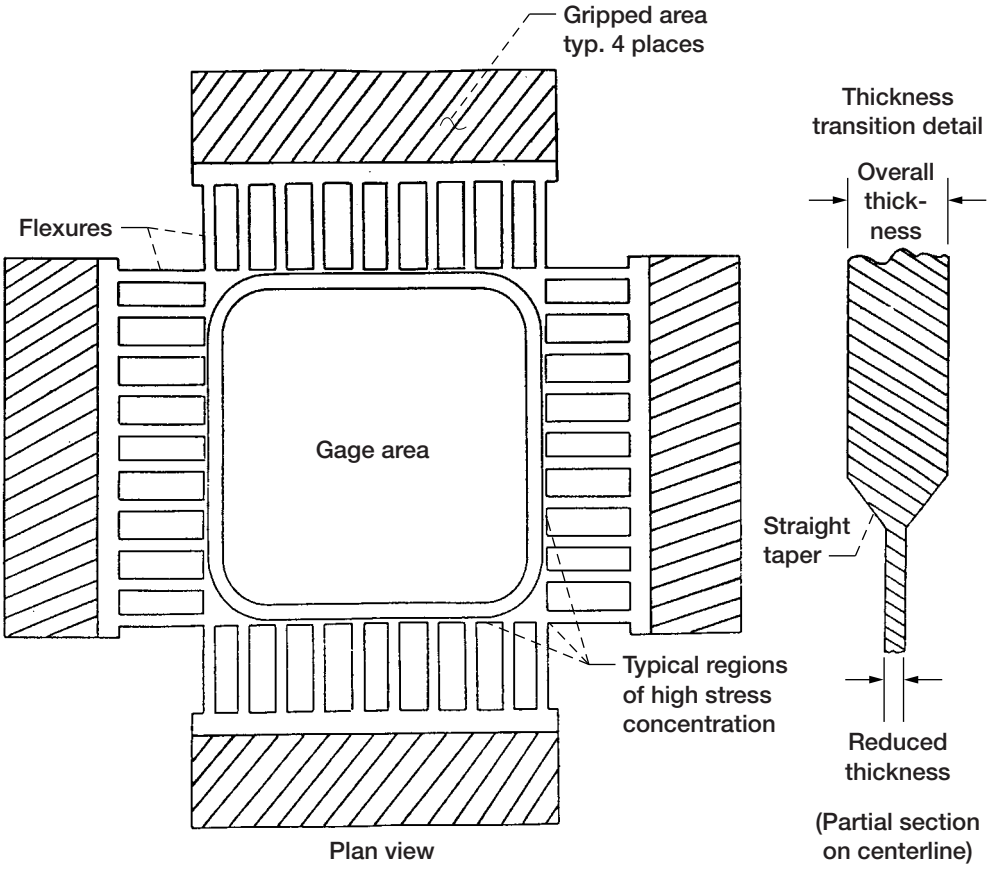

Figure 2.—In-plane biaxial test specimen (ref. 18).

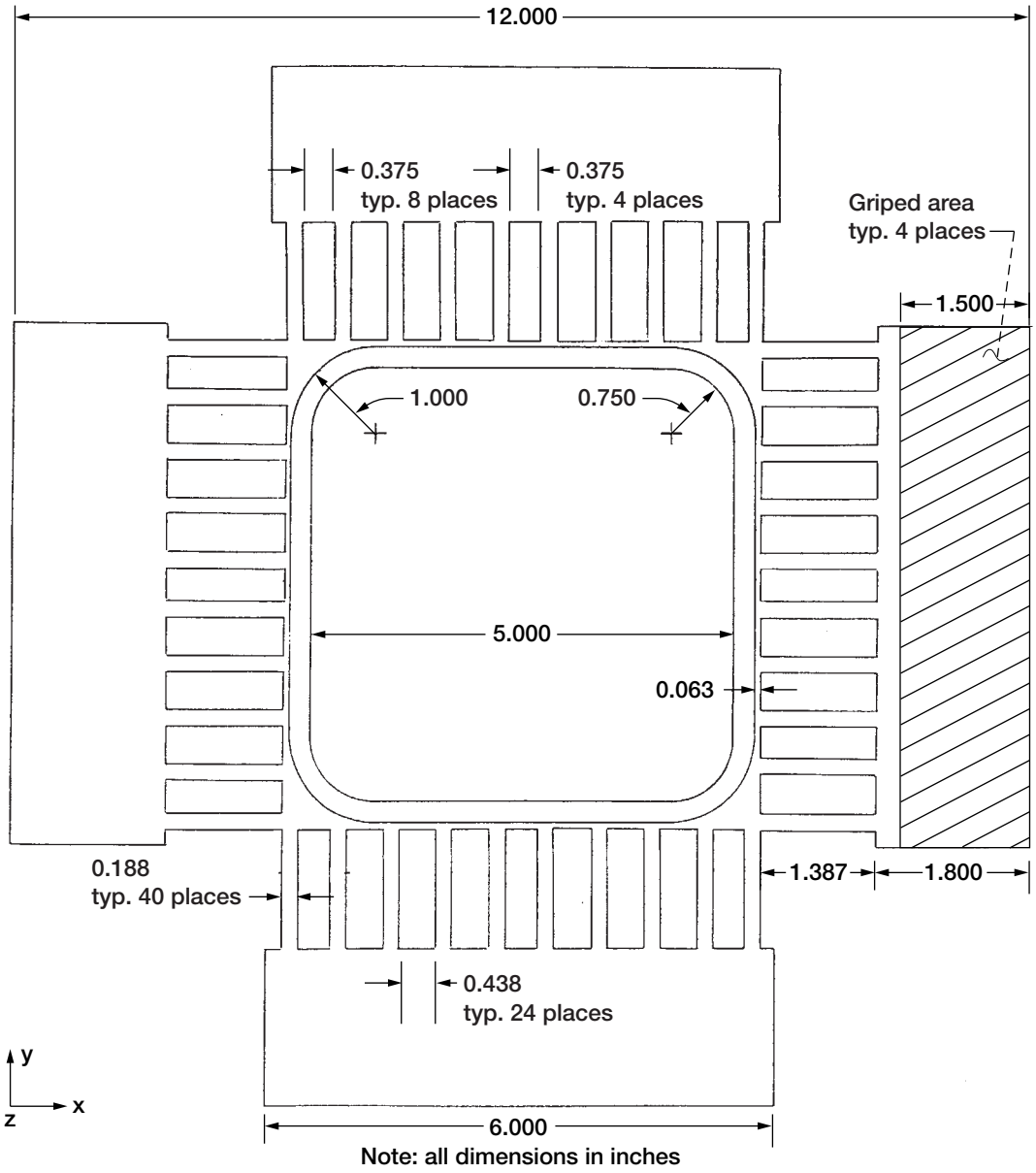

Figure 3.—Specimen design 146.1: plan view.

Partial section on centerline
Note: all dimensions in inches

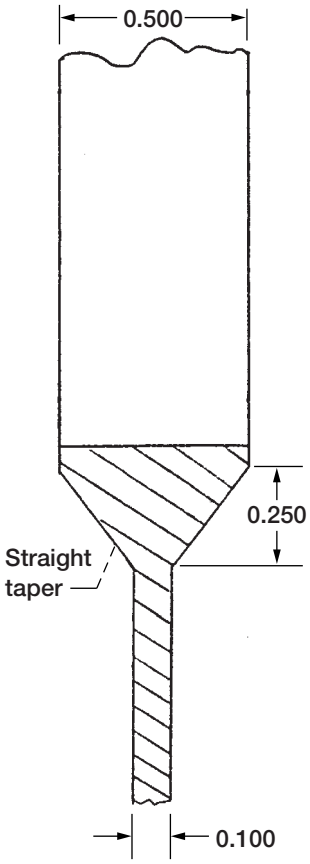

Figure 4.—Specimen design 146.1: Thickness transition.

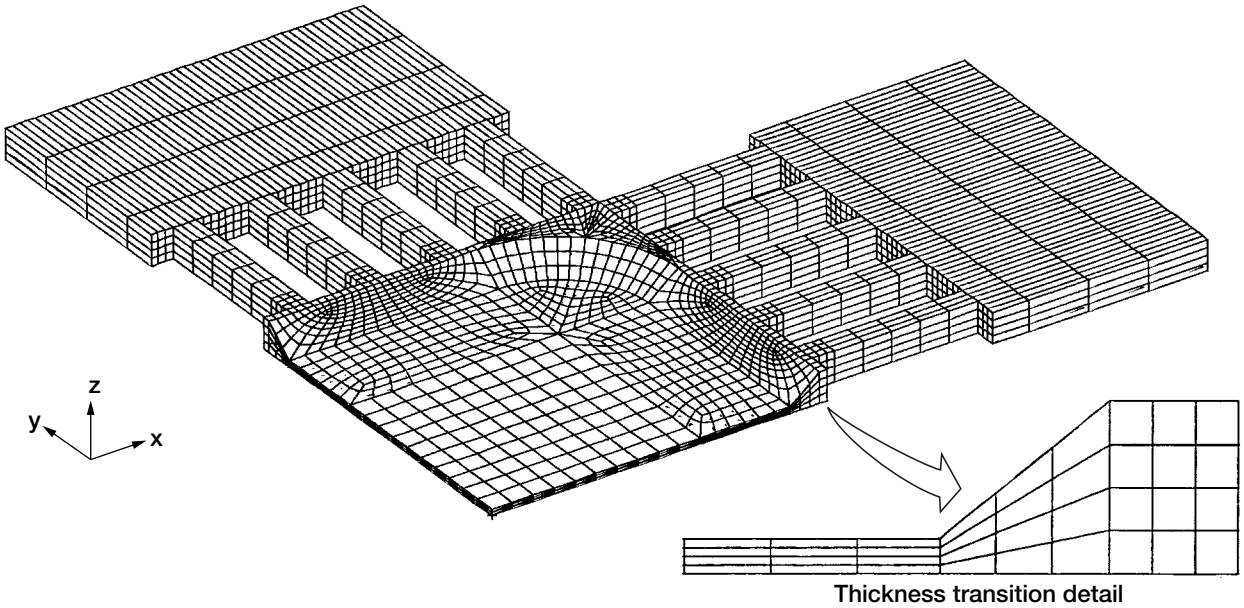

Figure 5.—Finite element model of specimen design 146.1: isometric view.

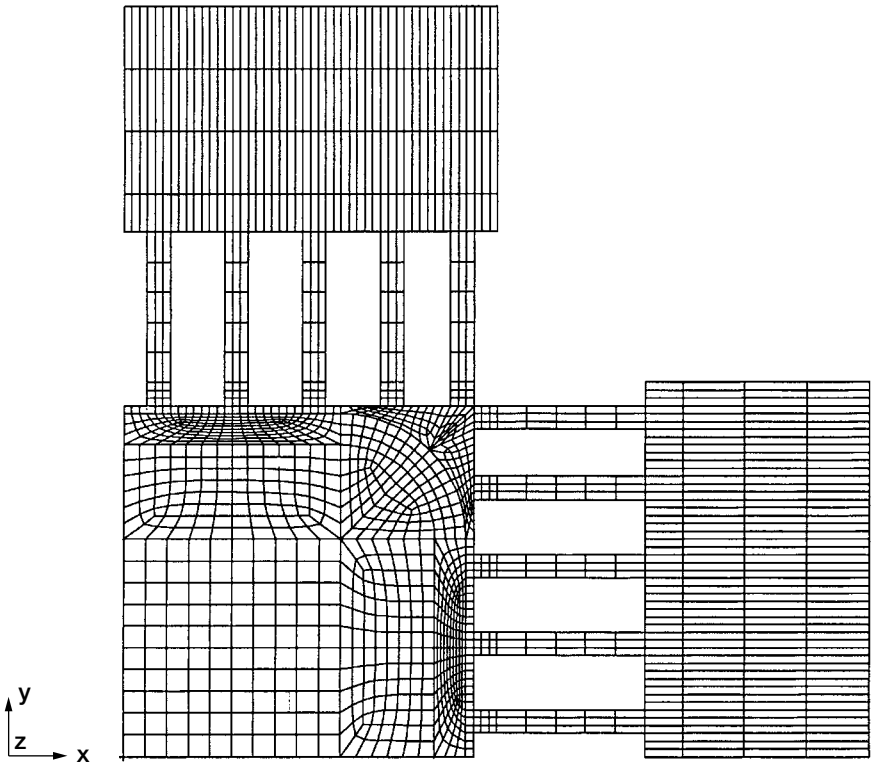

Figure 6.—Finite element model of specimen design 146.1: plan view.

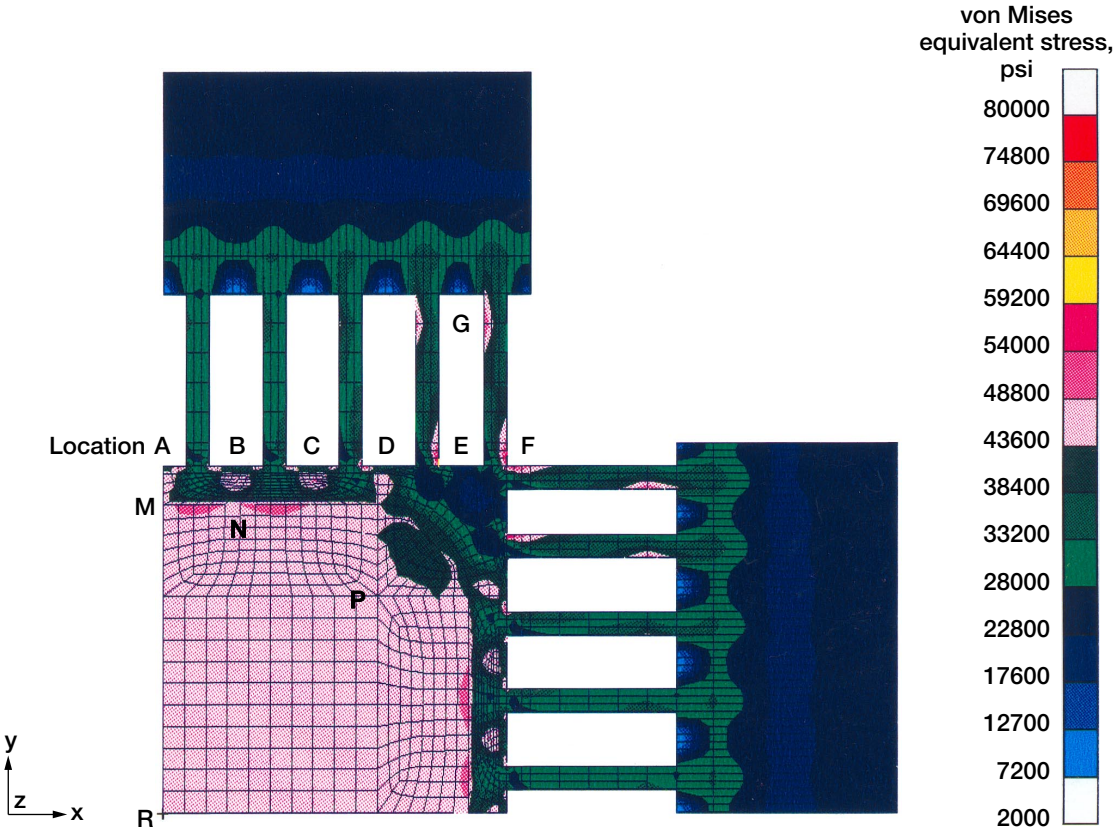

Figure 7.—Stress distribution on the top and bottom surfaces: specimen design 146.1.

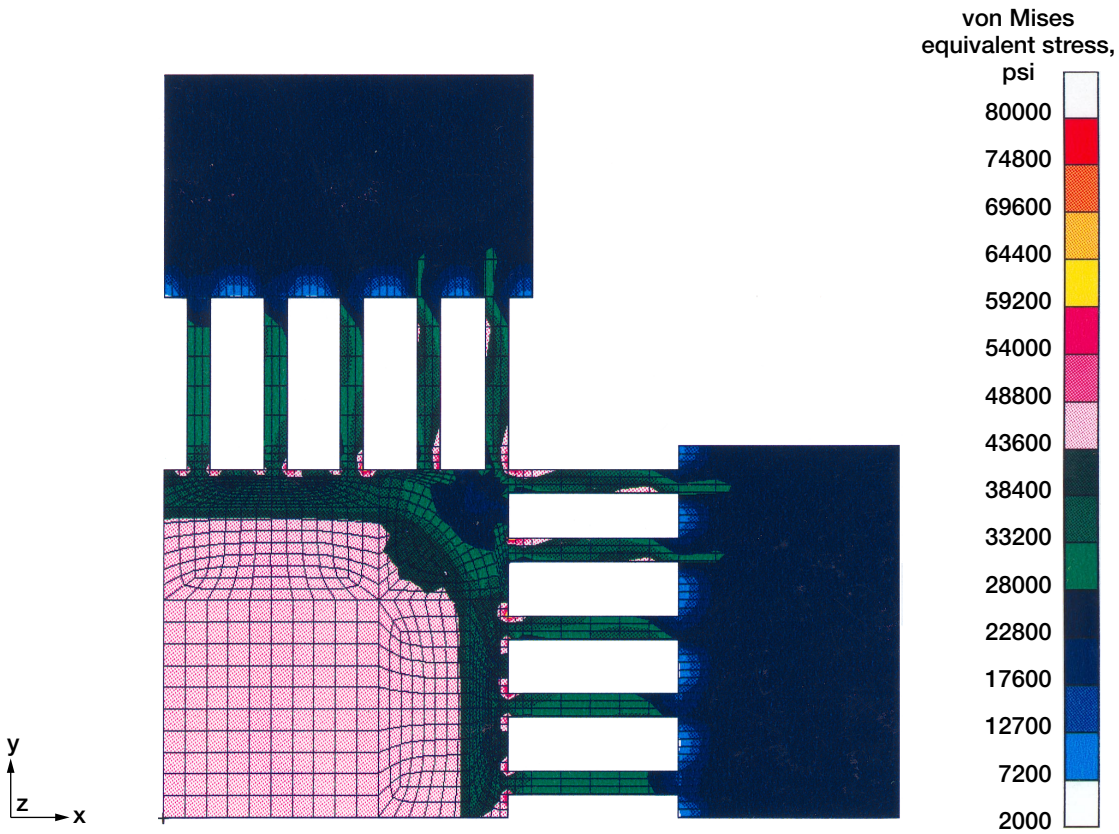

Figure 8.—Stress distribution at midsection: specimen design 146.1.

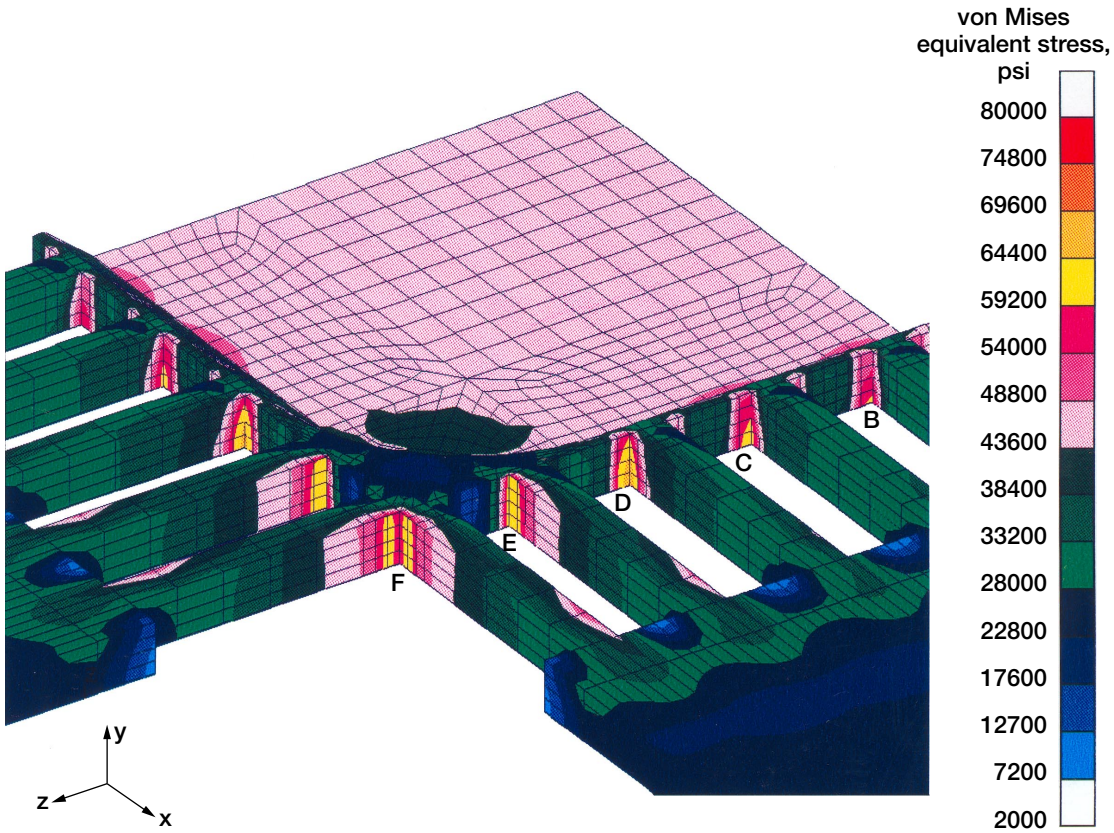

Figure 9.—Stress distribution in flexures: specimen design 146.1.

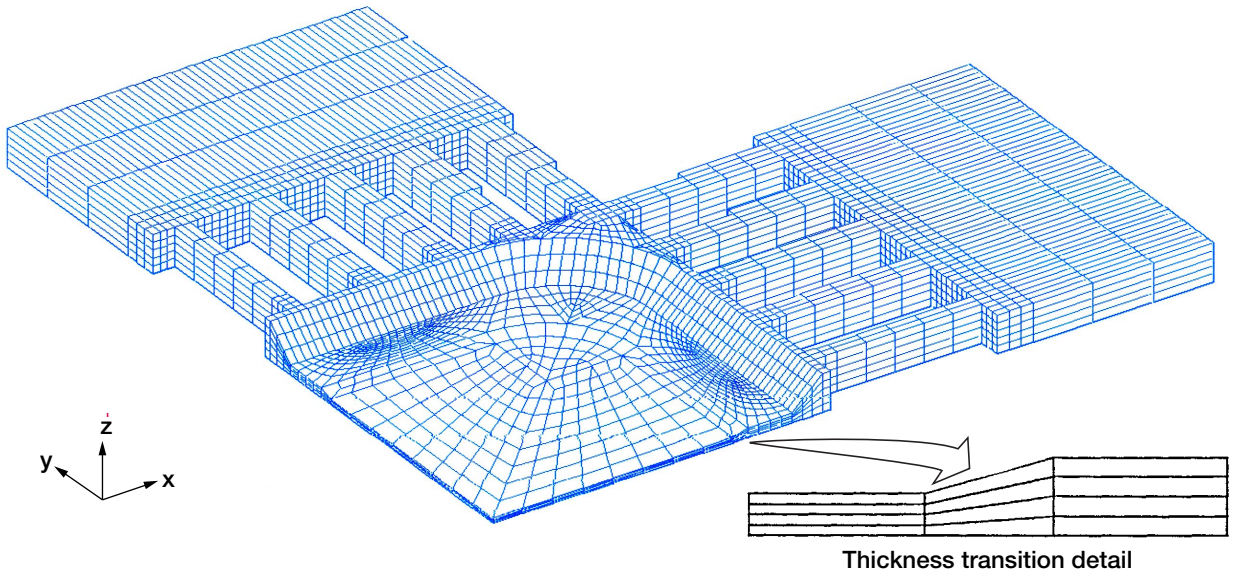

Figure 10.—Finite element model of specimen design 228.1: isometric view.

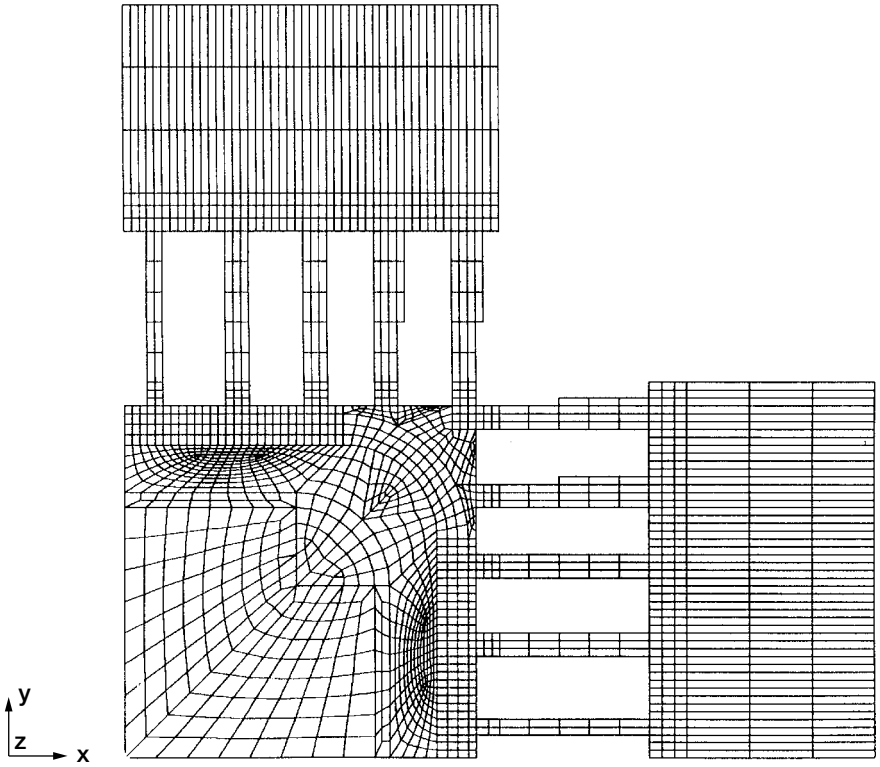

Figure 11.—Finite element model of specimen design 228.1: plan view.

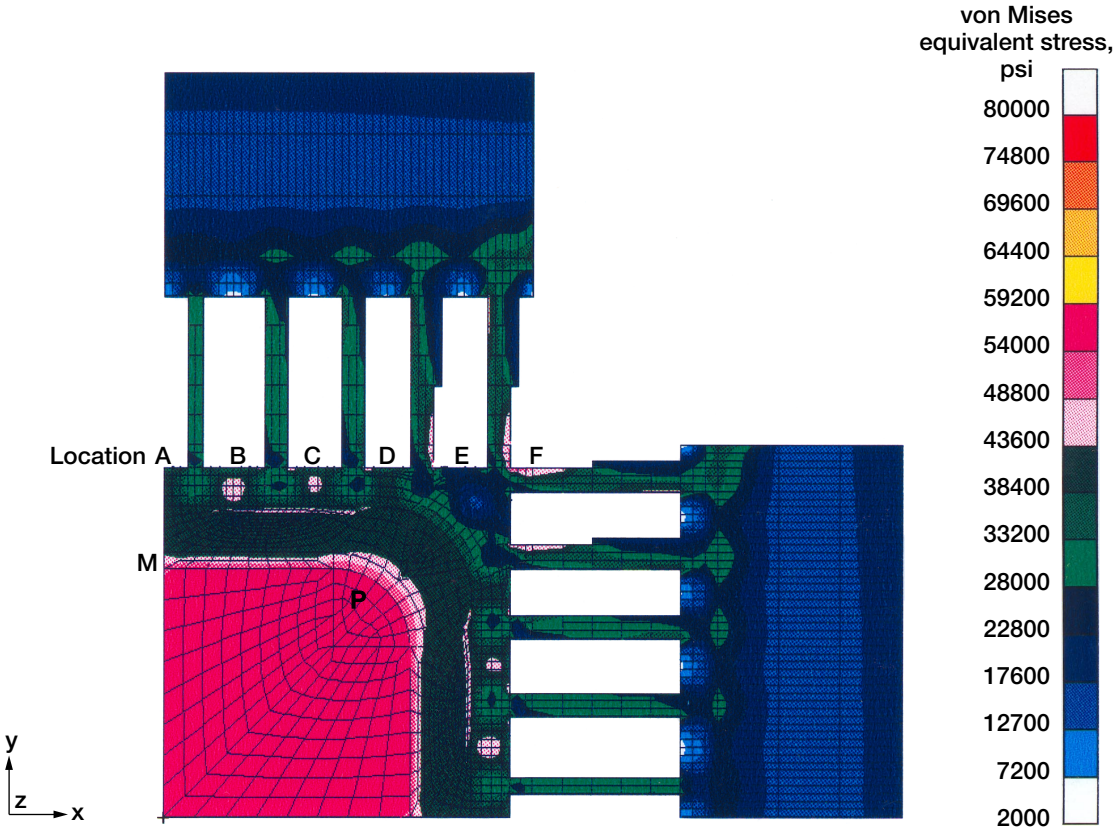

Figure 12.—Stress distribution on the top and bottom surfaces: specimen design 228.1.

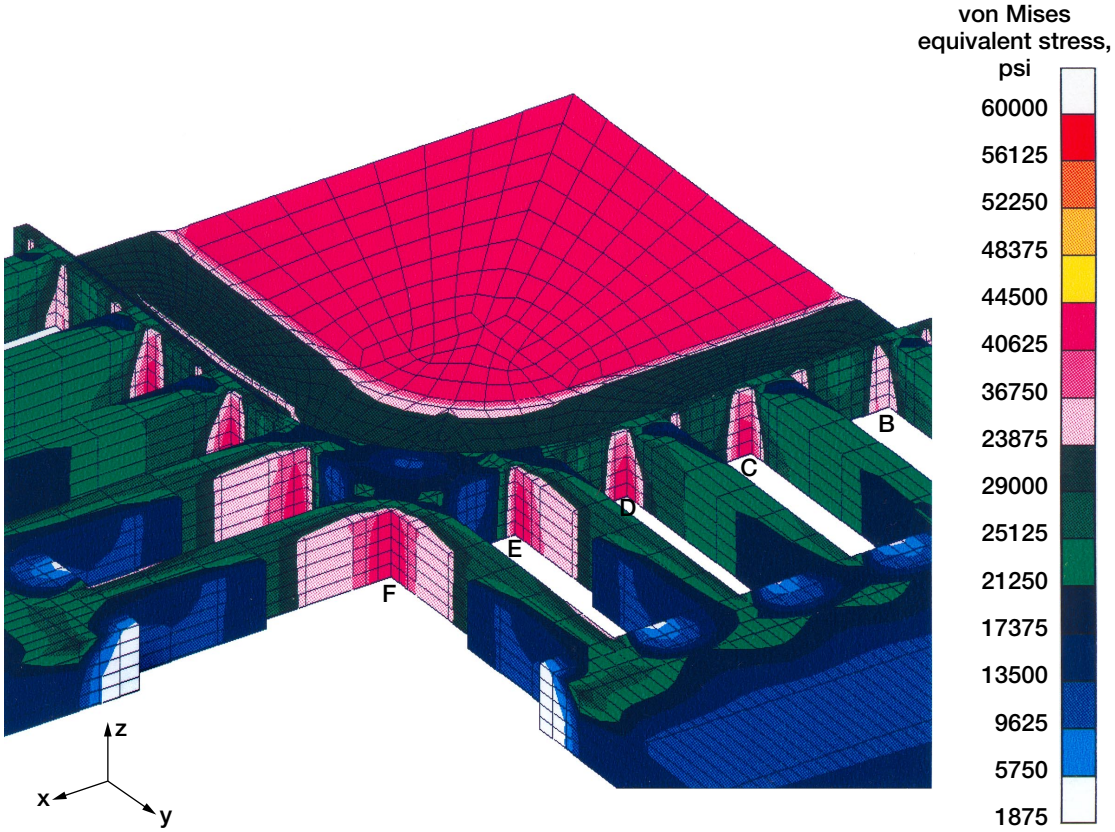

Figure 13.—Stress distribution flexures: specimen design 228.1.

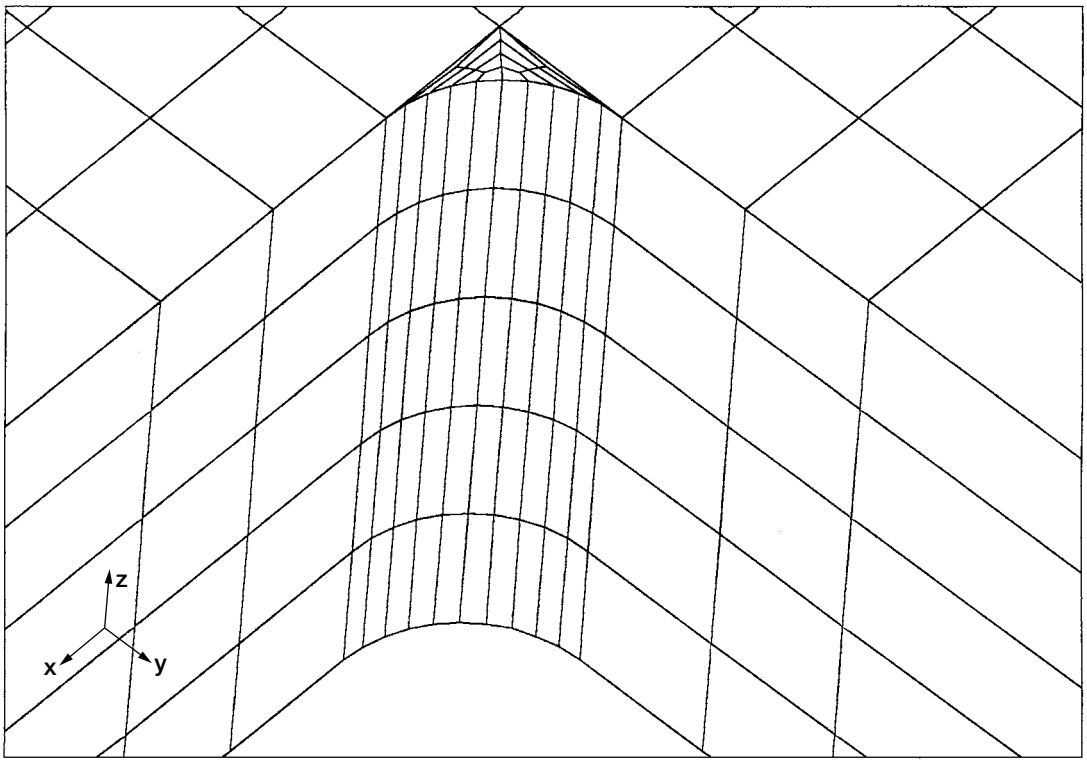

Figure 14.—Finite element model of corner fillet region: specimen design 228.2.

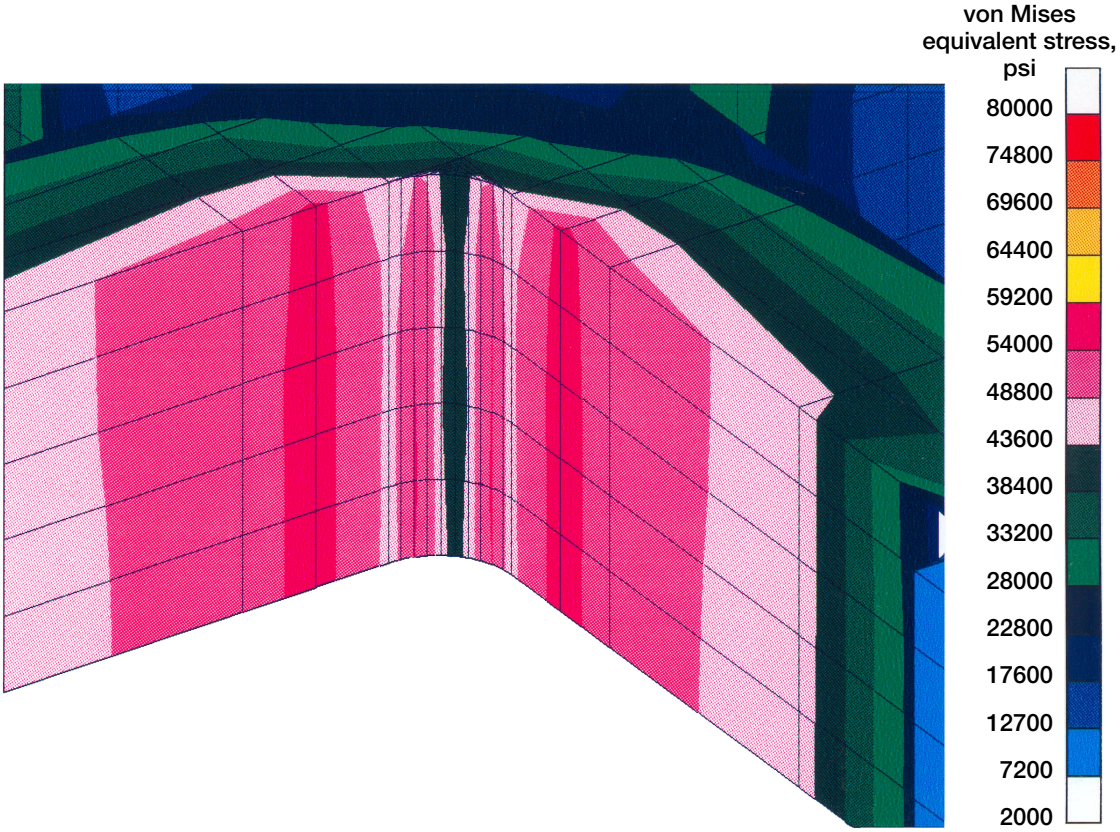

Figure 15.—Stress distribution in corner fillet region: specimen design 228.2.

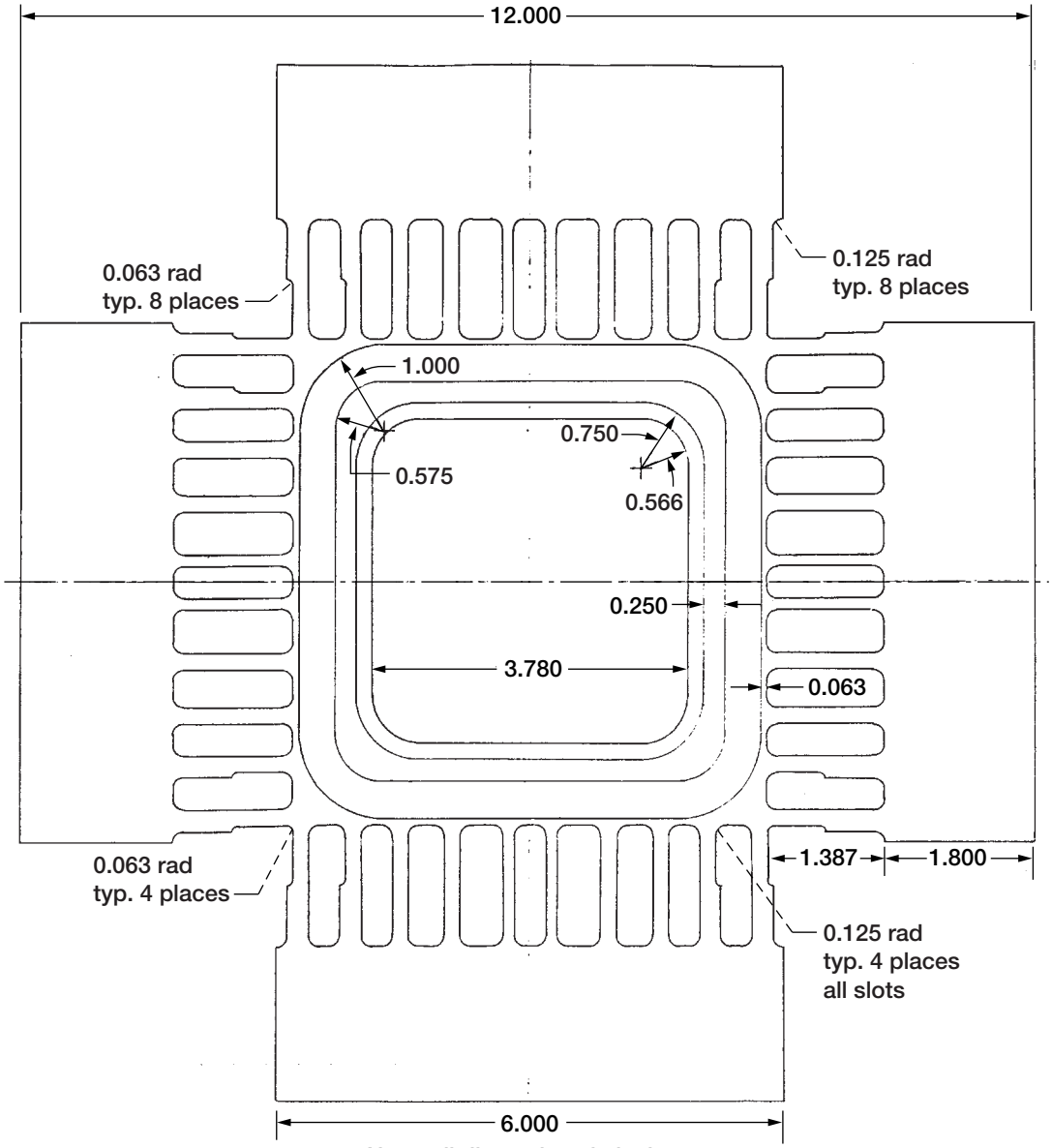

Note: all dimensions in inches

Figure 16.—Specimen design 228.2: plan view.

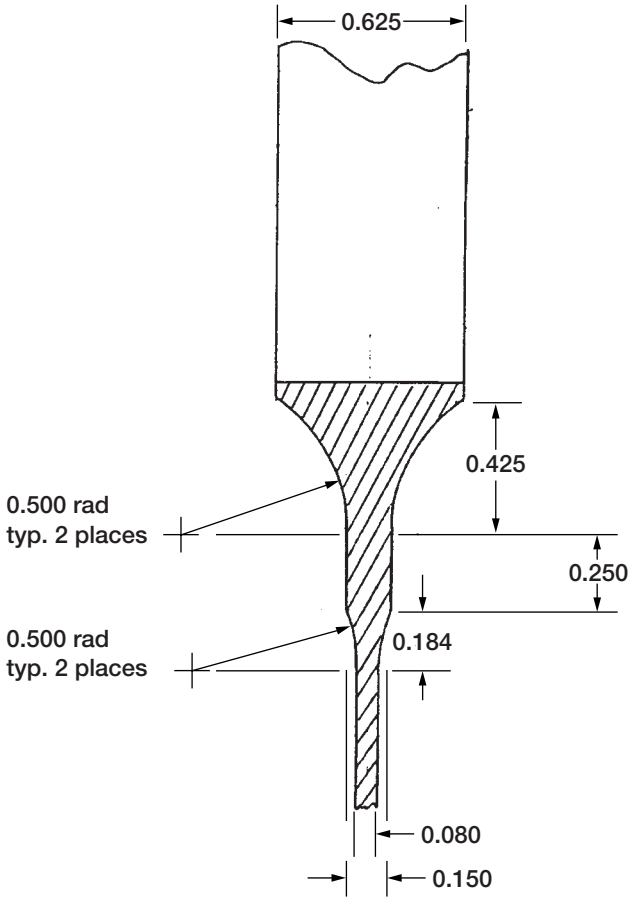

Note: all dimensions in inches

Figure 17.—Specimen design 228.2: thickness transition.

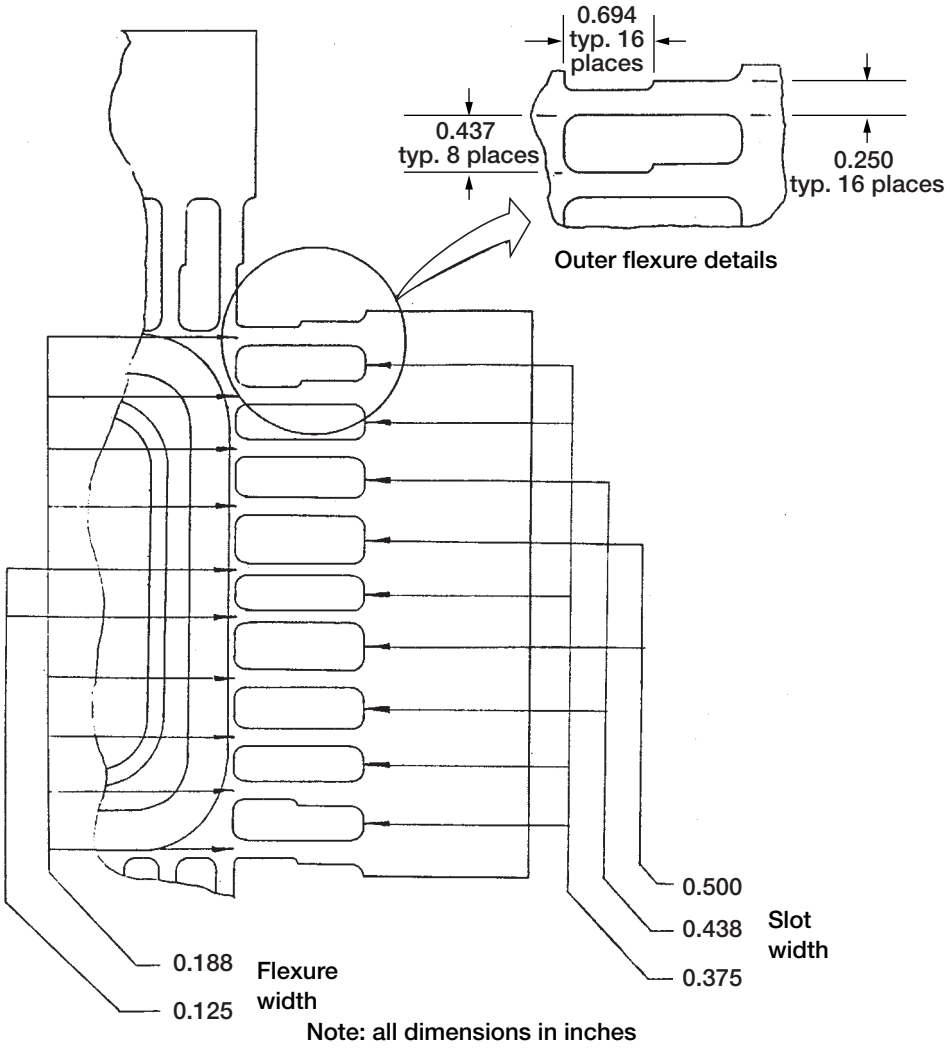

Figure 18.—Specimen design 228.2: flexure and slot details.

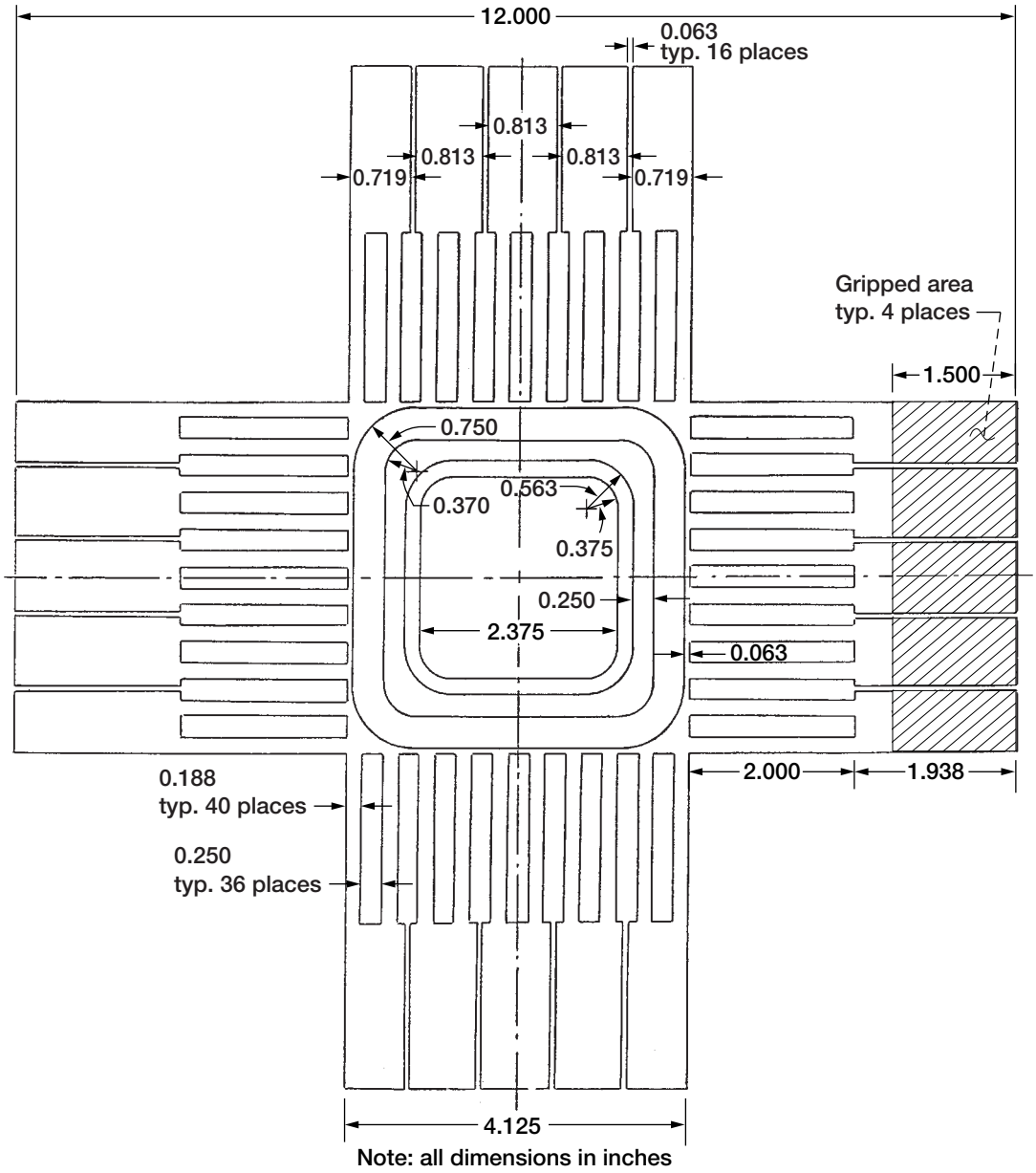

Figure 19.—Specimen design 232.1: plan view.

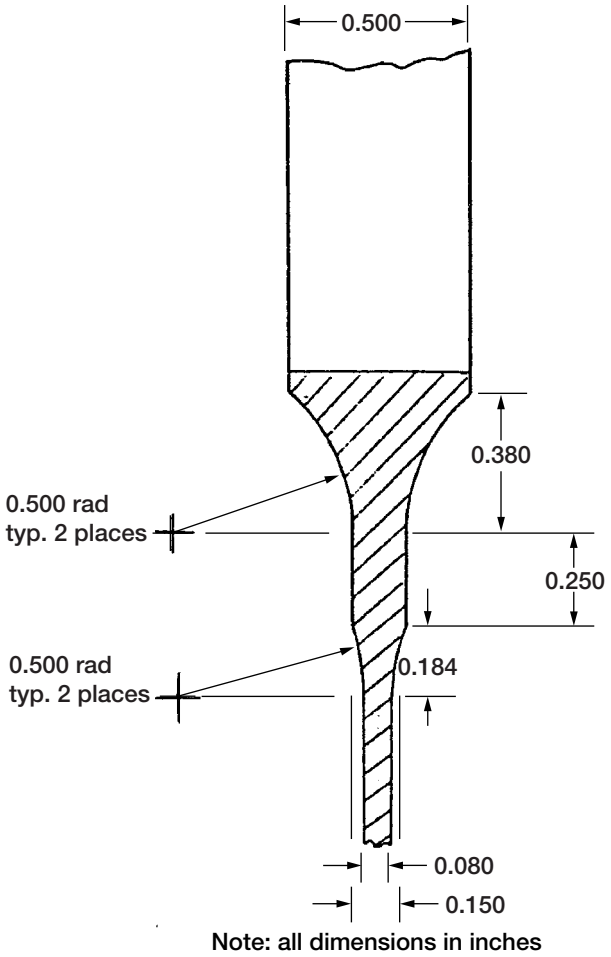

Figure 20.—Specimen design 232.1: thickness transition.

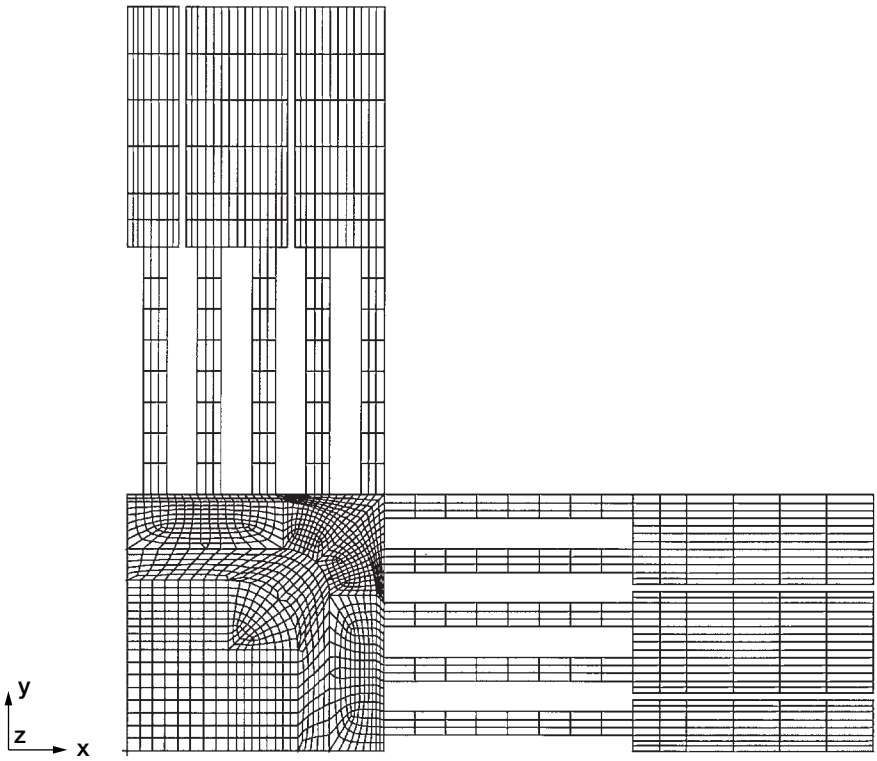

Figure 21.—Finite element model of specimen design 232.1: plan view.

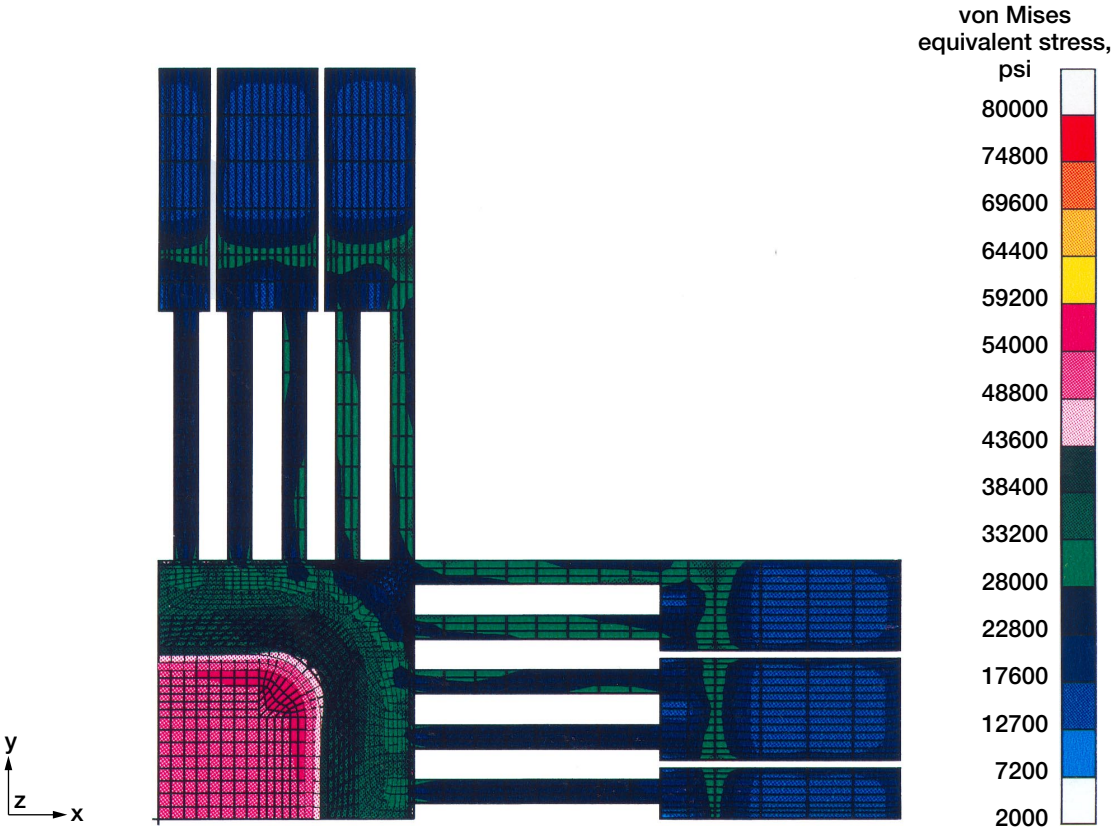

Figure 22.—Stress distribution on the top and bottom surfaces: specimen design 232.1.

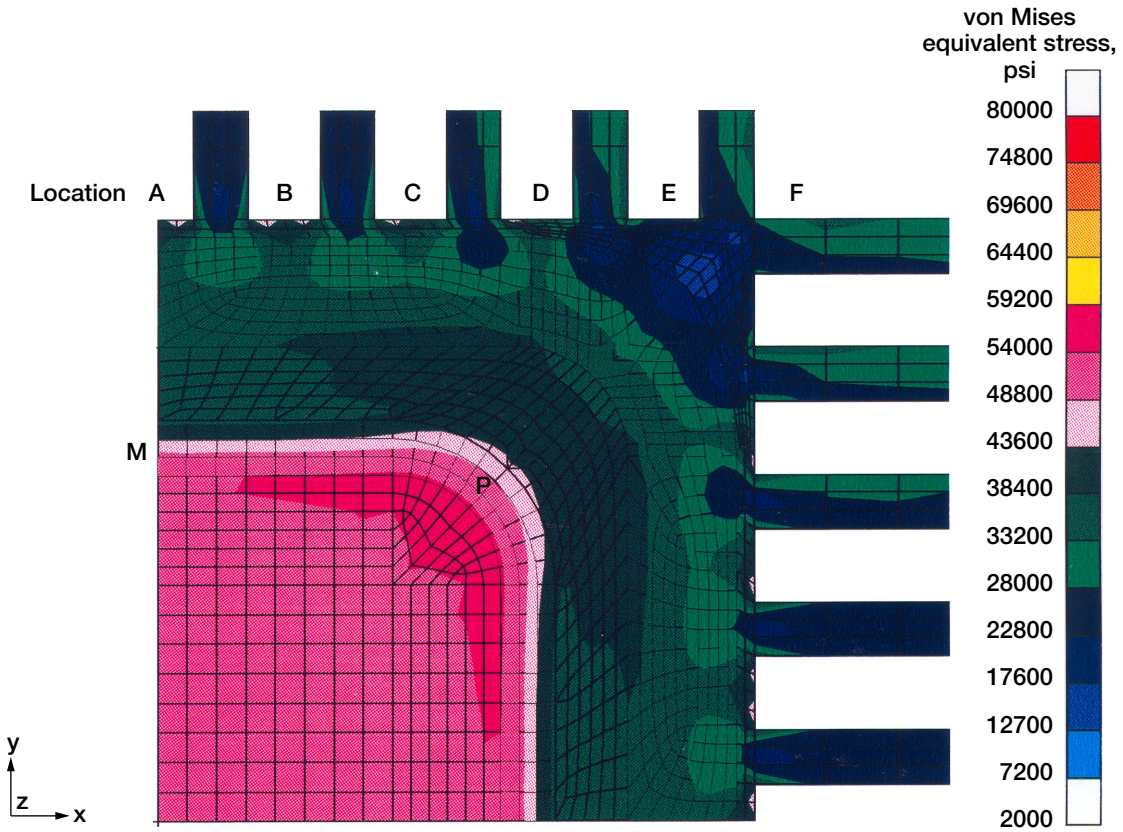

Figure 23.—Details of gage area stress distribution: specimen design 232.1.

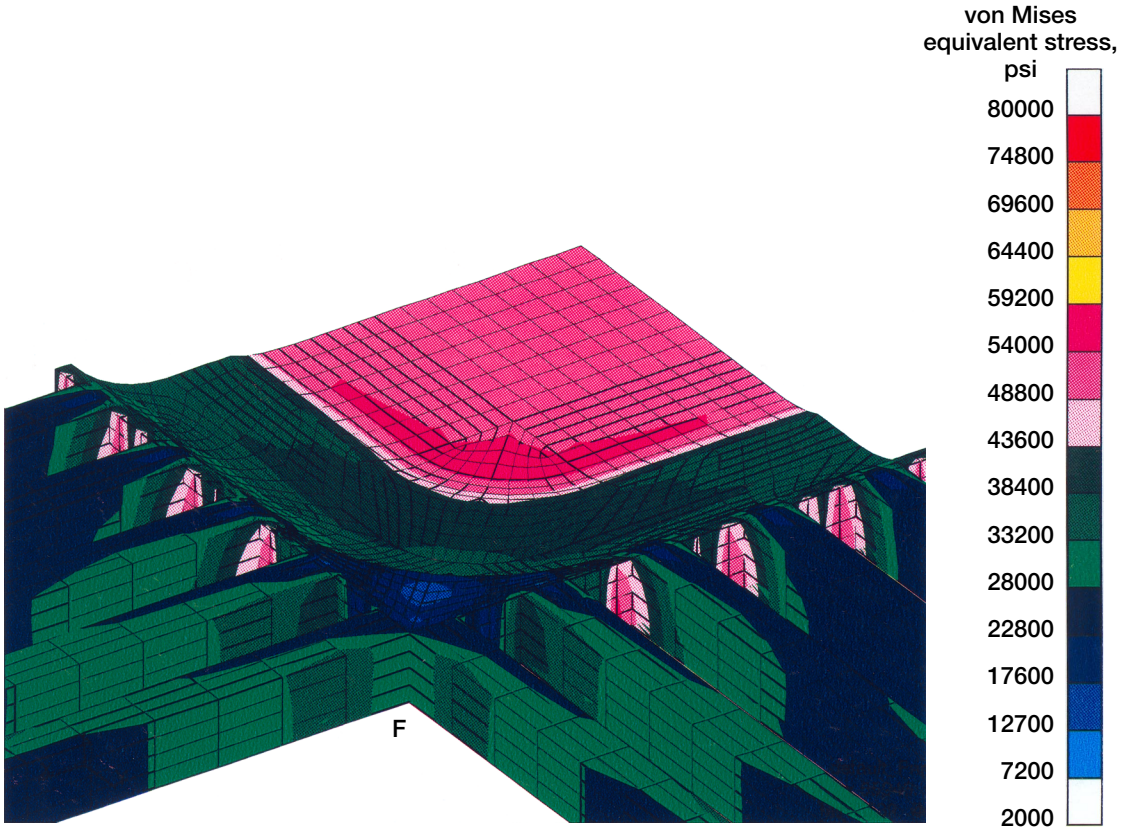

Figure 24.—Stress distribution in flexures: specimen design 232.1 viewed on corner.

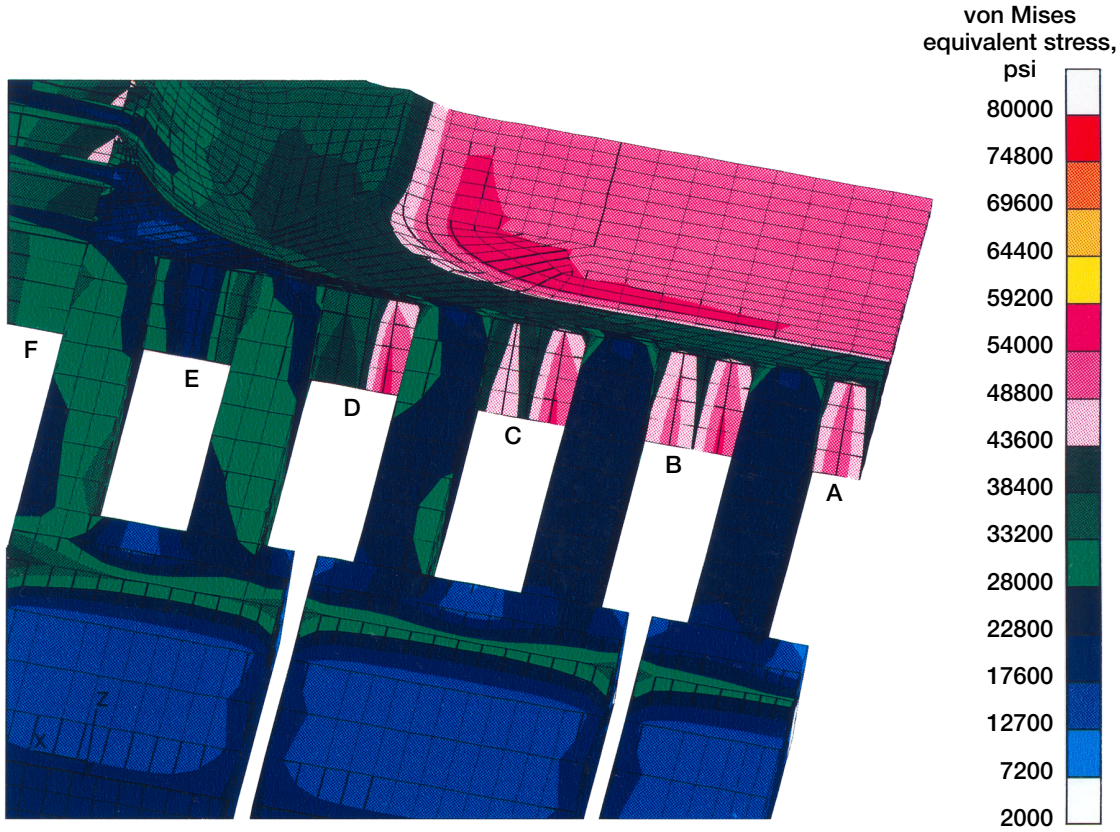

Figure 25.—Stress distribution in flexures: specimen design 232.1 viewed on centerline.

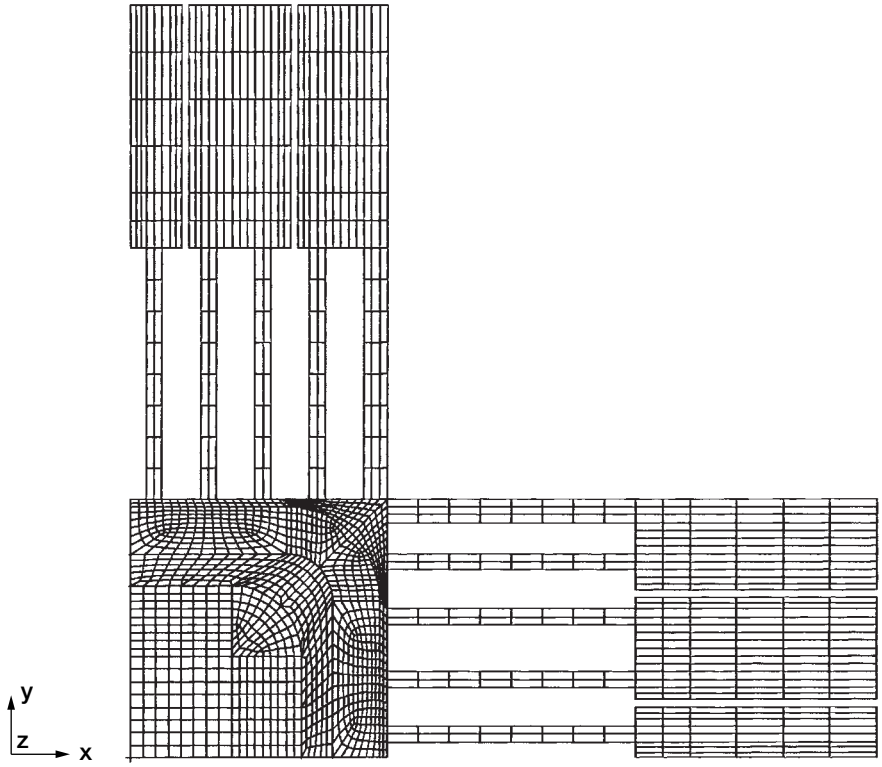

Figure 26.—Finite element model of specimen design 269.1: plan view.

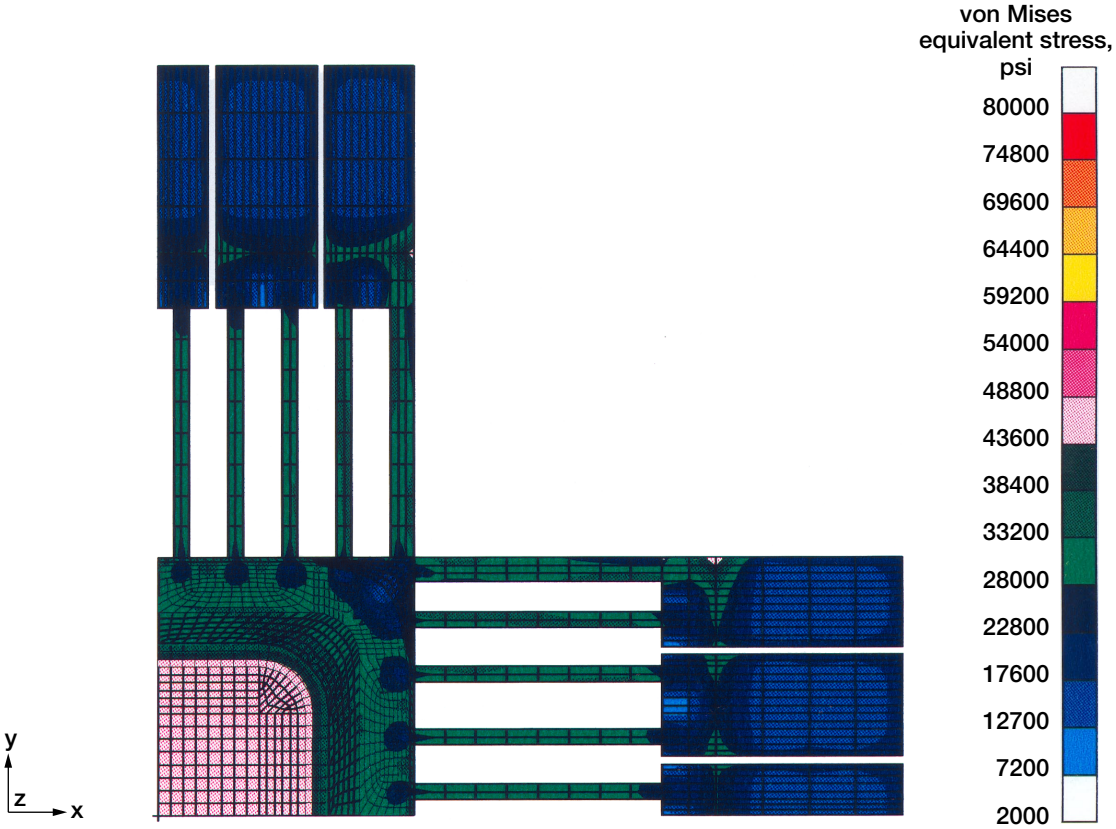

Figure 27.—Stress distribution on the top and bottom surfaces: specimen design 269.1.

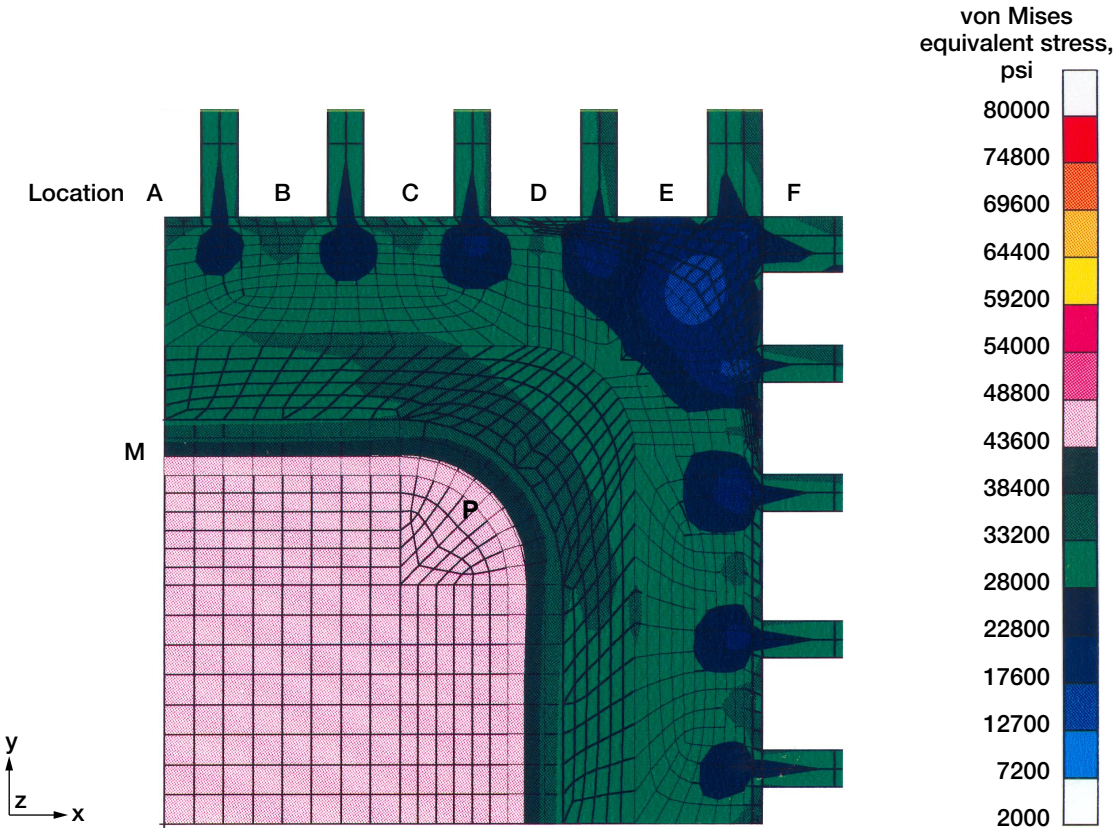

Figure 28.—Details of gage area stress distribution: specimen design 269.1.

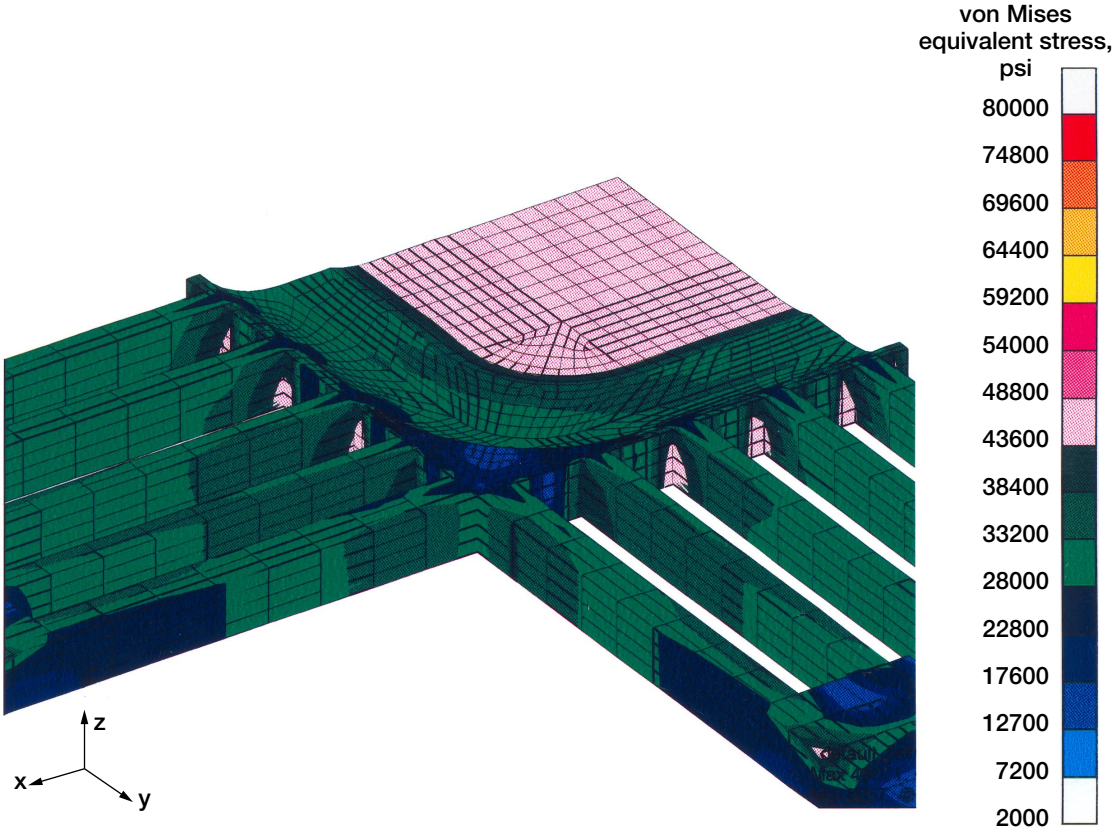

Figure 29.—Stress distribution in flexures: specimen design 269.1 viewed on corner.

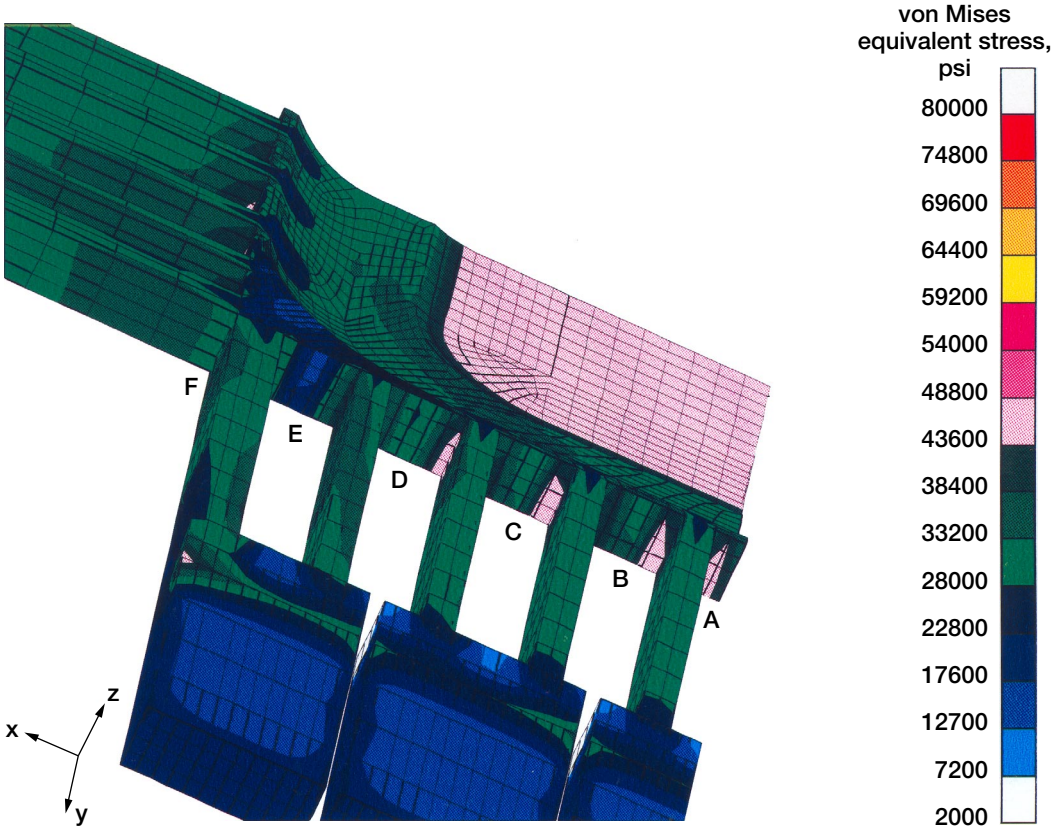

Figure 30.—Stress distribution in flexures: specimen design 269.1 viewed on centerline.

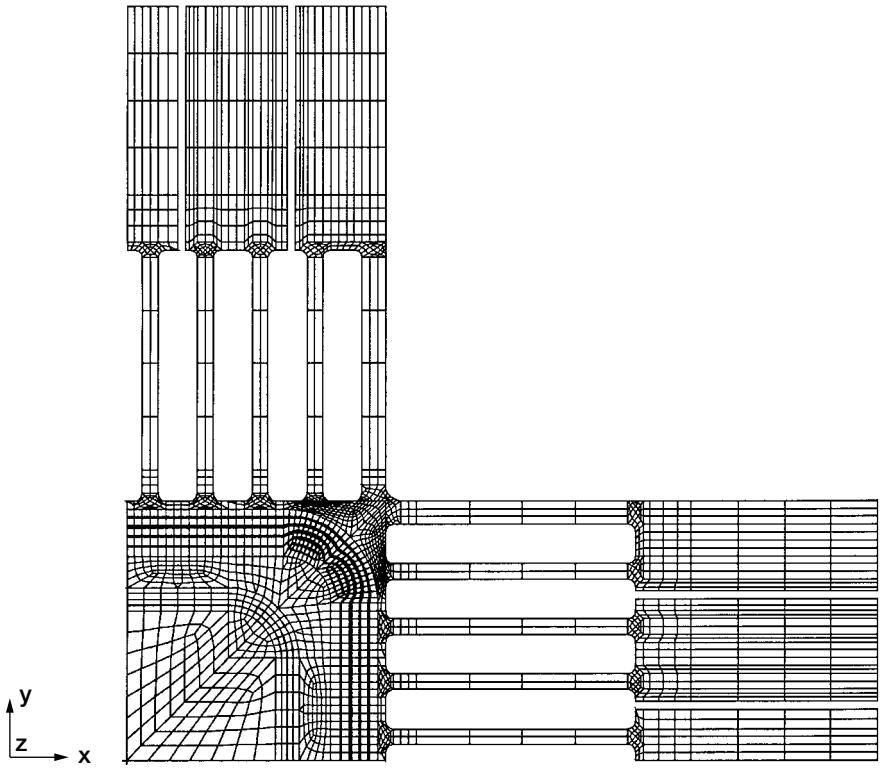

Figure 31.—Finite element model of specimen design 269.2: plan view.

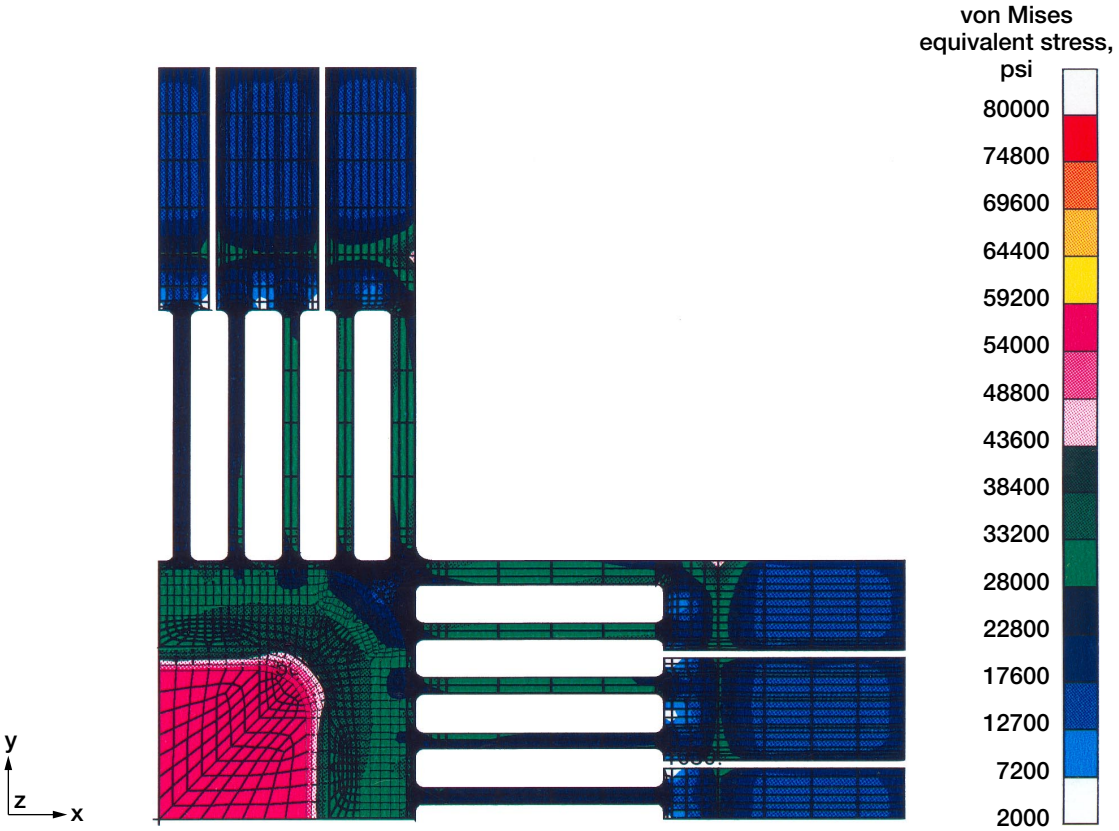

Figure 32.—Stress distribution on the top and bottom surfaces: specimen design 269.2.

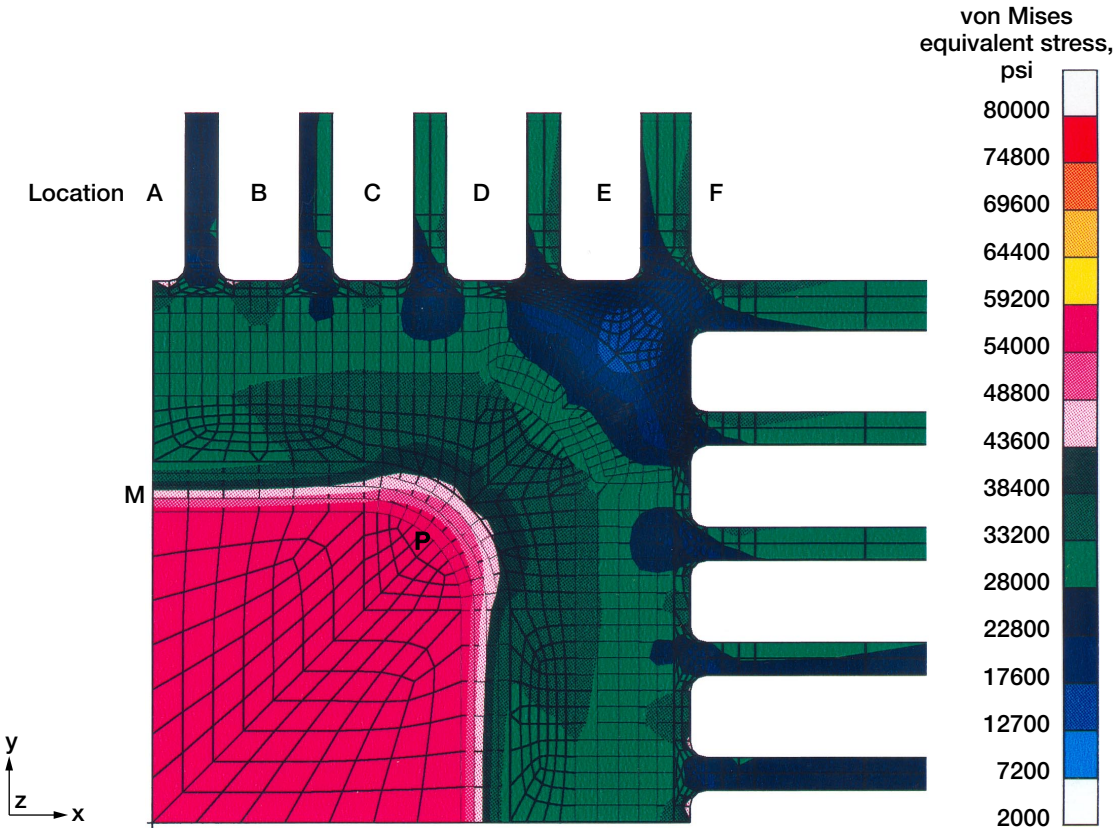

Figure 33.—Details of gage area stress distribution: specimen design 269.2.

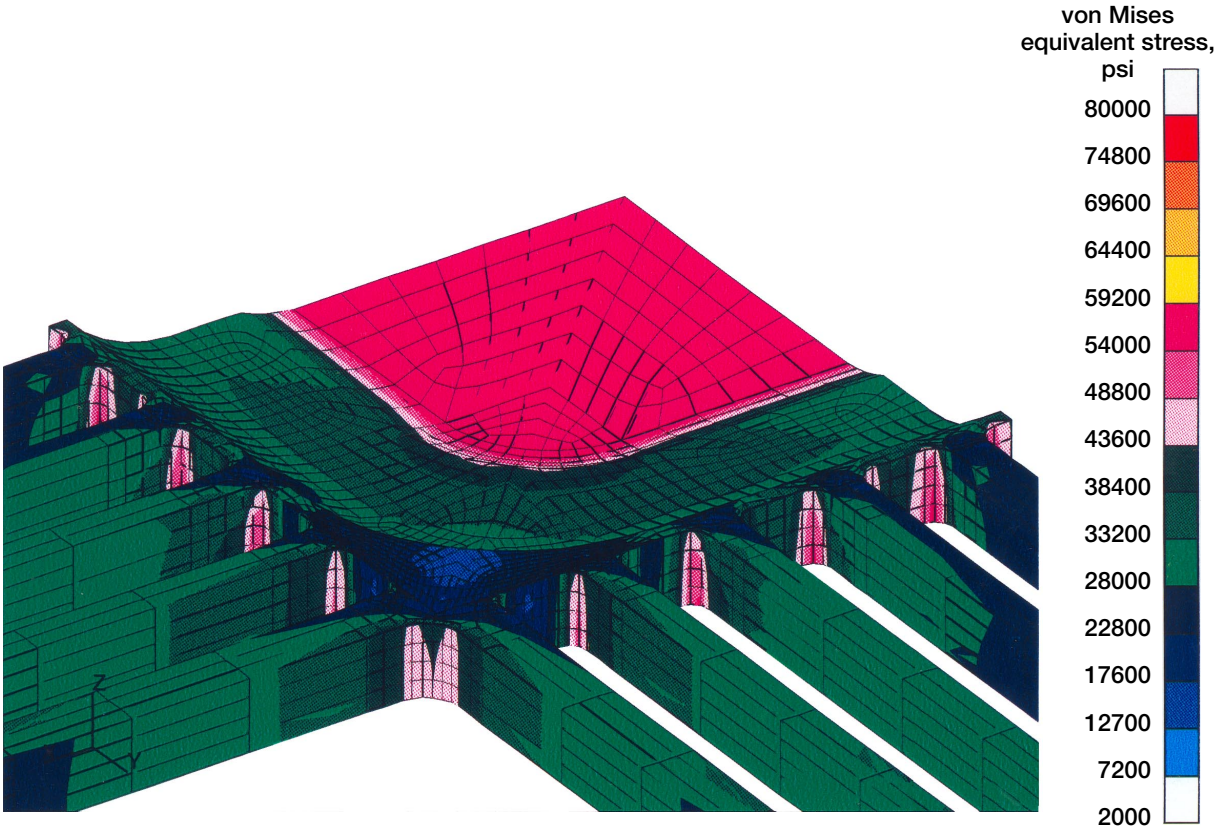

Figure 34.—Stress distribution in flexures: specimen design 269.2 viewed on corner.

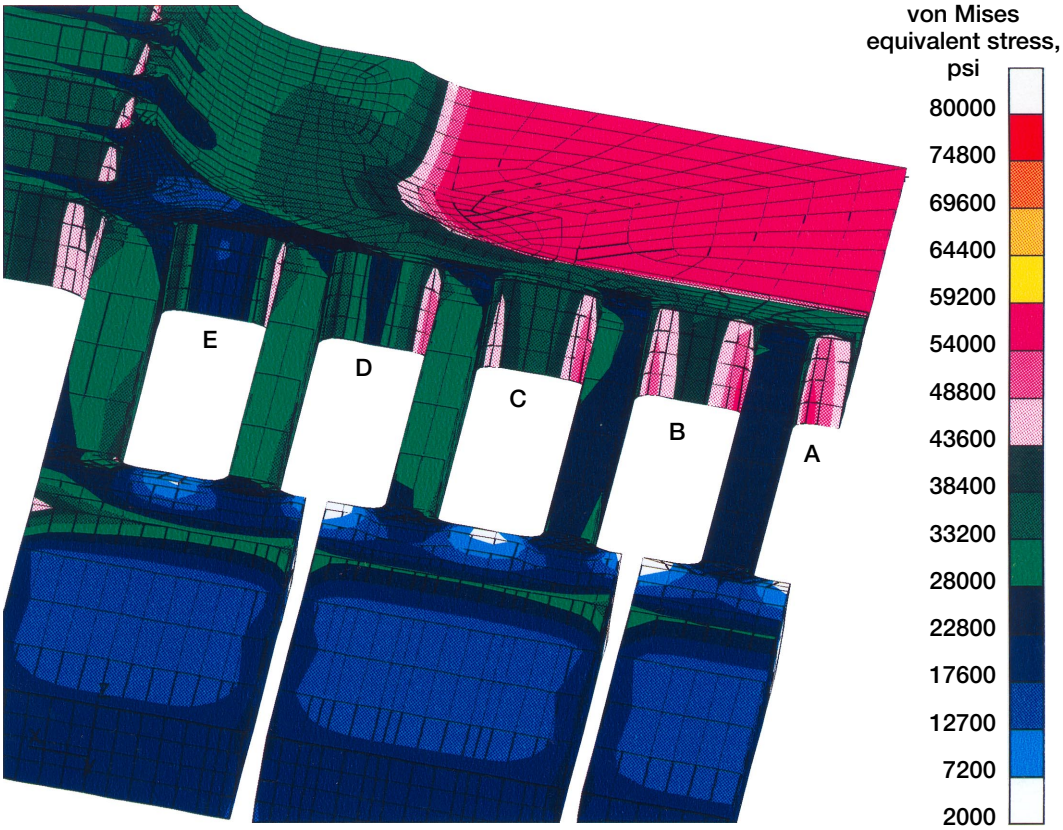

Figure 35.—Stress distribution in flexures: specimen design 269.2 viewed on centerline.

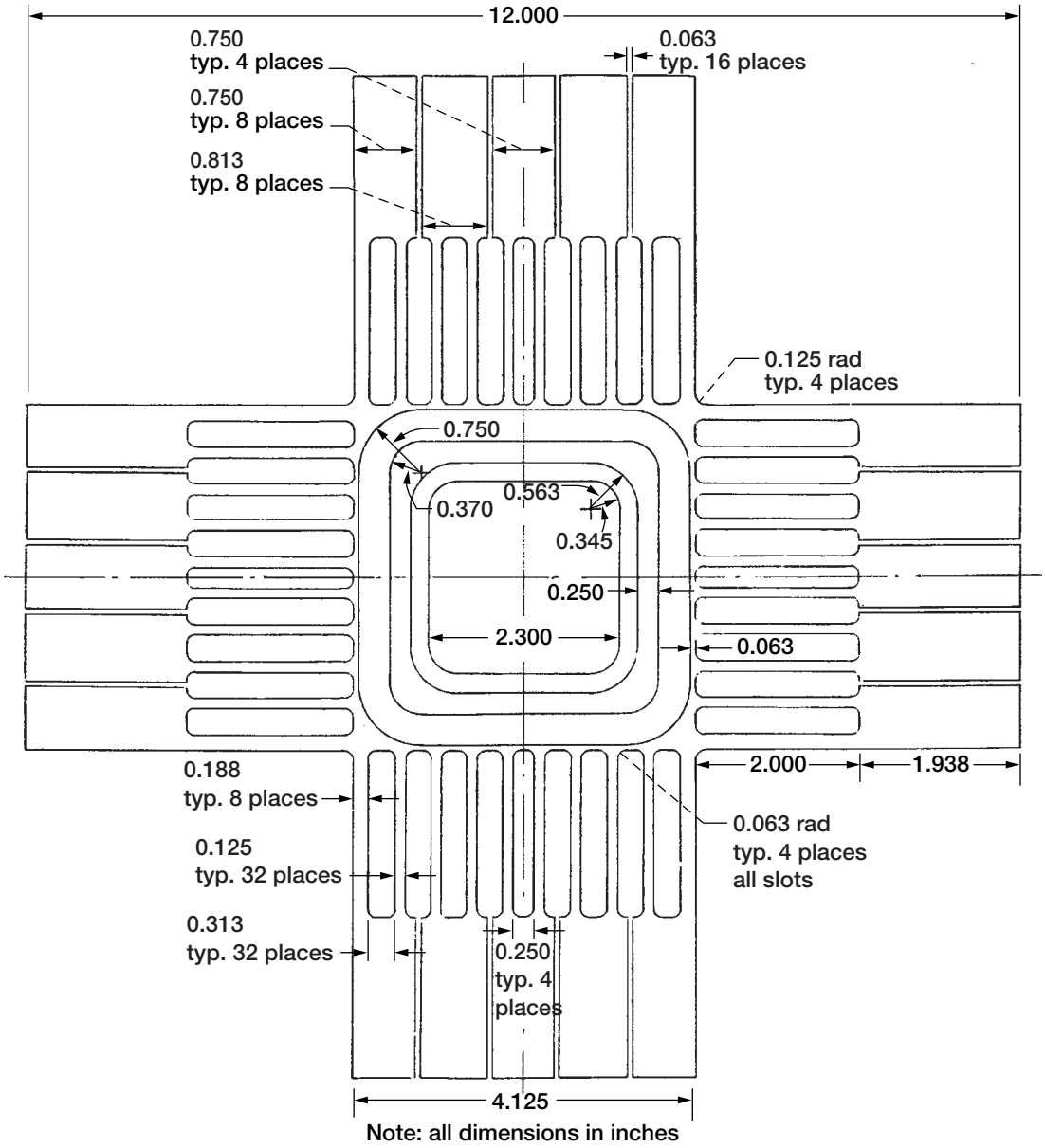

Figure 36.—Specimen design 269.2: plan view.

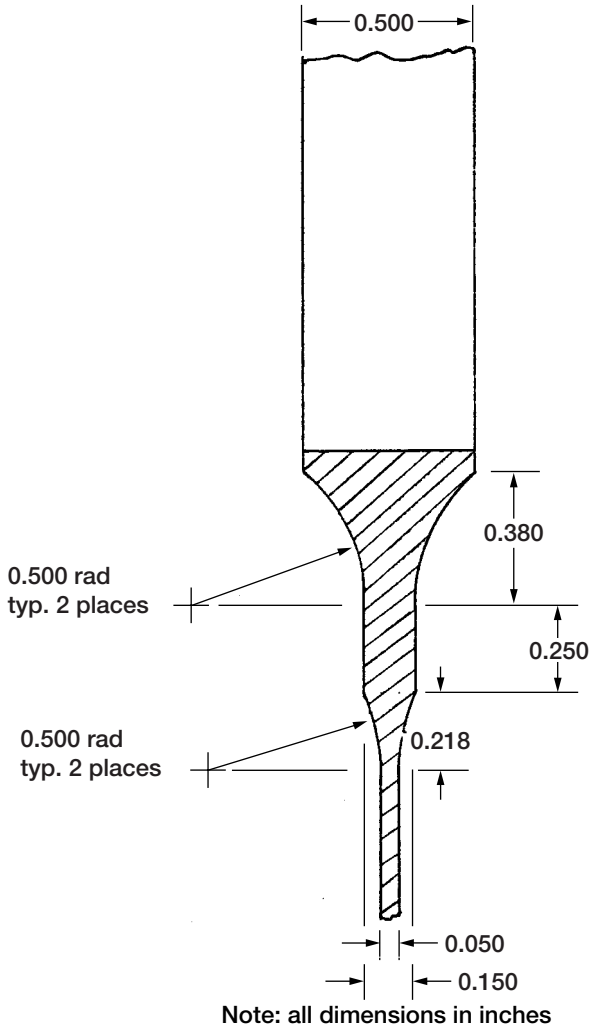

Figure 37.—Specimen design 269.2: thickness transition.

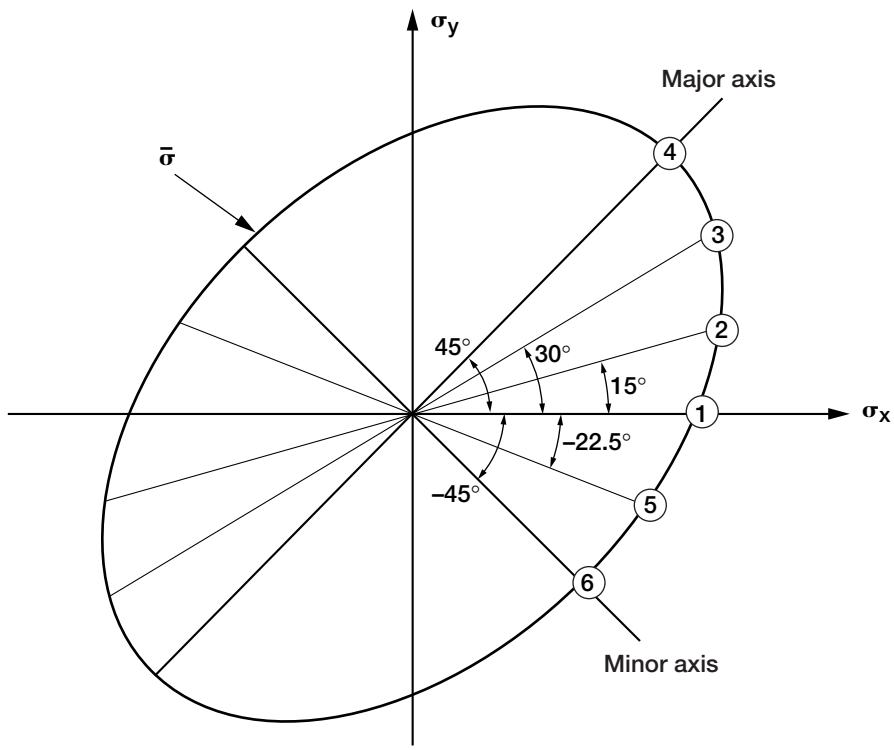

Where von Mises equivalent stress ($\bar{\sigma}$)

$$= (\sigma_x^2 - \sigma_x\sigma_y + \sigma_y^2)^{1/2} = 50{,}000 \text{ psi}$$

and stress ratio (θ)

$$= \text{Tan}^{-1}\,(\sigma_y/\sigma_x)$$

Figure 38.—Stress ratios (θ) used to investigate general forms of biaxial loading.

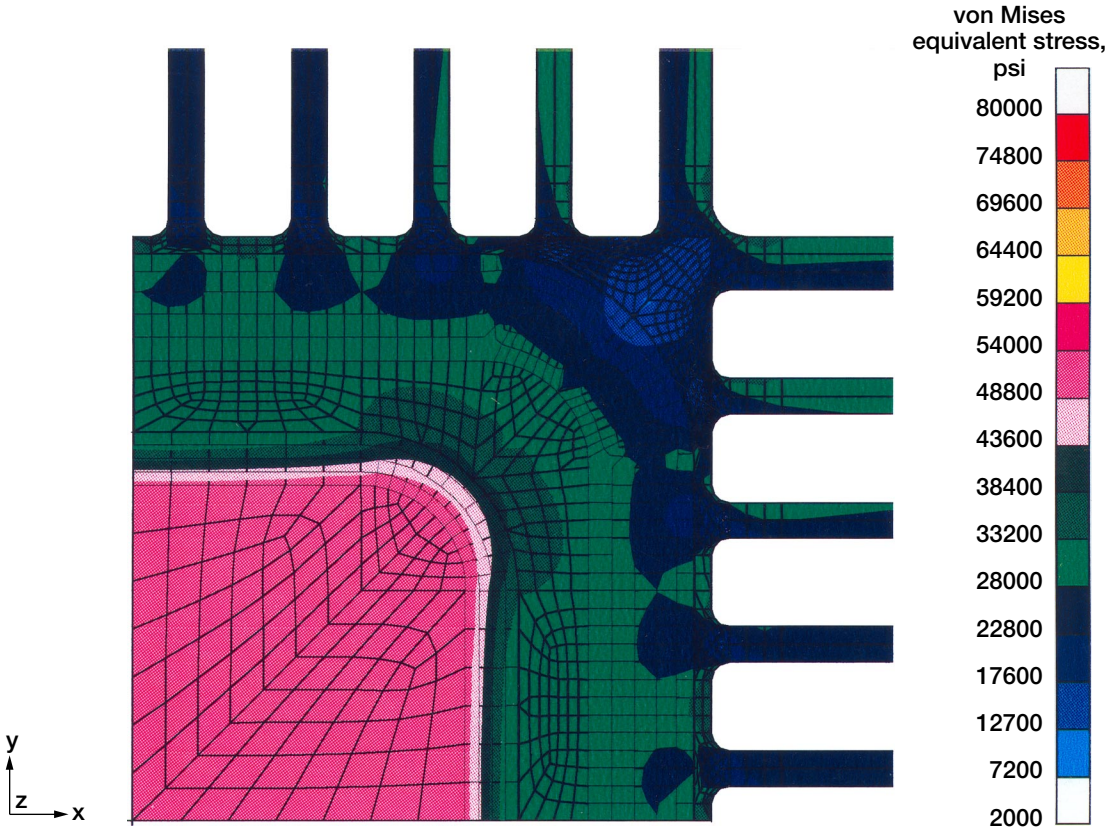

Figure 39.—Details of gage area stress distribution in specimen design 269.2: stress ratio (θ) = 45.0°.

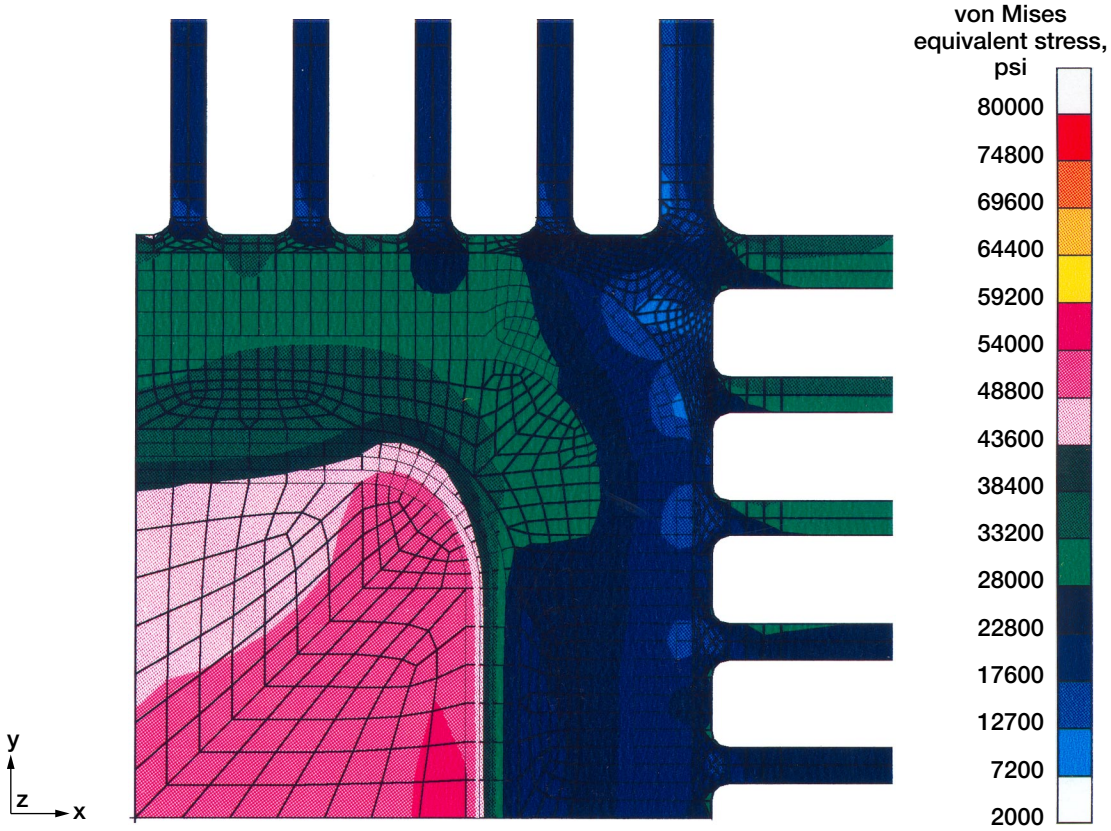

Figure 40.—Details of gage area stress distribution in specimen design 269.2: stress ratio (θ) = 30.0°.

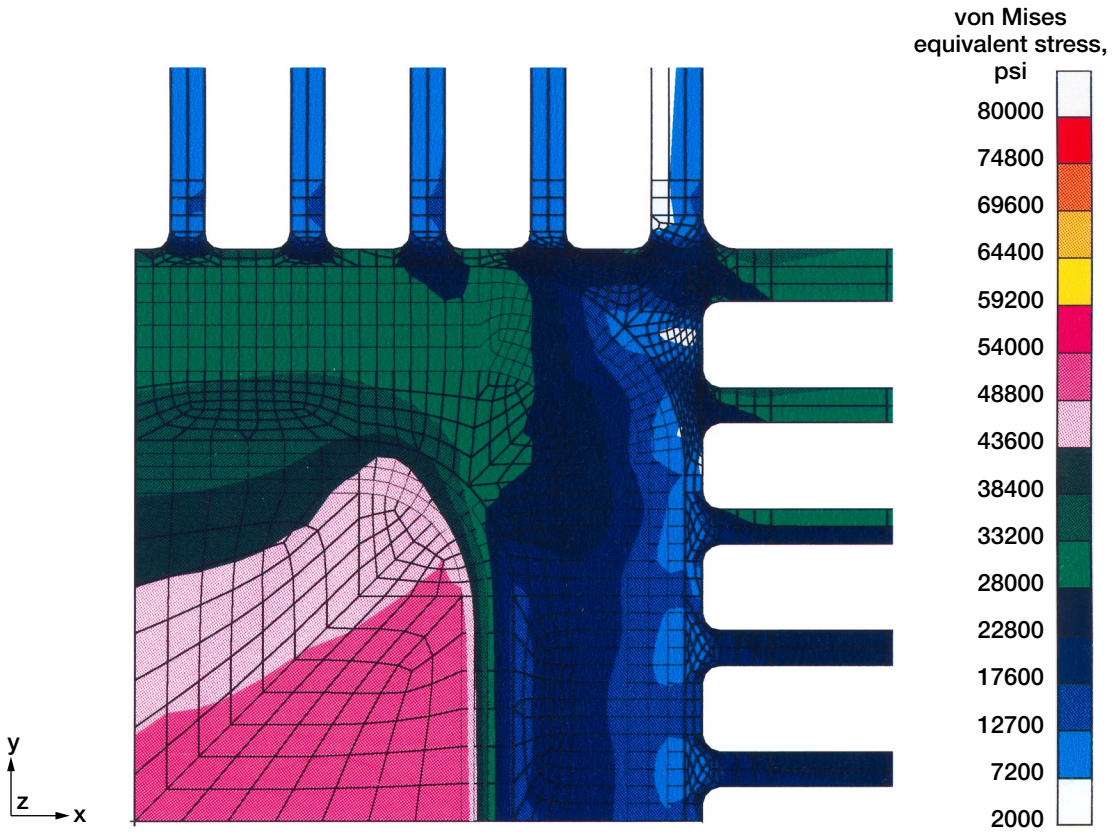

Figure 41.—Details of gage area stress distribution in specimen design 269.2: stress ratio (θ) = 15.0°.

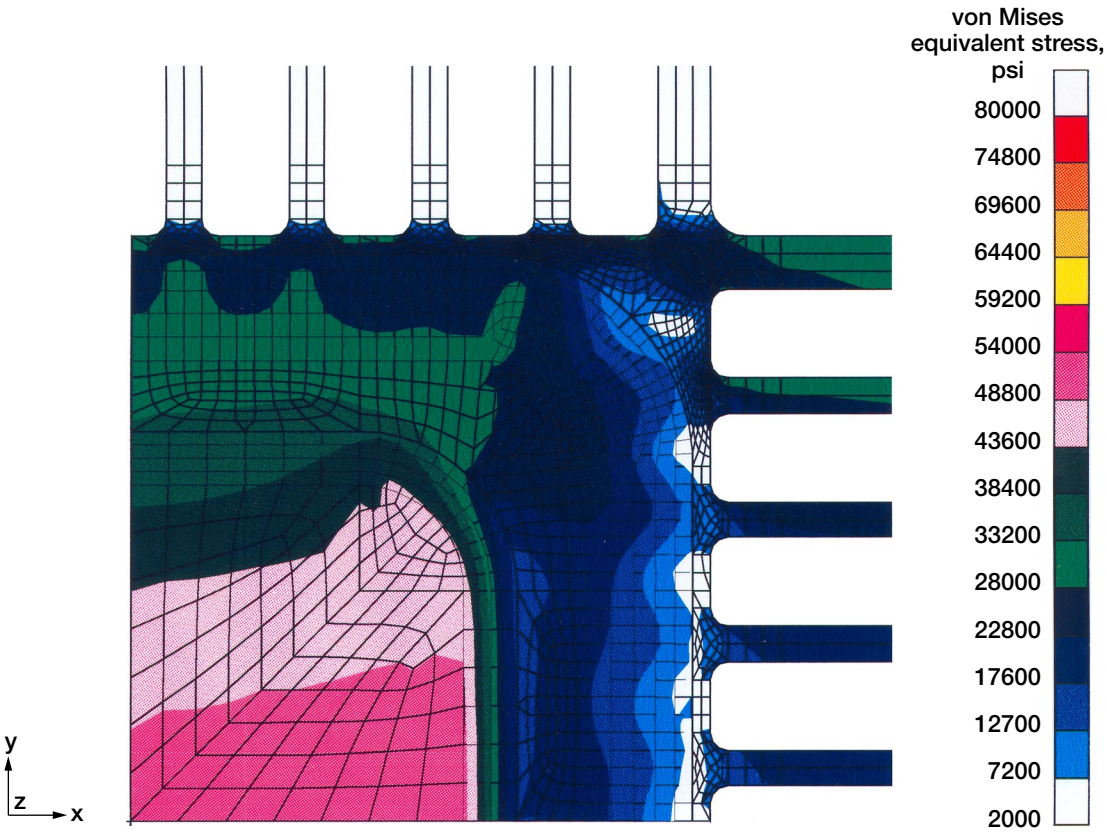

Figure 42.—Details of gage area stress distribution in specimen design 269.2: stress ratio (θ) = 0.0°.

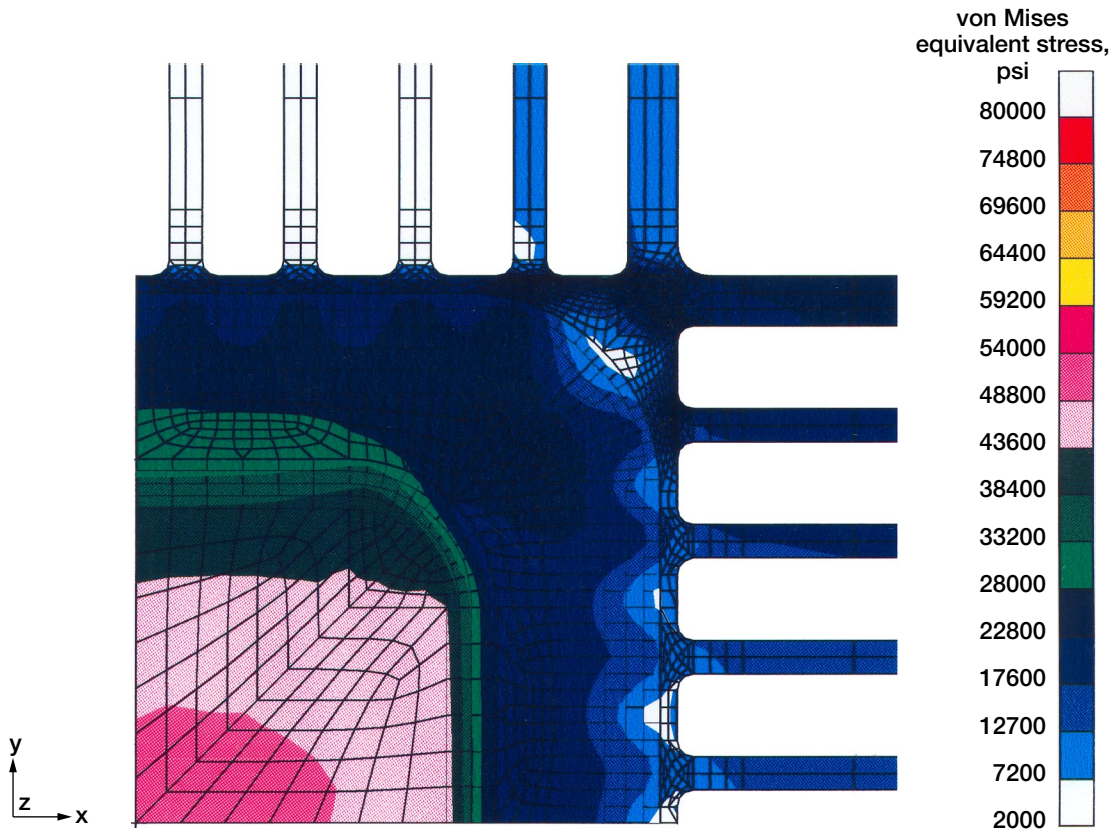

Figure 43.—Details of gage area stress distribution in specimen design 269.2: stress ratio (θ) = –22.5°.

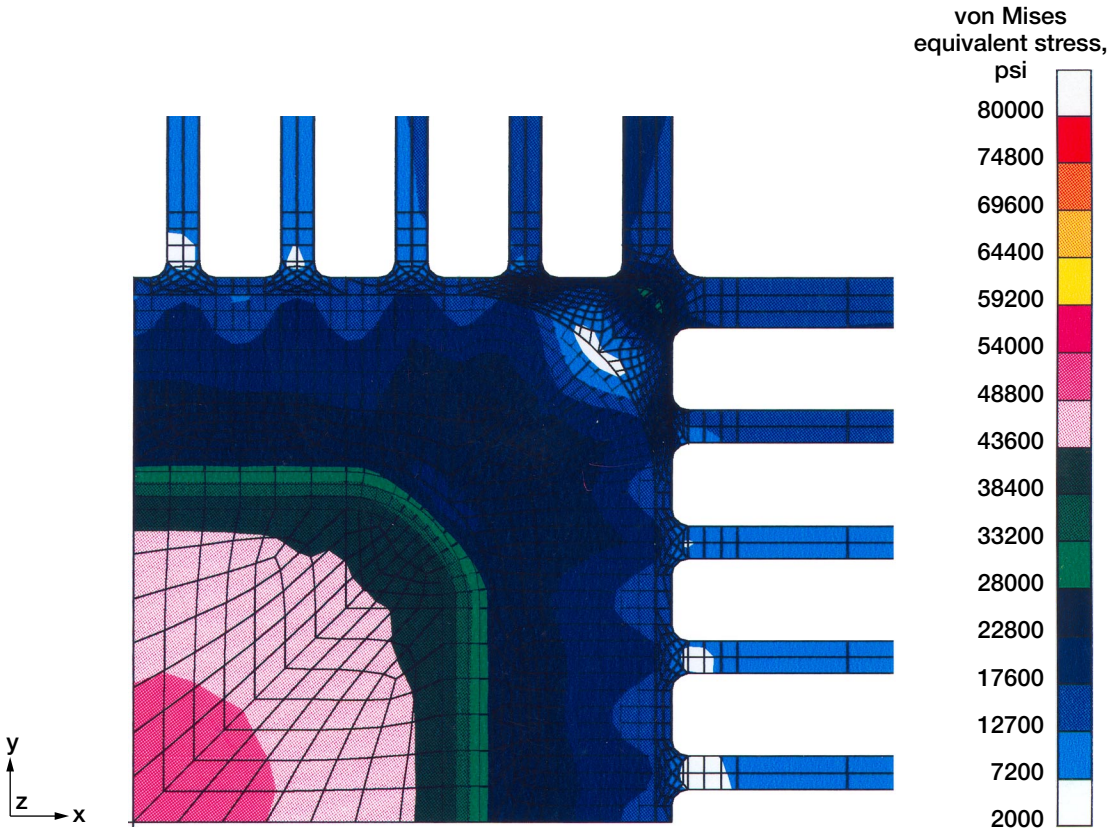

Figure 44.—Details of gage area stress distribution in specimen design 269.2: stress ratio (θ) = –45.0°.

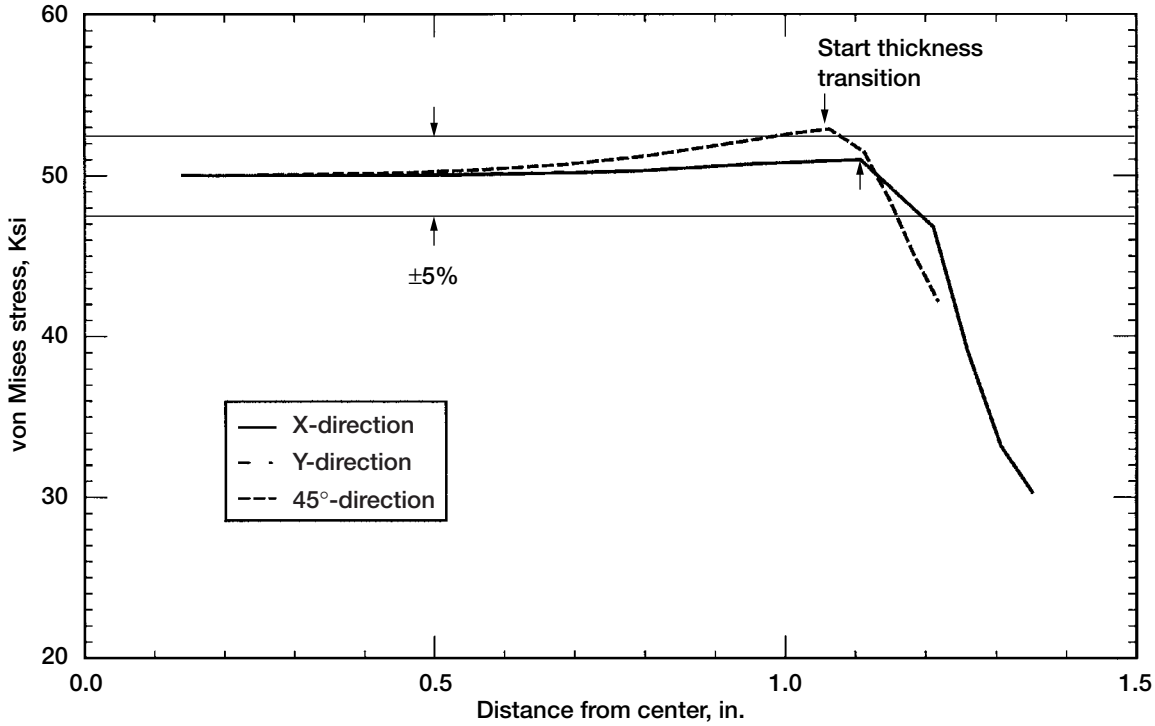

Note: The location of thickness transition occurs at the same distance in the x and y direction. The distance is reduced in the 45° direction because of the corner fillet radius.

Figure 45.—Variation of gage area stress in specimen design 269.2 in the x, y, and 45° directions: stress ratios (θ) = 45.0°.

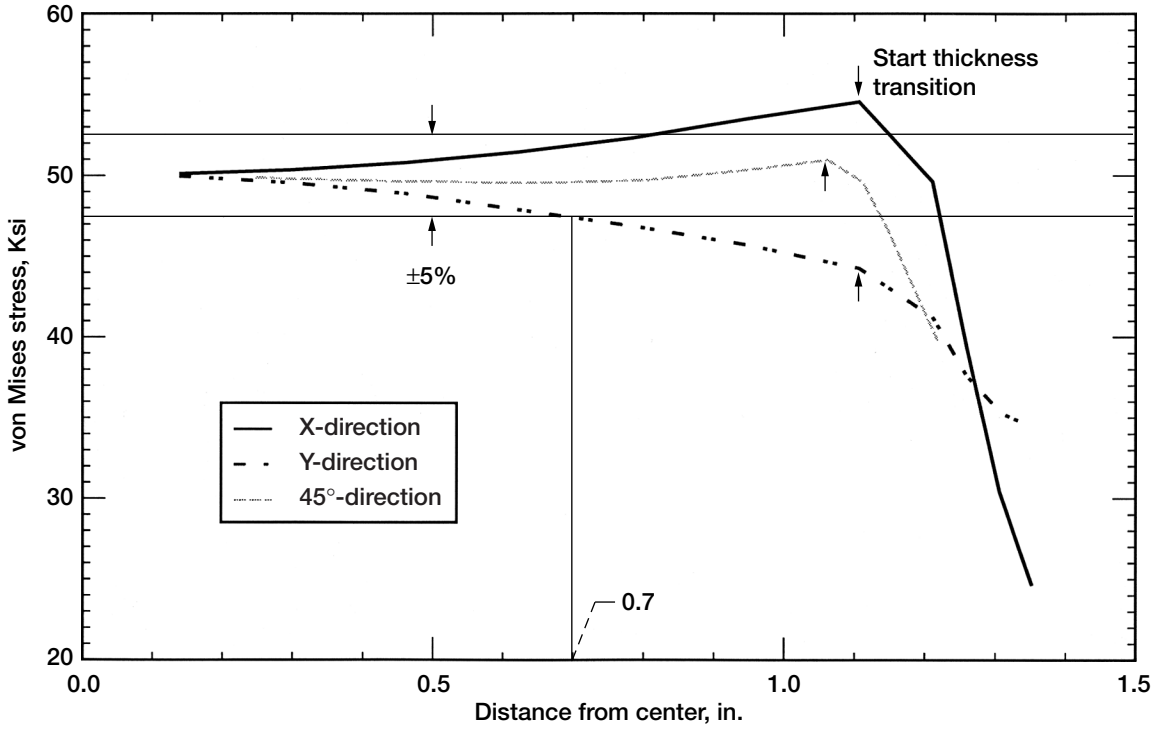

Figure 46.—Variation of gage area stress in specimen design 269.2 in the x, y, and 45° directions: stress ratio (θ) = 30.0°.

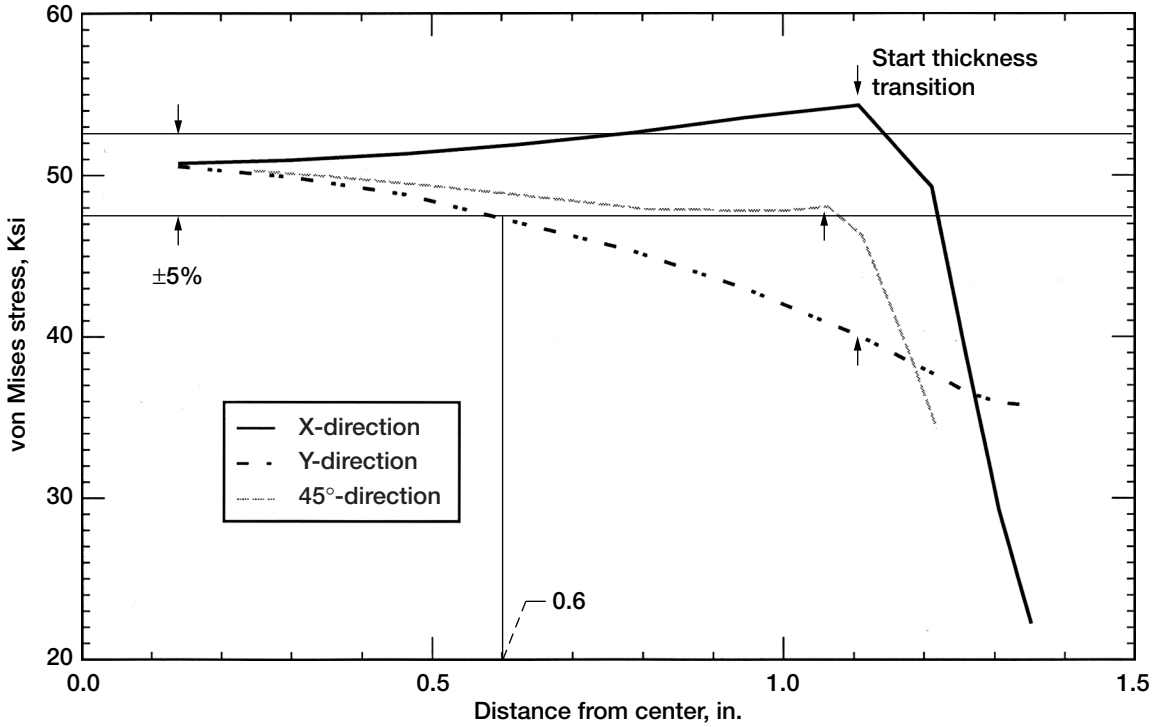

Figure 47.—Variation of gage area stress in specimen design 269.2 in the x, y, and 45° directions: stress ratio (θ) = 15.0°.

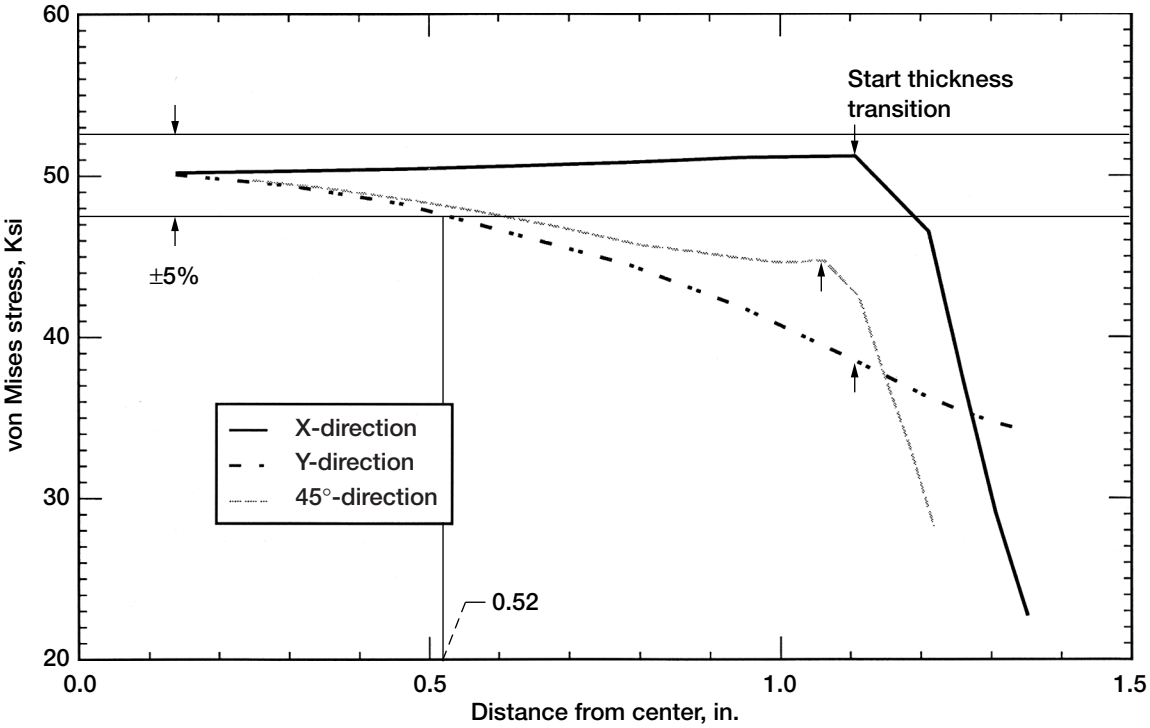

Figure 48.—Variation of gage area stress in specimen design 269.2 in the x, y, and 45° directions: stress ratio (θ) = 0.0°.

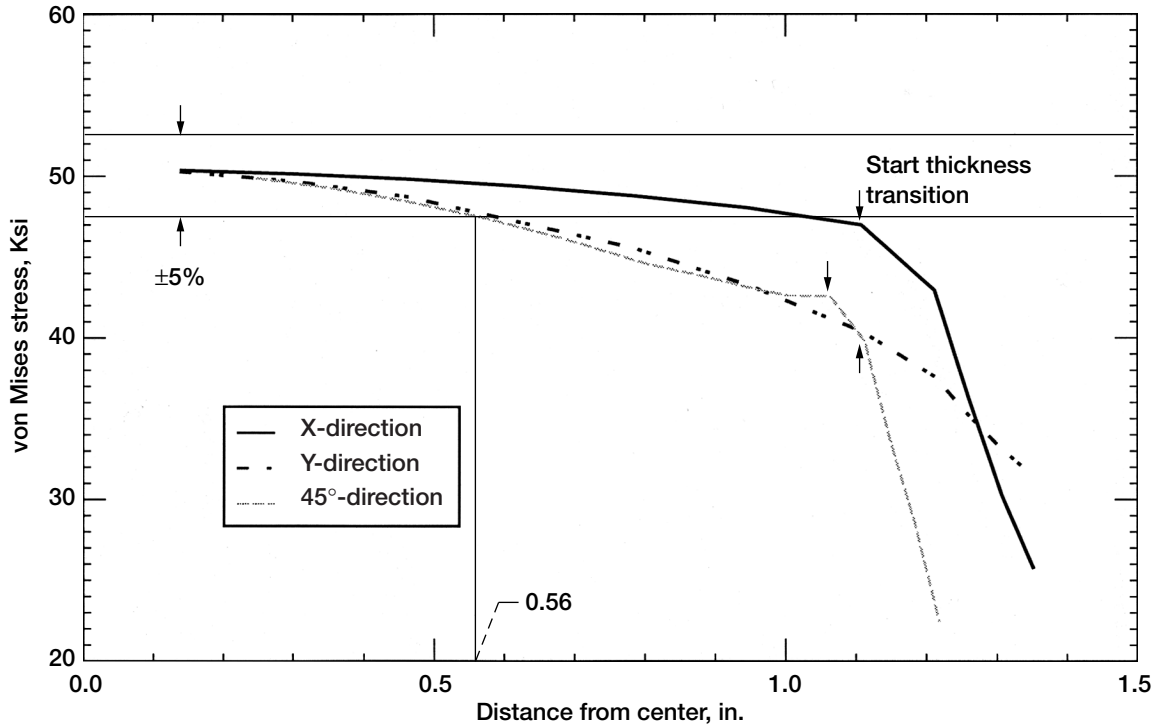

Figure 49.—Variation of gage area stress in specimen design 269.2 in the x, y, and 45° directions: stress ratio (θ) = –22.5°.

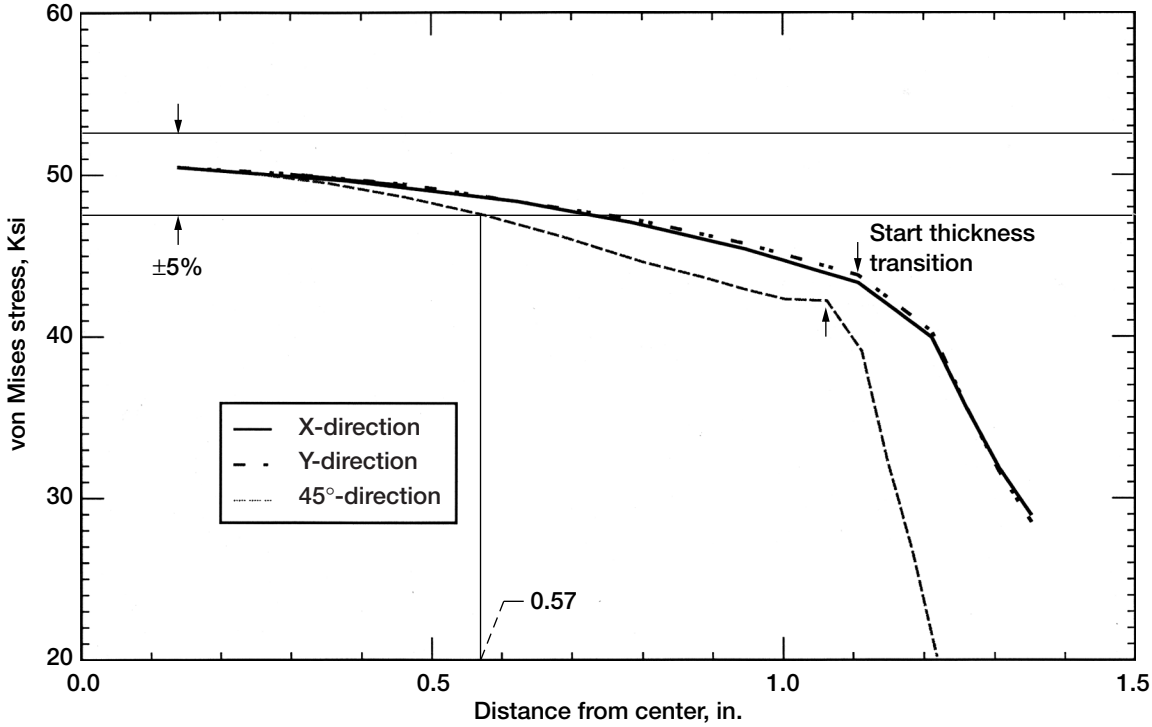

Figure 50.—Variation of gage area stress in specimen design 269.2 in the x, y, and 45° directions: stress ratio (θ) = –45.0°.

REPORT DOCUMENTATION PAGE

Form Approved
OMB No. 0704-0188

Public reporting burden for this collection of information is estimated to average 1 hour per response, including the time for reviewing instructions, searching existing data sources, gathering and maintaining the data needed, and completing and reviewing the collection of information. Send comments regarding this burden estimate or any other aspect of this collection of information, including suggestions for reducing this burden, to Washington Headquarters Services, Directorate for Information Operations and Reports, 1215 Jefferson Davis Highway, Suite 1204, Arlington, VA 22202-4302, and to the Office of Management and Budget, Paperwork Reduction Project (0704-0188), Washington, DC 20503.

1. AGENCY USE ONLY (*Leave blank*)

2. REPORT DATE
January 2003

3. REPORT TYPE AND DATES COVERED
Technical Memorandum

4. TITLE AND SUBTITLE

Specimen Designs for Testing Advanced Aeropropulsion Materials Under In-Plane Biaxial Loading

5. FUNDING NUMBERS

WBS–22–708–31–19

6. AUTHOR(S)

John R. Ellis and Ali Abul-Aziz

7. PERFORMING ORGANIZATION NAME(S) AND ADDRESS(ES)

National Aeronautics and Space Administration
John H. Glenn Research Center at Lewis Field
Cleveland, Ohio 44135–3191

8. PERFORMING ORGANIZATION REPORT NUMBER

E–13362

9. SPONSORING/MONITORING AGENCY NAME(S) AND ADDRESS(ES)

National Aeronautics and Space Administration
Washington, DC 20546–0001

10. SPONSORING/MONITORING AGENCY REPORT NUMBER

NASA TM—2003-212090

11. SUPPLEMENTARY NOTES

John R. Ellis, NASA Glenn Research Center, and Ali Abul-Aziz, Cleveland State University, Cleveland, Ohio 44115. Responsible person, John R. Ellis, organization code 5900, 216–433–3340.

12a. DISTRIBUTION/AVAILABILITY STATEMENT

Unclassified - Unlimited
Subject Category: 26 Distribution: Nonstandard

Available electronically at http://gltrs.grc.nasa.gov

This publication is available from the NASA Center for AeroSpace Information, 301–621–0390.

12b. DISTRIBUTION CODE

13. ABSTRACT ***(Maximum 200 words)***

A design study was undertaken to develop specimen designs for testing advanced aeropropulsion materials under in-plane biaxial loading. The focus of initial work was on developing a specimen design suitable for deformation and strength tests to be conducted under monotonic loading. The type of loading initially assumed in this study was the special case of equibiaxial, tensile loading. A specimen design was successfully developed after a lengthy design and optimization process with overall dimensions of 12 by12 by 0.625 in., and a gage area of 3.875 by 3.875 by 0.080 in. Subsequently, the scope of the work was extended to include the development of a second design tailored for tests involving cyclic loading. A specimen design suitably tailored to meet these requirements was successfully developed with overall dimensions of 12 by 12 by 0.500 in. and a gage area of 2.375 by 2.375 by 0.050 in. Finally, an investigation was made to determine whether the specimen designs developed in this study for equibiaxial, tensile loading could be used without modification to investigate general forms of biaxial loading. For best results, it was concluded that specimen designs need to be optimized and tailored to meet the specific loading requirements of individual research programs.

14. SUBJECT TERMS

In-Plane biaxial testing; Advanced aeropropulsion materials; Cruciform specimen designs

15. NUMBER OF PAGES
70

16. PRICE CODE

17. SECURITY CLASSIFICATION OF REPORT
Unclassified

18. SECURITY CLASSIFICATION OF THIS PAGE
Unclassified

19. SECURITY CLASSIFICATION OF ABSTRACT
Unclassified

20. LIMITATION OF ABSTRACT